Non-Nuclear Exploration of the Solar System

Final Report

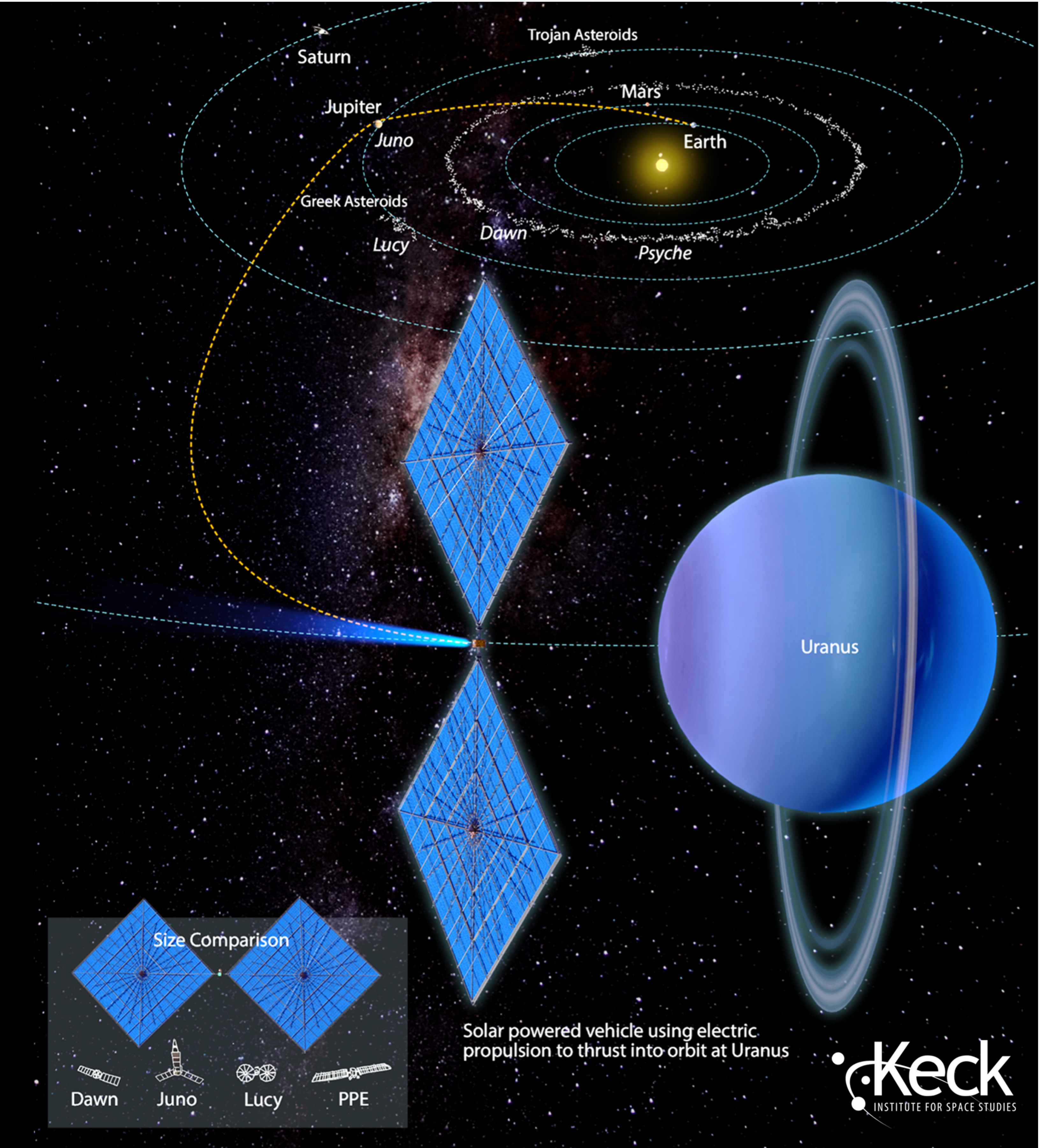

Solar powered vehicle using electric propulsion to thrust into orbit at Uranus

Keck
INSTITUTE FOR SPACE STUDIES

Non-Nuclear Exploration of the Solar System

Study Report prepared for the W. M. Keck Institute for Space Studies (KISS)

Team Leads: John Brophy, Sergio Pellegrino, and Phillip Lubin

The research was carried out in part at the Jet Propulsion Laboratory, California Institute of Technology, under a contract with the National Aeronautics and Space Administration (80NM0018D0004).

Pre-Decisional Information — For Planning and Discussion Purposes Only

Suggested citation: Keck Institute for Space Studies (KISS), 2022, Non-Nuclear Exploration of the Solar System. Brophy, J., Pellegrino, S., and Lubin, P., editors. Final Workshop Report for the W.M. Keck Institute for Space Studies, Pasadena, CA. DOI:10.7907/h62p−6328.

Director: Prof. Tom Prince
Executive Director: Michele Judd
Editing and Formatting: Meg Rosenburg
Cover Image: Chuck Carter/Keck Institute for Space Studies (KISS)

Workshop Participants:

John Brophy
Jet Propulsion Laboratory/
California Institute of Technology,
Principal Investigator

Sergio Pellegrino
California Institute of Technology
Principal Investigator

Phillip Lubin
University of California, Santa Barbara
Principal Investigator

Leon Alkalai
Mandala Space Ventures
Systems Engineering

Harry Atwater
California Institute of Technology
Photovoltaics

Abi Biswas
Jet Propulsion Laboratory/
California Institute of Technology
Beamed Power

Andreea Boca
Jet Propulsion Laboratory/
California Institute of Technology
Photovoltaics

Greg Carr
Jet Propulsion Laboratory/
California Institute of Technology
Power Systems

Artur Davoyan
University of California, Los Angeles
Advanced Propulsion

William Frazier
Jet Propulsion Laboratory/
California Institute of Technology
Systems Engineering

Terry Gdoutos
California Institute of Technology
Large Space Structures

Jonathan Grandidier
Jet Propulsion Laboratory/
California Institute of Technology
Photovoltaics

Kristina Hogstrom
Jet Propulsion Laboratory/
California Institute of Technology
Systems Engineering

Mike Hughes
Jet Propulsion Laboratory/
California Institute of Technology
Guidance Navigation & Control

Les Johnson
Marshall Space Flight Center
Solar Sails, Large Space Structures

Michael Kelzenberg
California Institute of Technology
Photovoltaics

Andrew Lee
California Institute of Technology
Lightweight Structures

Joseph Luther
National Renewable Energy Laboratory
Photovoltaics

Michael Marshall
California Institute of Technology
Large, Lightweight Structures

Colleen Marrese-Reading
Jet Propulsion Laboratory/
California Institute of Technology
Electric Propulsion

Steve McCarty
Glenn Research Center
Low-thrust Trajectory Design

Ralph McNutt
Johns Hopkins University
Applied Physics Laboratory
Power and Propulsion

Elaine Petro
Cornell University
Electric Propulsion

James Polk
Jet Propulsion Laboratory/
California Institute of Technology
Electric Propulsion

Jennifer Scully
Jet Propulsion Laboratory/
California Institute of Technology
Planetary Science

Michael Sekerak
Goddard Space Flight Center
Systems Engineering, Elec. Propulsion

Ian Sellers
University of Oklahoma
Photovoltaics

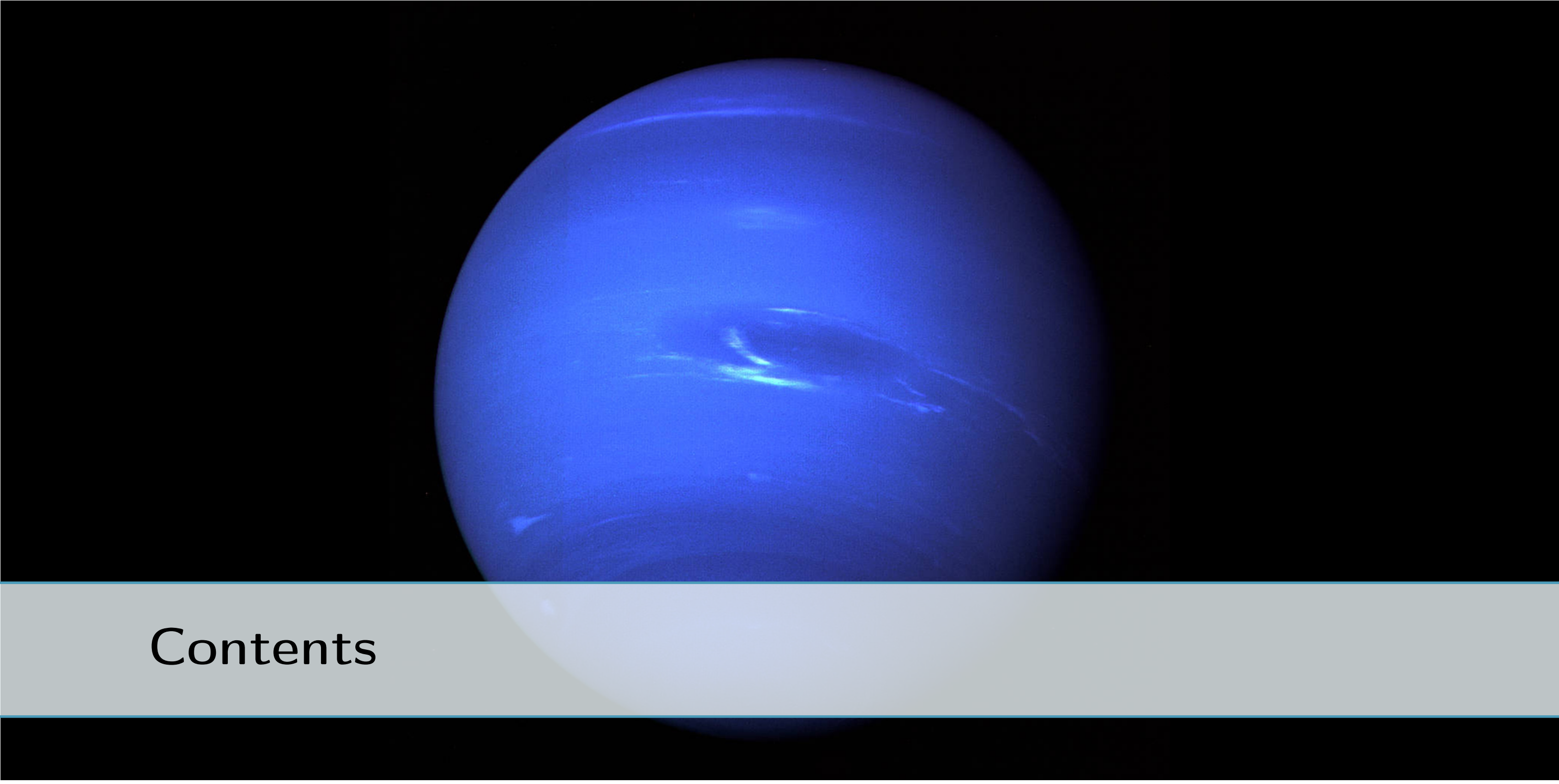

Contents

List of Figures

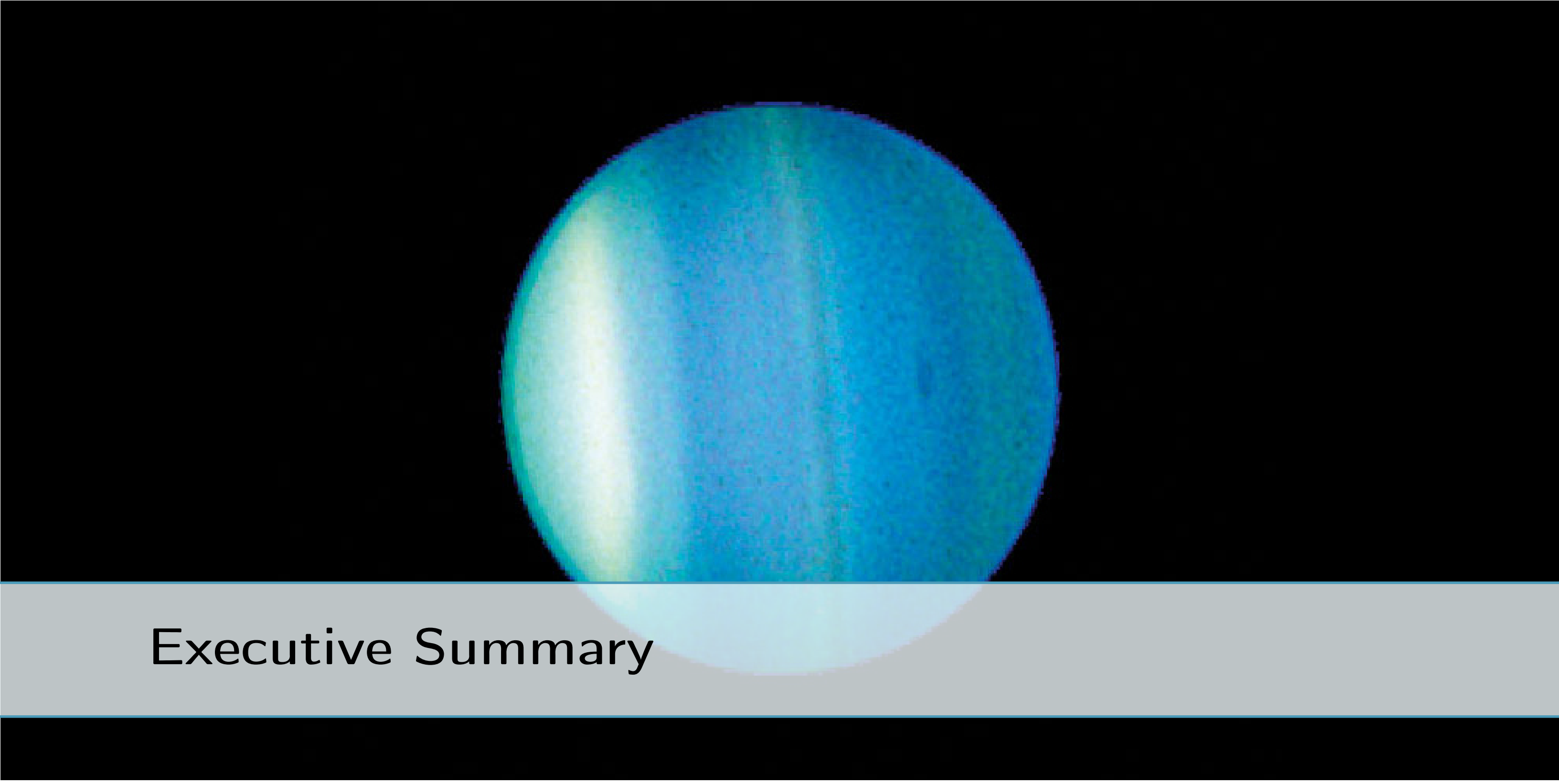

Executive Summary

Advances in solar array, electric propulsion (EP), and power beaming technologies will very likely enable future missions to the ice giants (Uranus and Neptune) by spacecraft that are completely solar powered. Between 1959 and 2001 the power from solar arrays on missions in Earth orbit have increased by five orders of magnitude (from 1 W to >100,000 W). Simultaneously, the use of solar power has been extended to ever larger distances from the Sun. Three solar powered missions out to solar ranges of just beyond 5 au have now been developed and flown (Rosetta, Juno, and Lucy). At these distances, the solar insolation is roughly 25 times lower than that at 1 au. Solar-powered spacecraft to Saturn, where the solar insolation is 100 times lower than that at 1 au have recently been proposed to NASA. A solar-powered mission to Uranus would have to function where solar insolation is only 4 times lower than it is at Saturn. For Neptune, it would be 9 times lower than at Saturn.

Three improvements in solar array technology are required to make this feasible. First, solar cells have to be able to function in the low-intensity, low-temperature (LILT) environment at Uranus and Neptune. Specially designed triple-junction solar cells have been tested at JPL under LILT conditions equivalent to the environment at 30 au have shown excellent performance (high efficiency and high fill factor). Second, the size of deployable solar arrays has to increase by one to two orders of magnitude relative to the current state of the art. Third, the areal density of solar arrays has to be reduced by an order of magnitude. This will most likely be accomplished through a combination of new thin-film solar cell technology like the Perovskite cells under development worldwide and the development of new deployable solar array structures such as those under investigation for solar-powered satellites.

The solar insolation at Uranus and Neptune is 400 to 900 times lower, respectively, than it is at 1 au. To provide sufficient power for a spacecraft at these destinations requires very large solar arrays. To be practical, such arrays will necessarily need to be very lightweight with a minimum structure mass. The gentle, low-thrust nature of electric propulsion is a good match for such solar arrays since the continuous acceleration of order 10–5g will not drive increases in structure mass. In addition, the availability of large amounts of power provided by these arrays between 1 au and 5 to 10 au enables the design of low-thrust trajectories to the ice giants with attractive flight times. Existing ion propulsion technologies, such as NASA's NEXT ion propulsion system enable flight times of conventionally sized spacecraft ($\geq$1000 kg, not including the solar array) to Uranus of less than 10 years with reasonable propellant masses. For example, a conventionally sized spacecraft with a 150-kg complement of instruments could be delivered to Uranus orbit with a vehicle that has two 60-m × 60-m solar array wings and an areal density of 100 g/m^2 in a flight time of less than 10 years. The same-sized vehicle could be delivered to orbit around Neptune in a flight time of less than 18 years if the solar array areal density is reduced to 50 g/m^2. In both cases, larger payload masses can be delivered in similar flight times by increasing the size of the solar array wings. A 440-kg payload mass could be delivered to Neptune orbit in less than 17 years by increasing the solar array size to 70 m ×70 m.

Smaller spacecraft may offer nearer-term opportunities. For example, coupling large, lightweight solar arrays with low-power ion propulsion systems (maximum input power of ~3 kW) can deliver net spacecraft masses to Uranus orbit of several hundred kilograms in flight times of less than 10 years. The only new development for such missions would be solar array wings with dimensions of 30 m × 30 m to 60 m ×60 m with an areal density of 100 g/m^2. The same EP system could deliver net spacecraft masses of 300 to 500 kg (inclusive of the payload, but not including the solar array, xenon tank, and xenon mass margin, which are tracked separately) to Neptune orbit with flight times of around 15 years with a 60-m × 60-m solar array that has an areal density of 50 g/m^2. Such an array would provide roughly 2.4 kW at Neptune.

The development of directed energy (DE) systems could potentially provide hundreds of watts of power continuously to landed assets from solar-powered orbiting spacecraft. Using a DE system to convert electrical power to light on the orbiting spacecraft and a photo-converter system on the landed asset to convert the DE light back to electricity is effectively a "photonic extension cord." For the DE side, a series of lasers in an array is used to beam power to distant landed assets over distances of hundreds to thousands of kilometers. The landed assets use high efficiency photovoltaics tuned to the laser frequency to convert the laser power back to electrical power. Thermal power from the photon power not converted to electricity may, in some applications, also be useful to the landed asset. State-of-the-art directed-energy systems are solid state, efficient (~50%), low mass (~1 kg/kW$_{\text{optical}}$), and long lifetime (~10^5 hrs).

This technology is improving rapidly, driven by the photonic revolution along with consumer and industrial demand. It is likely even possible to beam power to multiple stationary and even moving targets using unique optical beacons from each target.

The technologies required for non-nuclear exploration of the solar system would also enable or enhance a wide variety of other missions of national interest. The large, ultra-light solar arrays combined with a state-of-the-art electric propulsion system would make possible the orbital exploration of Pluto, as well as a tour of its large moon Charon and smaller moons, with a reasonable mass margin and could potentially eliminate the need for RTGs for this mission. Large, ultra-light solar arrays and state-of-the-art electric propulsion systems could enable missions to chase down and encounter long-period comets and potentially even interstellar objects. This combination of technologies could enable solar electric propulsion (SEP) mission architectures farther out in the solar system, including: a Kuiper belt tour, centaur tour, or maybe even a 'Grand Tour' of the gas and ice giants without need for the most optimal planetary alignment, as with the Voyager missions. Sample returns are the next frontier in planetary exploration. The SEP and solar array technologies discussed here would facilitate sample return from a wide range of bodies, including possibly Ceres, Mars, Enceladus, Titan, Triton, and maybe even Mercury. Beaming power from a large, ultra-light solar array in orbit to a landed asset could enable non-nuclear surface exploration of the ice giant's moons. In the nearer term, directed energy systems could deliver power to the surface of the Moon or Mars. Large, lighter solar arrays could facilitate lower-risk human missions to Mars using very high-power solar electric propulsion systems in mission architectures that don't require rendezvousing with pre-deployed assets for the return trip. Finally, large, ultra-light solar arrays could power an Arecibo-like radar in space, to enhance characterization of potentially hazardous objects. Such high-power solar arrays combined with ion-beam deflection would be greatly enhance the nations's planetary defense capabilities.

1. Introduction

The history of deep space exploration has seen solar power used at ever greater distances from the Sun. The solar-powered Juno spacecraft is currently in operation at Jupiter and solar-powered Discovery-class missions to Saturn have been proposed. Simultaneously, solar arrays have been getting larger, lighter, less expensive, and more efficient (cell efficiency has more than doubled in the last 30 years). In 2021, NASA launched the solar-powered Lucy mission with solar arrays that have sufficient area to provide roughly 21 kW of power at 1 au (10.5 kW/wing). This is approximately twice the size of the solar arrays on NASA's Dawn mission, launched in 2007, and 50% larger than the solar arrays on NASA's Juno spacecraft, launched in 2011. The iROSA solar arrays, recently deployed on the International Space Station, are roughly 25 kW/wing. The Power and Propulsion Element of NASA's Lunar Gateway, with a targeted launch readiness date in 2024, is developing a solar array nearly three times the area of the Lucy arrays (~30 kW/wing for a total of >60 kW at 1 au).

In stark contrast, NASA has flown exactly one fission reactor in the history of the space program (the SNAP-10A launched in 1965; *SNAP-10A* n.d.). It produced about 0.5 kW of electrical power and had an unshielded mass of 290 kg, for a specific mass of 580 kg/kW. NASA is currently developing the Kilopower (*Kilopower* n.d.) fission reactor to produce 1-kW-electric with an estimated mass of 400 kg (specific mass including shielding of 400 kg/kW). Radioisotope Thermoelectric Generators (RTGs) have been used successfully for decades to provide power to spacecraft throughout the solar system and beyond. But RTGs are difficult and expensive to develop—as evidenced by the difficulties with the Advanced Stirling Radioisotope Generator (ASRG) (*Advanced Stirling radioisotope generator* n.d.) and the enhanced Multi-Mission RGT (eMMRTG) development activities (*Enhanced Multi-Mission Radioisotope Thermoelectric Generator (eMMRTG) Concept* n.d.)—take decades to mature, are expensive to fly, and have large specific masses. The Multi-Mission RGT (MMRTG) specific mass is 417 kg/kW (*Multi-mission radioisotope thermoelectric generator* n.d.). Limited plutonium and high cost make RTGs a precious resource that could constrain outer planet exploration.

Advanced solar array technologies are compared to nuclear power sources in Figure 1.1. This figure shows that the state of the art in solar array technologies, represented by the Lucy Ultraflex array, has a higher specific power than either the existing MMRTGs or the still-under-development 1-kW version of the Kilopower reactor out to a solar range of about 7 au—well past the orbit of Jupiter. The Lucy array is almost as good as the to-be-developed NextGen RTG and the 10-kW Kilopower reactor at Jupiter.

Advanced solar array technologies, for the purposes of this study, are characterized by their areal density, i.e., mass per unit area. The Lucy Ultraflex solar array, for example, has an areal density of about 3,000 g/m^2. The cell efficiency has a smaller effect on the array performance at large solar ranges and we assume that the cells for the low areal density array will have an efficiency of 25% under low-intensity, low-temperature conditions.

An advanced solar array with an areal density of 400 g/m^2 and a cell efficiency of 25% is almost as good as the MMRTG and the 1-kW Kilopower reactor as far from the Sun as Uranus and is better than the NexGen MMRTG and the 10-kW Kilopower reactor at Saturn. A 200 g/m^2 array with 25% efficient cells is better than the MMRTG and the 1-kW Kilopower reactor all the way out to Neptune and is better than the NexGen MMRTG and the 10-kW Kilopower reactor at Uranus. A 50 g/m^2 array with 25% cells is better than the NexGen MMRTG and the 10-kW Kilopower reactor across all planets in the entire solar system all the way to Neptune.

The vision for this study is the development of the capability for solar-powered missions to the ice giants (Uranus and Neptune) in order to enable a more robust outer planet exploration program unconstrained by the development of fission reactors or the availability of RTGs. This would potentially have the side benefit of reserving scarce RTG resources for a few select missions. The objective of the study is to determine the system architectures and technologies necessary to extend solar-powered missions to the ice giants.

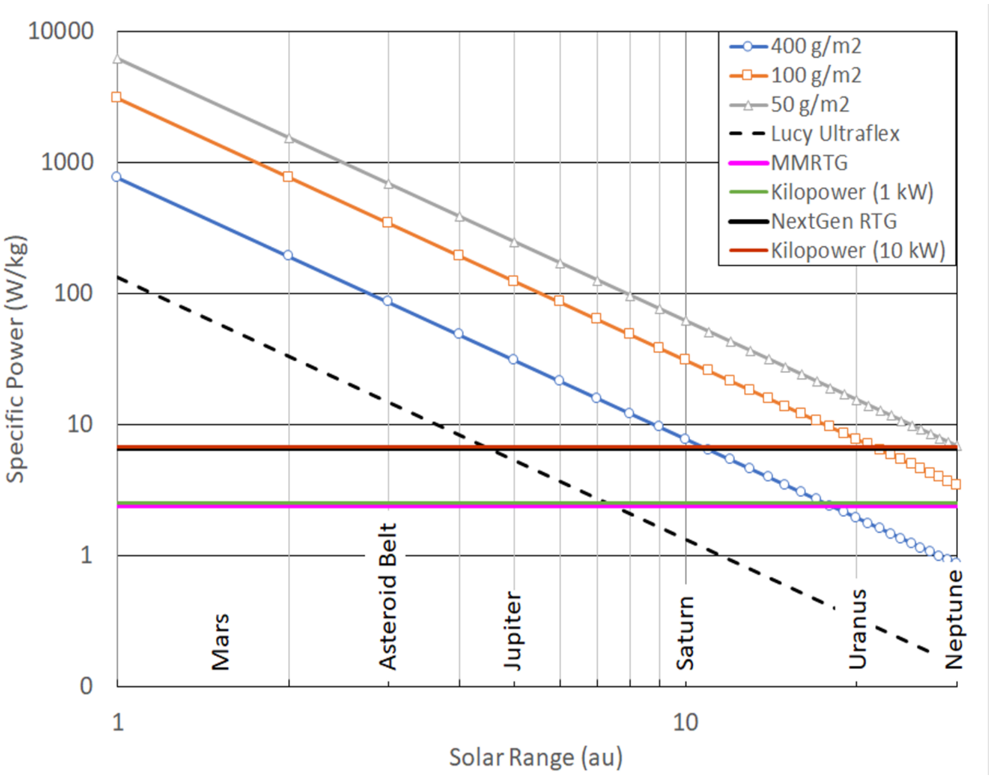

Figure 1.1: Comparison of solar array technologies characterized by specific power (W/kg) with existing and near-term nuclear power technologies. The state-of-the-art Lucy array has an areal density of 3035 g/m^2 and conventional triple-junction cells (efficiency of 29.5% at 1 au). The advanced solar array technologies, with areal densities of 50 g/m^2 to 400 g/m^2, are assumed to have solar cell efficiencies of 25% and cell packing factors of 0.9.

2. Reference Mission Concepts

The reference mission concepts used in this report are to Uranus and Neptune, which make up the ice giant planet class. Voyager 2 and Earth-based telescopic data have revealed the ice giants to be a unique class of planets. However, our understanding of these bodies has greatly fallen behind our knowledge of the gas giants (Jupiter and Saturn) and the terrestrial planets because only a single spacecraft (Voyager 2 in the late 1980s) has visited the ice giants. Ice giants are fundamentally different from the gas giants and terrestrial planets. They are mostly composed of water and other ‘ices’, such as methane and ammonia, which are likely primarily concentrated in a supercritical fluid layer. As discussed by authors such as Hofstadter et al. (2017) and Beddingfield et al. (2020), big-picture questions remain about their interior structures, compositions, atmospheres, magnetospheres, satellites and rings, which when answered, will revolutionize our understanding of the formation and evolution of this class of planets and the solar system as a whole (because the ice giants make up a third of the types of planets in our solar system). Moreover, ice-giant-sized exoplanets are frequently discovered, which means that observation of Uranus and Neptune is also an exceptional tool to calibrate our knowledge of exoplanets. Our insights into the gas giants Jupiter and Saturn have been revolutionized by the orbital missions Galileo, Cassini and Juno, and the time has come for a similar exploration of the ice giants, in the form of a comprehensive orbital exploration of the Uranus and/or Neptune systems.

This report investigates two types of design reference missions to Uranus and Neptune: orbiter-only missions; and orbiter missions that also include landers on the moons of these planets. The orbiter-only missions include a tour of the planet’s moons. The lander missions are assumed to use beamed power to provide long-duration power to landed assets. For these cases, the power is assumed to be beamed from an orbiting solar-powered spacecraft.

Very large solar array areas are required to power a spacecraft at Uranus or Neptune. Table 2.1 indicates that to provide 1 kW of power at Uranus an array size equivalent to a 360-kW solar array at 1 au would be required. Similarly, providing 1 kW at Neptune would require the equivalent of a 900-kW solar array at 1 au. While these arrays are enormous, it should be noted the original solar arrays for the International Space Station (ISS) had sufficient area that if covered with modern triple-junction cells and wired appropriately, would be capable of producing approximately 700 kW at 1 au.

Because of the high power available in the inner solar system as indicated in Table 2.1, it makes sense to consider the use of solar electric propulsion (SEP) for delivery of the spacecraft to Uranus or Neptune. In this study, we assumed that SEP is used for all propulsive functions including orbit insertion at Uranus or Neptune and the grand tours of the moons of these planets as illustrated in Figure 2.1. This architectural requirement further increases the size of the solar arrays required, but eliminates the need to deal with the effects of chemical propulsion induced acceleration loads on these very large, very lightweight solar arrays in their deployed configurations, or the need to retract them for high-thrust maneuvers and then redeploy them. It also significantly reduces the required launch mass (~system cost) as a result of the much higher specific impulse available from SEP as compared with chemical propulsion.

Target Location	Required Power at Target Location (kW)	Solar Range (au)	Solar Insolation (W/m^2)	Active Cell Area Required with 25% Efficient Cells (m^2)	Equivalent Power at 1 au (kW)	Power at 5 au (kW)	Wing Dimensions for a Square Wing with 2 Wings per Spacecraft (m^2)
Earth	1.0	1	1360	2.94	1.0	0.04	1.2 m × 1.2 m
Uranus	1.0	19	3.7	1080	360	14	23 m × 23 m
Neptune	1.0	30	1.5	2670	900	36	37 m × 37 m

Table 2.1: Solar Array Size Example to Provide 1 kW at the Target Location.

2.1 Orbiter Missions to Uranus and Neptune

A Planetary Mission Concept Study (PMCS) report titled, "Neptune Odyssey: Mission to the Neptune-Triton System," was recently published (Rymer et al., 2020)]. This PMCS report describes an orbiter mission to Neptune that is clearly designed to be a Flagship-class. It assumes the use of three Next-Generation Radioisotope Thermoelectric Generators, a Block 2 Space Launch System (SLS) launch vehicle, and a cost (not including the launch vehicle) of $3.5B (in FY'25 $). This report provides an excellent mission concept against which we can compare the results of this KISS study. This PMCS concept includes both an orbiter and a probe dropped into Neptune's atmosphere. The instrument suite on the orbiter is listed in Table 2.2 and has a total Maximum Expected Value (MEV) mass of 194 kg. Per Rymer et al. (2020), the MEV mass is 16% greater than the Current Best Estimate (CBE) mass. The probe in the Neptune Odyssey concept has a CBE mass of 210 kg. For our KISS study, we assumed this same instrument suite plus probe for Flagship mission options resulting in a total payload CBE mass of 377 kg (437 kg MEV). We also defined a simpler instrument suit that may be suitable for a New Frontiers class mission. This simplified instrument suite is also given in Table 2.2 with an MEV mass of 152 kg.

The performance results for our all solar-powered orbiter missions to Uranus and Neptune are given Section 3.2 and compared the results of the all solar-powered missions to Neptune with the nuclear-powered Neptune Odyssey PMCS mission concept.

Instrument	**Flagship Class MEV Mass (kg)**	**New Frontiers Class MEV Mass (kg)**
Magnetometer and Boom	4.7	4.7
Color Narrow-Angle Camera	9.9	9.9
UV Imaging Spectrometer	5.0	5.0
Ion and Neutral Mass Spectrometer	10.6	—
Laser Altimeter	8.5	—
Vis-NIR Imaging Spectrometer	35.65	35.65
Radio and Plasma Wave Detector	14.6	14.6
Thermal Infrared Imager	11.5	11.5
Microwave Radiometer	52.9	52.9
Thermal Plasma Spectrometer	14.71	—
Energetic Charged Particle Detector	3.91	3.91
Energetic Neutral Atom Imager	8.2	—
Dust Detector	13.28	13.28
EPO Camera	0.8	0.8
MEV TOTAL	**194**	**152**

Table 2.2: Suite of Instruments for Flagship (from Rymer et al., 2020) and New Frontiers Class Missions.

2.2 Lander Missions to the Moons of Uranus and Neptune

This study also investigated mission concepts that included landing a vehicle on one of the Ice Giant's moons. A key assumption is that it is not practical to land and/or deploy a solar array of sufficient size—typically of order the equivalent of a 100-kW array at 1 au—on the surface of one of these moons. A mission to land a spacecraft on Miranda, the innermost large moon of Uranus, was selected as our Design Reference Mission in order to help identify

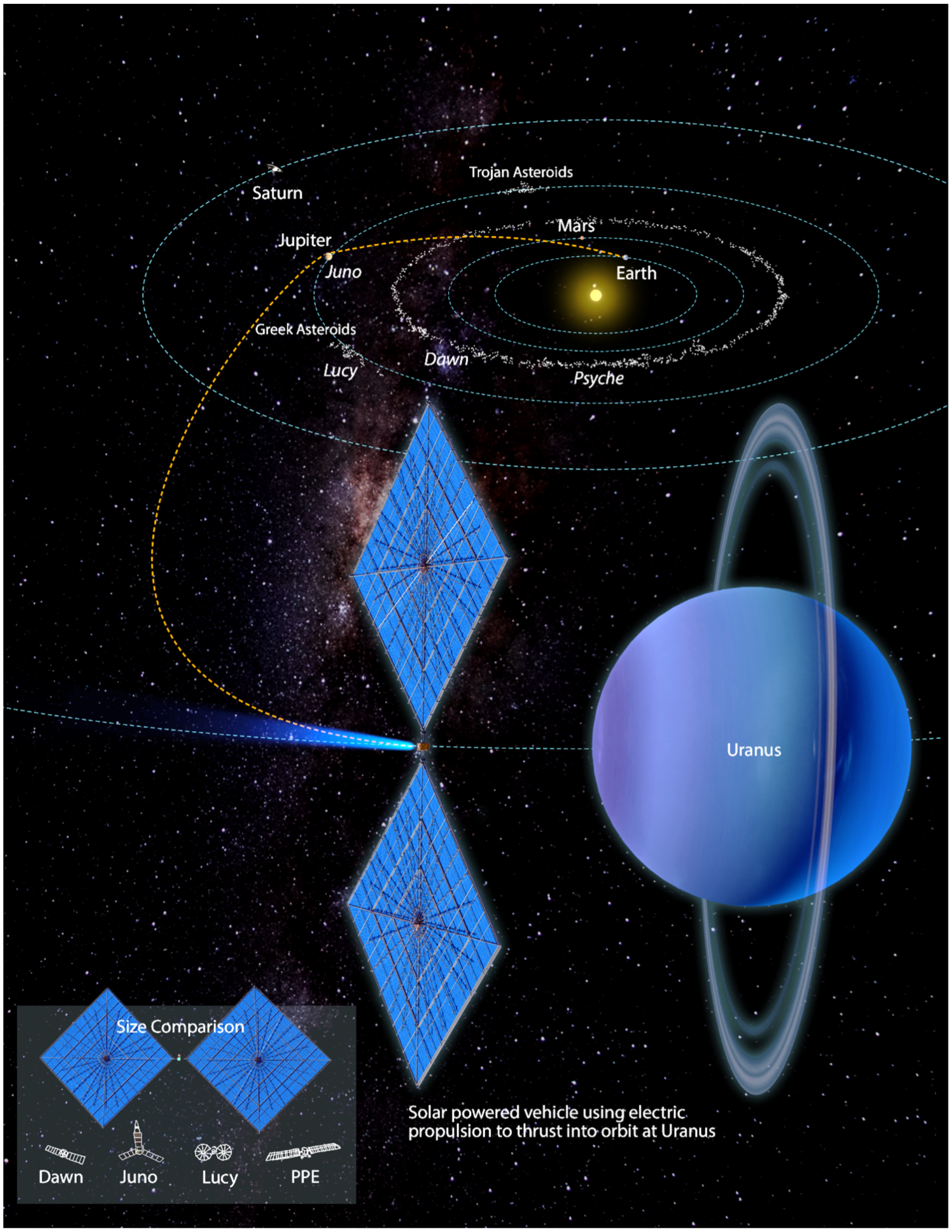

Solar powered vehicle using electric propulsion to thrust into orbit at Uranus

Figure 2.1: A solar-powered spacecraft approaches Uranus 20 au from the Sun using ion propulsion to gently thrust into orbit. The spacecraft is powered by two 60-m × 60-m solar array wings. Credit: Chuck Carter/Keck Institute for Space Studies

and quantify the driving technical issues associated with performing this mission without the use of nuclear power sources. The architecture evaluated in this study beams power to the lander from a solar-powered orbiting spacecraft. An overview of the concept is given in Figure 2.2.

The orbiting spacecraft is assumed to be located at the Uranus-Miranda Lagrange point 2 (UM L2). Because Miranda is small and Uranus is big, UM L2 is only 820 km from the center of Mirada (roughly 600 km above the surface). In comparison, the Earth-Moon L2 point is about 60,000 km from the lunar surface. Therefore, the orbiting spacecraft has to beam power over a distance of about 600 km and since UM L2 moves with Miranda as it orbits Uranus, and its orbit eccentricity is low (0.0013), this distance is approximately fixed. In addition, Miranda is tidally locked with Uranus and so a spacecraft at UM L2 could potentially provide continuous beamed power to the lander.

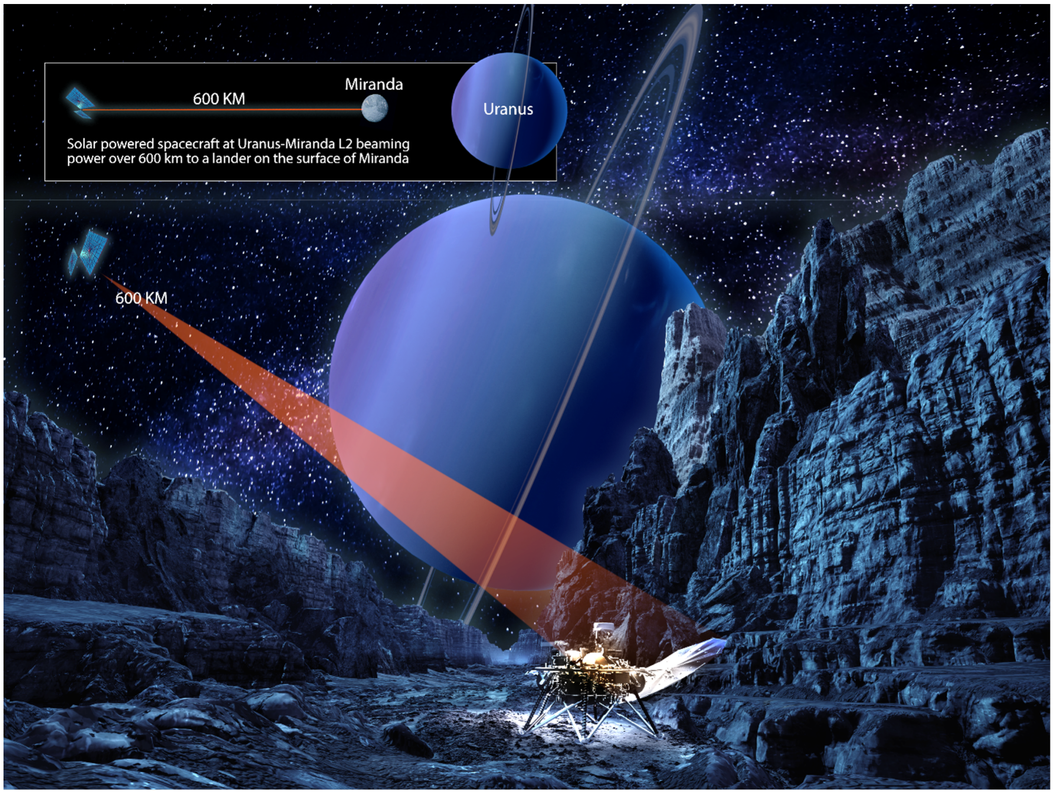

Figure 2.2: A solar-powered spacecraft beams power from the Uranus-Miranda Lagrange point L2 across 600 km, providing power to a lander on the surface of Miranda. Credit: Chuck Carter/Keck Institute for Space Studies

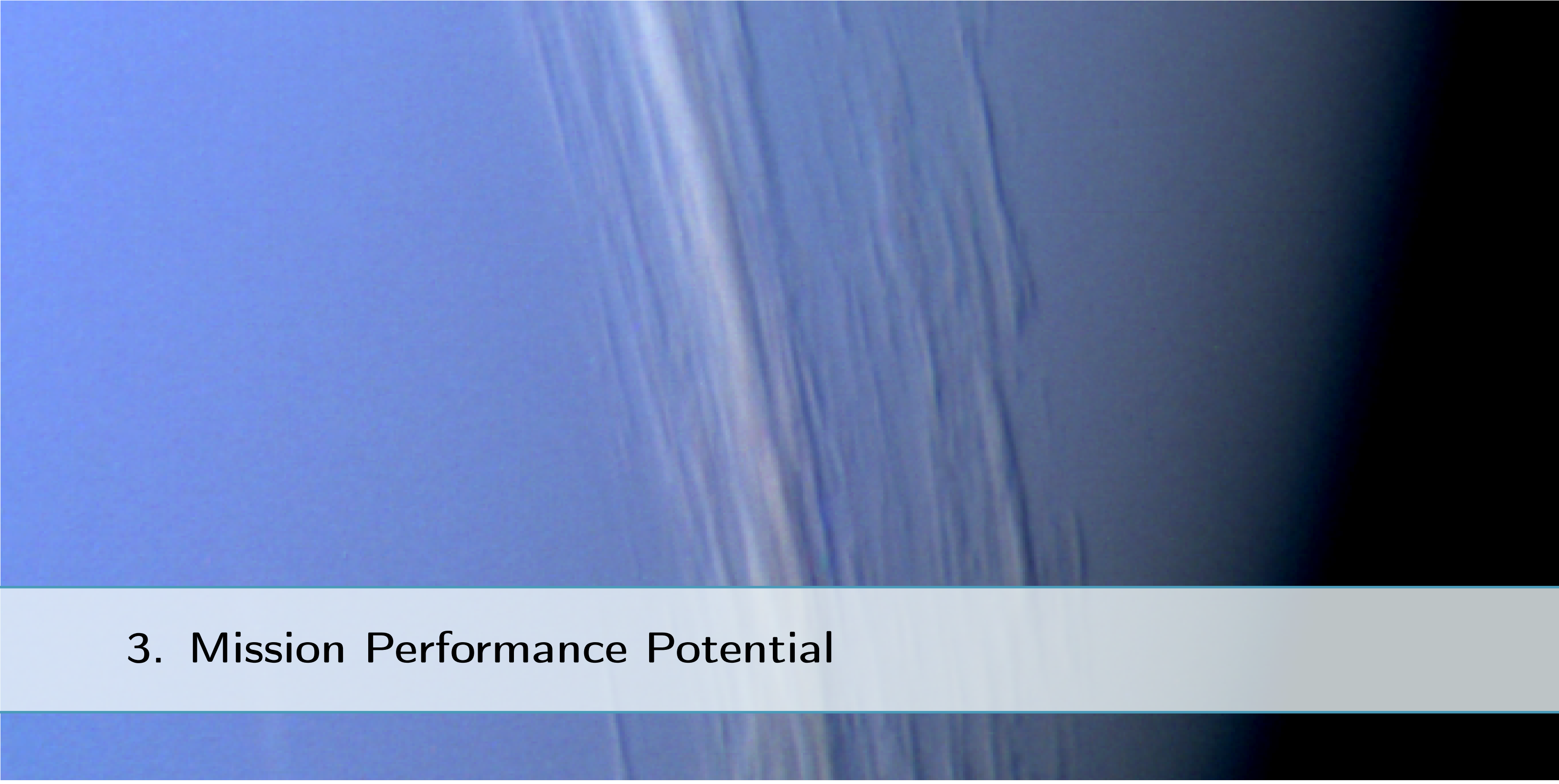

3. Mission Performance Potential

This section provides the results of mission analyses to the ice giants for all solar-powered spacecraft using SEP for all spacecraft maneuvers. The primary figures of merit are the flight time and delivered mass to orbit around Uranus or Neptune. The analyses are done parametrically over a range of parameters for the key technologies that enable all solar-powered missions to the outer planets: solar arrays, electric propulsion, and power beaming.

3.1 Technical Requirements

Technical performance requirements are provided for the key technologies including the solar array (size and areal density), the electric propulsion system (specific impulse, specific mass, maximum input power and throttle range), and the power beam technology (aperture size, power level, and laser frequency).

3.1.1 Large, Lightweight Solar Arrays

The size range of solar array wings considered in this study is illustrated in Figure 3.1. The solar array wings are assumed to be square-shaped and the spacecraft configurations are assumed to include two wings as illustrated in Figure 2.2. The equivalent power at 1 au is given in Figure 3.1 as a function of the length of the side of a square solar array wing. This equivalent power is used as a figure of merit for the solar array assuming a cell efficiency of 25%. But, the solar array wings would not be wired to be able to extract the power indicated in this figure. The corresponding mass of the solar array versus the wing linear dimension is given in Figure 3.2 for areal densities of 50 g/m^2 and 100 g/m^2.

3.1.2 Electric Propulsion

Electric propulsion (EP) is used to achieve the high ΔV values necessary for outer solar system rendezvous in reasonable flight times. EP systems offer specific impulse values over 10× that of traditional chemical propulsion systems and thus can provide ΔVs of order 10 km/s with reasonable propellant mass fractions. For example, the Dawn ion propulsion system provide a ΔV of 11.5 km/s with a maximum specific impulse of 3080 s (Brophy, 2011).

The goal of putting a spacecraft in orbit around Uranus or Neptune places new requirements on the EP system. There are two functions of EP technologies in the mission concept studied here. First, EP imparts ΔV on the spacecraft in the form of outbound acceleration near Earth and deceleration for orbit capture. For this application, the characteristics of NASA's NEXT ion propulsion technology were assumed (Thomas et al., 2019). Second, distributed EP thrusters, such as electrospray thrusters, may be able to provide attitude control for the large-array structure. This distributed mode of operation is indicated by the illustration in Figure 3.3, with array-mounted thrusters providing attitude control and/or momentum management. A unique challenge with this mission arises from the drastic differences in available power at the beginning and end of the trajectories.

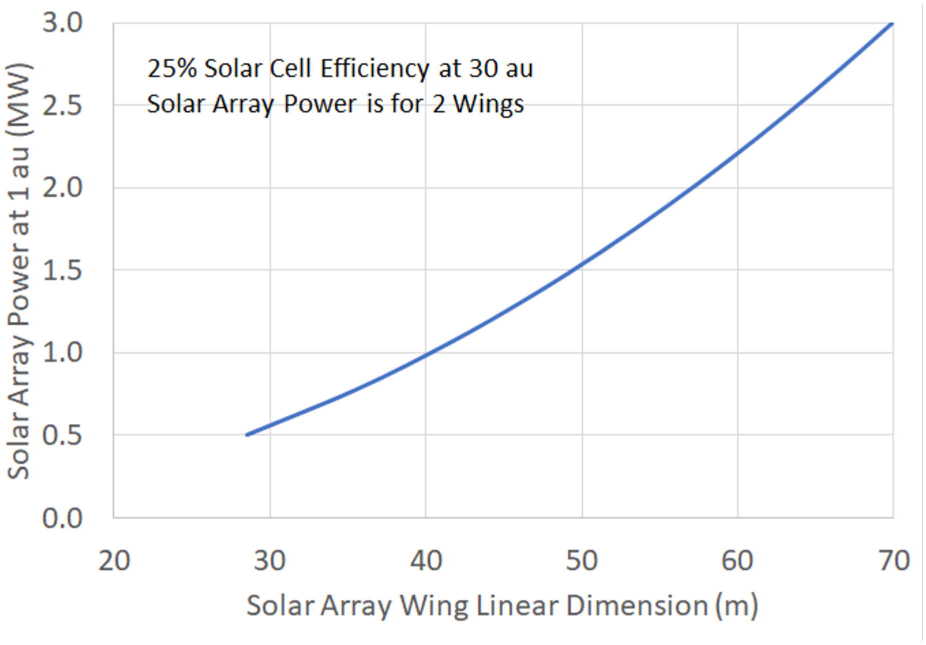

Figure 3.1: Equivalent solar array power at 1 au for two square shaped wings with the linear dimensions indicated (assuming a cell efficiency of 25% independent of solar range). This is for illustration purposes only. The solar arrays would not be wired to handle the total power indicated on the vertical axis. Instead, the array harnessing would be designed to just handle the maximum power expected to be drawn from the array during the mission.

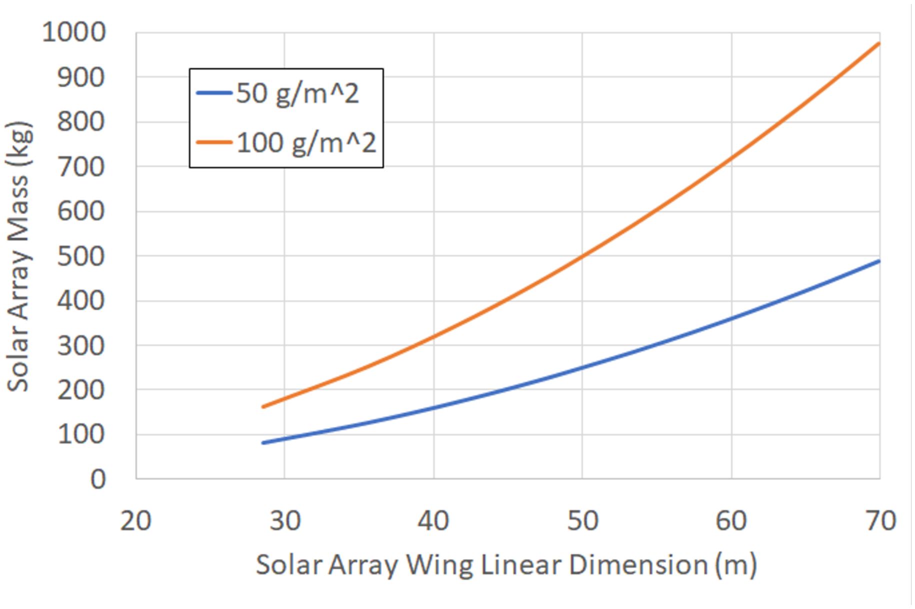

Figure 3.2: Solar array mass for two square wings with the indicated linear dimensions for areal densities of 50 g/m^2 and 100 g/m^2.

Figure 3.3: Illustration of a potential concept for electrospray thrusters distributed on the back-side of the solar arrays of a solar-powered exploration vehicle. Credit: Chuck Carter/Keck Institute for Space Studies

3.1.3 Power Beaming

The development of directed energy (DE) systems is required to provide power to landed assets from solar-powered orbiting spacecraft. Using a DE system to convert electrical power to light on the orbiting spacecraft and a photo-converter system on the landed asset to convert the DE light back to electricity is effectively a "photonic extension cord." For the DE side we assume the use of a laser or series of lasers in an array to beam power to distant assets. The landed asset uses very high efficiency photovoltaics to form a laser power converter (LPC) tuned to the laser frequency to convert the laser power back to electrical power. In addition, the thermal power from the photon power not converted to electricity may, in some applications, also be useful to the landed asset.

The DE systems are required to have a high efficiency for the conversion of electrical power to laser power (~50%), high efficiency for the conversion of laser power back to electrical power (~50%), low mass (~1 $\mathrm{kg/kW_{optical}}$), and a long lifetime (~10^5 hrs). Both the DE server and the landed asset LPC must operate over a reasonably wide range of temperatures with the DE side operating between 40°C to +50°C and the LPV operating over –100°C to +100°C. We assume that the DE system is generally run in a CW mode rather than in a high peak power pulsed mode. The DE server must have a sufficiently large aperture and frequency combination to produce a spot size at the landed asset of reasonable dimensions. Distances between the DE server spacecraft and the landed asset will typically be hundreds to thousands of kilometers. It is 600 km for the example given in Figure 2.2.

3.2 Projected Mission Performance to Uranus and Neptune

The mission performance trade space for orbiter-only missions is divided into conventionally sized spacecraft with masses, exclusive of the solar array, greater than 1000 kg and "smallsats" with masses in the range from 200 kg to less than 1000 kg (also exclusive of the solar array).

3.2.1 Trajectory Analysis

Preliminary trajectory analyses were completed in order to inform key system trades and demonstrate potential mission performance to both Uranus and Neptune. Low-thrust trajectories were designed for over 4,000 unique spacecraft configurations, each of which departs Earth in the early-mid 2030s on a Falcon Heavy launch vehicle (or equivalent), includes a Jupiter gravity assist, and uses the low-thrust ion propulsion system to rendezvous with the planetary sphere of influence (SOI). The low-thrust propulsion system was assumed to operate at a specific impulse of 4107 s, efficiency of 65%, and 90% duty cycle during thrusting arcs. With this baseline mission, multiple spacecraft system parameters were varied in order to better understand the mission sensitivities.

The total spacecraft mass delivered to the planet SOI was varied from 500–3500 kg. This represents the mass available for the remainder of the mission at the destination, including any additional propellant, landers, probes, tankage, solar arrays, etc. The solar array equivalent power available at 1 au was varied from 0.5–3.0 MW and is assumed to decrease by $1/r^2$ as distance to the Sun increases. This array power is intended for use exclusively by the electric propulsion system—any power required for the spacecraft bus would require increased array size. This parameter ultimately determines the power available at the destination for EP thrusting.

The maximum power useable by the SEP system was varied from 3–40 kW. This parameter, along with the resultant propellant throughput, is used to determine the number of thrusters required on the spacecraft. Significantly more power is available early in the mission when the spacecraft is closer to the Sun, but it is generally not beneficial to design the EP system to be capable of using all of this power.

Representative interplanetary trajectories for missions to Uranus and Neptune are shown in Figures 3.4 and 3.5. In each figure, thrust arcs are shown in orange and coast arcs are shown in blue. These types of trajectories commonly start with an acceleration phase through the Jupiter gravity assist, a coast period in the middle, and a deceleration phase where the low-thrust system is used to match the orbit of the target planet. While this structure is common, the duration of each phase is highly dependent upon the launch vehicle, thruster performance solar array power, and vehicle specific mass. It is important to emphasize that the design of any particular trajectory of this type is very tightly coupled with the spacecraft design, propulsion system, and launch vehicle performance. This preliminary analysis provides significant insight into the mission possibilities, but there is much more work that could be done in this area to improve overall performance.

In addition to this work, it would also be interesting to investigate the potential use of a hybrid propulsion architecture, wherein the low-thrust system is used in deep space and a high-thrust system is used to aid in capturing at the destination. The optimization between these two types of systems may provide an intriguing mission with reduced total time of flight.

It is also important to note that an alternative mission approach that uses an Earth Gravity Assist (EGA) rather than JGA, as studied in Brophy et al. (2019), would enable yearly launch opportunities and reduce the spacecraft radiation shielding requirements.

3.2.2 Conventionally Sized Spacecraft

To extract mission performance information from the trajectory analyses, the approximate Master Equipment List (MEL) shown in Table 3.1 was created. This MEL has fixed masses for all of the spacecraft subsystems except for the solar array, the ion propulsion subsystem, the mechanical subsystem, the xenon tankage fraction, and the xenon margin. The solar array mass varies as a function of the solar array wing size and areal density according to Figure 3.2.

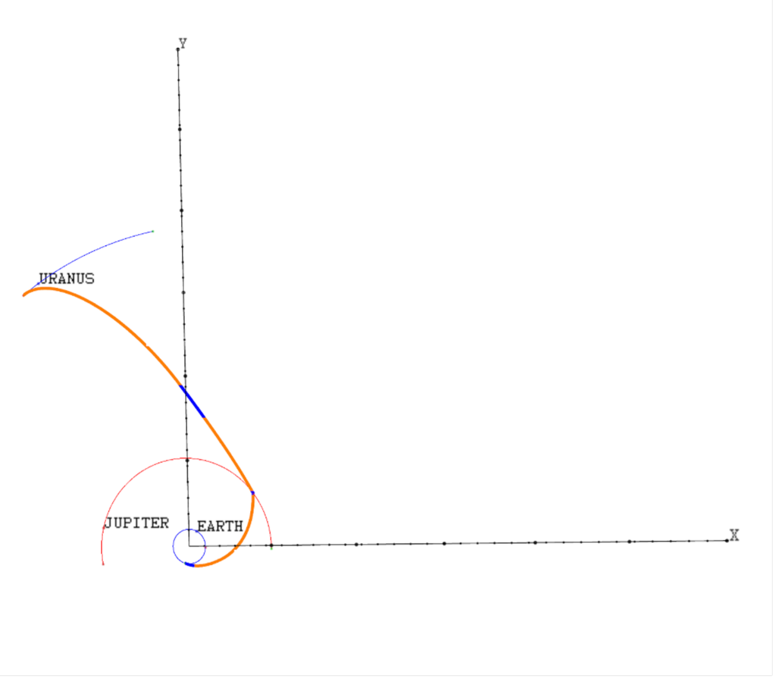

Figure 3.4: Representative interplanetary trajectory to Uranus. Low-thrust arcs are shown in orange indicating that thrusting takes place over the vast majority of the trajectory.

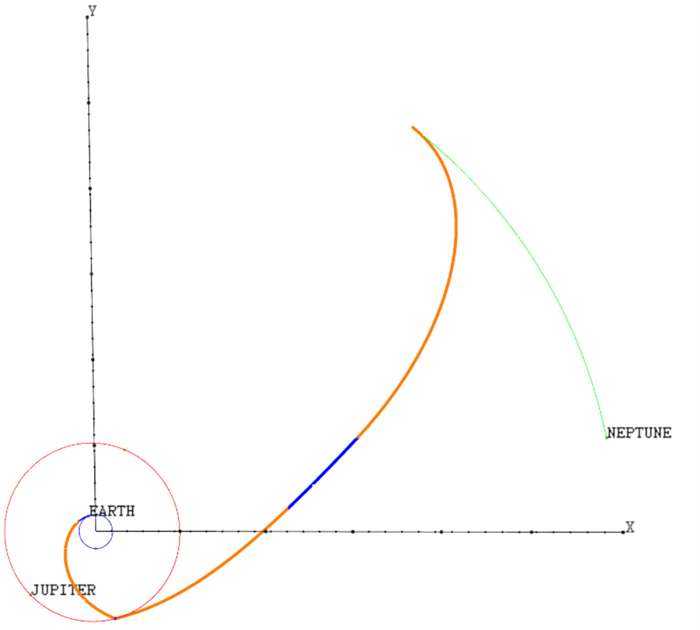

Figure 3.5: Representative interplanetary trajectory to Neptune. Low-thrust arcs are shown in orange.

The xenon tank mass is assumed to be 5% of the total xenon mass stored. Total xenon mass stored includes the deterministic xenon from the trajectory analysis plus 10% margin.

An example mass estimate of the ion propulsion subsystem (IPS) is detailed in Table 3.2. The IPS is based on the NEXT (Thomas et al., 2019) ion thruster similar to that which will fly on the DART mission (*DART* n.d.). The maximum number of simultaneously operating NEXT ion thrusters is calculated from the maximum input power to the IPS used in the trajectory analysis. The maximum input power to the NEXT power processor unit PPU is 7.78 kW including a 5% power growth contingency. The total number of NEXT thrusters is calculated by dividing the total xenon required for the mission by the throughput capability of the NEXT thruster (assume here to be 750 kg/thruster). One additional thruster and PPU are added as cold spares for single fault tolerance. The example in Table 3.2 shows a "2+4" configuration (2 active thrusters + 4 additional thrusters for throughput and redundancy).

Subsystem	CBE (kg)	Mass Growth Contingency	MEV (kg)
Command & Data Handling	3.3	50%	5
Guidance Navigation & Control	60	30%	78
Power Distribution Assembly	50	30%	65
Solar Array	81	30%	106
Harness	80	30%	104
Thermal	80	30%	104
Telecom	50	30%	65
Ion Propulsion System	201	19%	239
Mechanical	198	30%	257
Xenon Tank (5% of Xe stored)	206	0	206
Xenon Margin (10% of deterministic Xe)	413	0	413
Spacecraft Total	1423	15%	1642
Payload	377		467
Instruments	167	16%	194
Probe	210	30%	273
Flight System Dry	1800	17%	2109
JPL Dry Mass Margin	774		30%
MPV System Dry			2574

Table 3.1: Rough Spacecraft MEL used in the mission performance assessment. The items in the CBE column with green backgrounds vary with solar array size and propellant load. All other masses in the CBE column remain fixed.

Item	Unit Mass (kg)	# of Units	CBE (kg)	Mass Growth Contingency	MEV (kg)	Comments
Thruster	13.3	6	79.8	10%	87.8	Assume 750 kg Xe throughput per thruster
PPU	10	3	30.0	30%	39.0	Direct-drive PPU
Gimbal	7.0	6	42.0	30%	54.6	2-axis mechanical gimbal
High Pressure Feed System	5.0	1	5.0	30%	6.5	Xenon tank not included
XCA	2.5	6	15.0	10%	16.5	Xe control assembly
Cabling	3.0	6	18.0	30%	23.4	Subsystem cabling
Misc	11.4	1	11.4	0%	11.4	Tubing, brackets, etc.
		Total	**201**	**19%**	**239**	**Values for Table 3.1**

Table 3.2: Ion Propulsion Subsystem Mass Breakdown Example for a 2+4 Configuration (not including the xenon tank).

3.2.2.1 Uranus Orbiter Mission Performance

The low-thrust trajectory analyses described in Section 3.2.1 were post-processed using the MELs in Tables 3.1 and 3.2 over the range of parameter values given in Table 3.3. The solar array size was varied in the trajectory analysis from (29 m)^2 to (70 m)^2. This resulted in solar array areas for two wings ranging from 1680 m^2 to 9800 m^2. Assuming 25% efficient solar cells and a packing fraction of 0.9, this range of solar array sizes would provide 0.51 to 3.0 MW at 1 au if the arrays were harnessed to exact the full available power at 1 au. At Uranus, this range of solar array sizes provides between 1.4 and 8.3 kW. The maximum input power to the IPS ranged from 3.0 to 40 kW. This represents approximately the maximum power that is drawn from the array over the mission and, therefore, sets the wiring requirements for the solar array. It also determines the number of simultaneously operating NEXT thrusters and the number of PPUs. The amount of xenon required ranges from 515 kg to 4440 kg and determines the total number of NEXT thrusters required.

Parameter	Value Range
Solar Array Square Wing Side Length (m)	29–70
Total Solar Array Area for Two Wings (m^2)	1680–9800
Solar Array Areal Density (g/m^2)	50–100
Equivalent Power at 1 au[a] (MW)	0.51–3.0
S/A Output Power at Uranus[a] (kW)	1.4–8.3
Mass Delivered to Uranus Orbit (kg)	1170–3500
Max. Input Power to the IPS (kW)	3–40
Xenon Required (kg)	515–4440
Launch Mass (kg)	1930–7670
Launch C3 (km^2/s^2)	33.3–83.8
Payload Mass (kg)	130–377

Table 3.3: Range of Parameter Values Used in the Performance Analysis for an Orbiter Mission to Uranus.

---

[a] 25% cell efficiency, 90% packing fraction

For each trajectory, the system CBE dry mass is estimated and compared to the spacecraft mass delivered to Uranus orbit. A system dry mass margin is then calculated as $(M_{\text{delivered}} - M_{\text{CBE}})/M_{\text{delivered}}$. This margin is plotted as a function of flight time as indicated in Figure 3.3. The results in Figure 3.3 assume a solar array areal density of 50 g/m^2 and a payload CBE mass of 377 kg (from Section 2.1). Three solar array sizes are highlighted by the black, orange, and green data symbols corresponding to solar array wings that are 29 m, 60 m, and 70 m on a side. The 70-m array (green symbols) can deliver the spacecraft into Uranus orbit in a flight time of 8.6 years with a dry mass margin of just over 30%. The 60-m array (orange symbols) requires a flight time of 9.2 years for the same mass margin, while the much smaller, 29-m array takes much longer, ~15.5 years.

Reducing the payload mass from 377 kg to the New Frontiers-like 152 kg (from Table 2.2) reduces the flight times by roughly half a year for the same mass margin as indicated in Figure 3.4. Increasing the areal density to the less aggressive 100 g/m^2 increased the flight times by more than a year as indicated in Figure 3.5.

An interesting feature of these results are that for a given solar array size and areal density, significant mass margin can be gained by slight increases in flight time. This can be seen, for example, by examining the orange data symbols in Figure 3.3. The lowest orange symbol indicates a mass margin of 25% for a flight time of 9.1 years. Seven symbols above that is a point that has a mass margin of 39% with a flight time of 9.6 years, representing a significant increase in mass margin for a 5% increase in flight time.

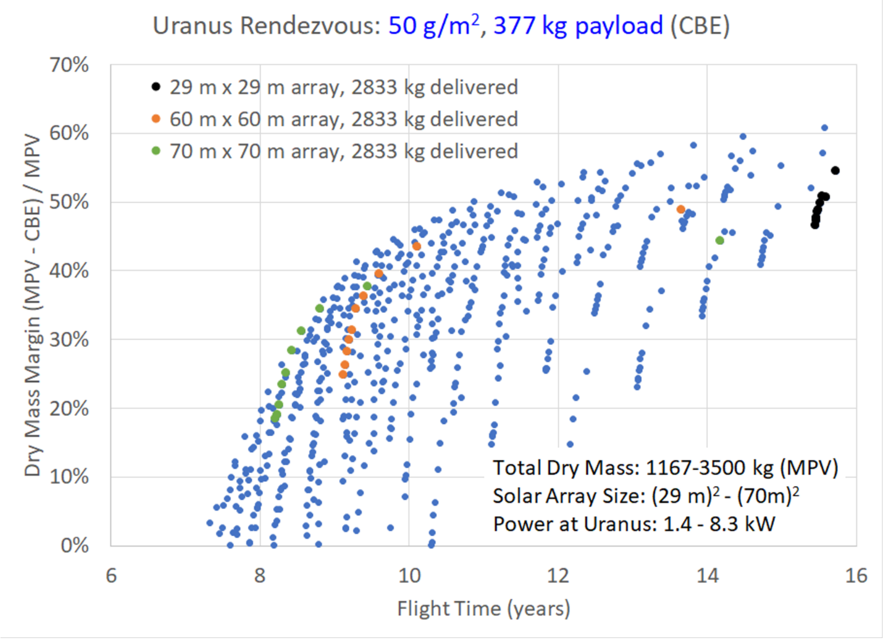

Figure 3.6: Dry mass margin versus flight time for a Uranus orbiter mission with a solar array areal density of 50 g/m^2 and a payload CBE mass of 377 kg. Flight times to enter Uranus orbit are as short as ~8.5 years with mass margins greater than 30%.

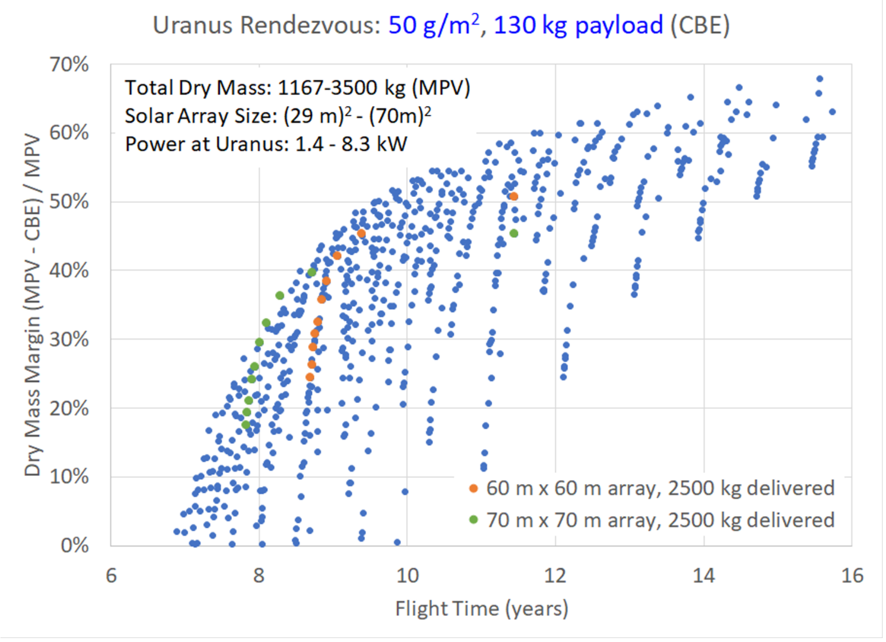

Figure 3.7: Reducing the payload mass from 377 kg to 130 kg, with all else being equal, reduces the flight times about half a year relative to the results in Figure 3.3.

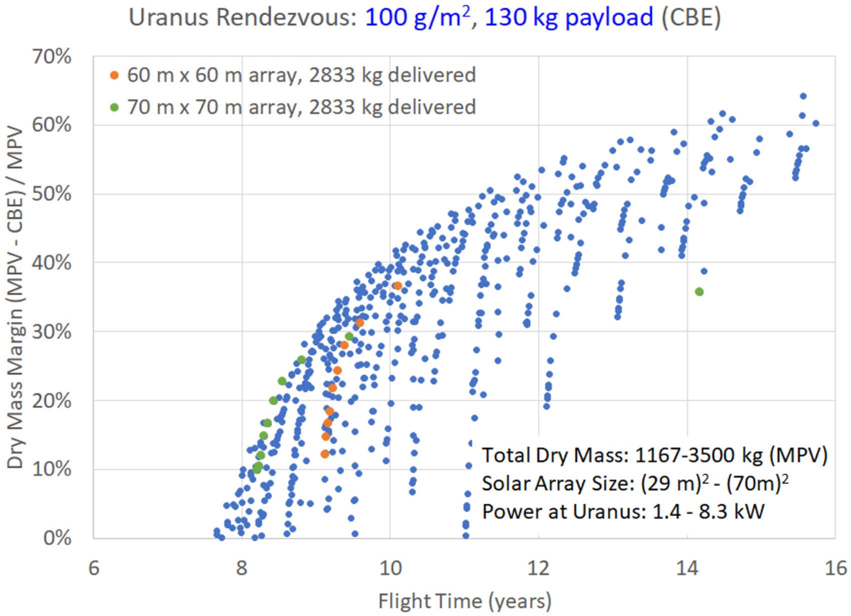

Figure 3.8: Using a less aggressive solar array areal density of 100 g/m^2, with all else being equal, increases the flight times by more than a year relative to the results in Figure 3.4.

3.2.2.2 Neptune Orbiter Mission Performance

Similar to Uranus, the low-thrust trajectory results for missions to Neptune were post-processed using the MELs in Tables 3.1 and 3.2 over the range of parameter values given in Table 3.4. The same solar array size range was used, (29 m)^2 to (70 m)^2 along with the same cell efficiency (25%) and packing fraction (0.9). At Neptune, this range of solar array sizes provides between 0.6 kW and 3.3 kW. As for the Uranus missions, the maximum input power to the IPS for missions to Neptune ranged from 3.0 to 40 kW. The amount of xenon required ranges from 623 kg to 5980 kg.

Parameter	Value Range
Solar Array Square Wing Side Length (m)	29–70
Total Solar Array Area for Two Wings (m^2)	1680–9800
Solar Array Areal Density (g/m^2)	50–100
Equivalent Power at 1 au[a] (MW)	0.51–3.0
S/A Output Power at Neptune[a] (kW)	0.6–3.3
Mass Delivered to Neptune Orbit (kg)	1170–3500
Max. Input Power to the IPS (kW)	3–40
Xenon Required (kg)	623–5980
Launch Mass (kg)	1790–9480
Launch C3 (km^2/s^2)	23.3–85.6
Payload Mass (kg)	130–377

Table 3.4: Range of Parameter Values Used in the Performance Analysis for an Orbiter Mission to Neptune.

---

[a] 25% cell efficiency, 90% packing fraction

The resulting system dry mass margins for Neptune, calculated as $(M_{\text{delivered}} - M_{\text{CBE}})/\text{M}_{\text{delivered}}$, are given in Figures 3.6 through 3.8. The mass margins are given in Figure 3.6 for a solar array areal density of 50 g/m^2 and a payload CBE mass of 377 kg. The orange and green data symbols correspond to solar array wings 60 m and 70 m on a side, respectively. The 70-m array (green symbols) can deliver the spacecraft into Neptune orbit in a flight time of 16.6 years with a dry mass margin of just under 30%. The 60-m array (orange symbols) requires a flight time of 18.2 years for a margin just over 30%.

Reducing the payload mass from 377 kg to the New Frontiers-like 130 kg (from Table 2-3) reduces the flight time to about 15.7 for a mass margin of 30% indicated by the green symbols in Figure 3.7. Increasing the areal density to the less aggressive 100 g/m^2 increases the flight times to over 18 years for mass margins >30% as indicated in Figure 3.8. Even though these flight times are of order 15 years and greater, there the use of solar power eliminates the effect of RTG power decrease over missions of this duration.

3.2.3 Smallsats

The trajectory data for Uranus was re-analyzed to investigate the ability of lower-power ion propulsion subsystems coupled with large lightweight solar arrays to deliver relatively small spacecraft to Uranus orbit. In these analyses the input power to the IPS was limited to 3 kW. Two different solar array sizes were considered: arrays with wings 29 m on a side, and arrays with wings 60 m on a side. As before, each vehicle was assumed to have two solar array wings. These solar arrays would provide 1.4 kW to 6.0 W at Uranus. To determine

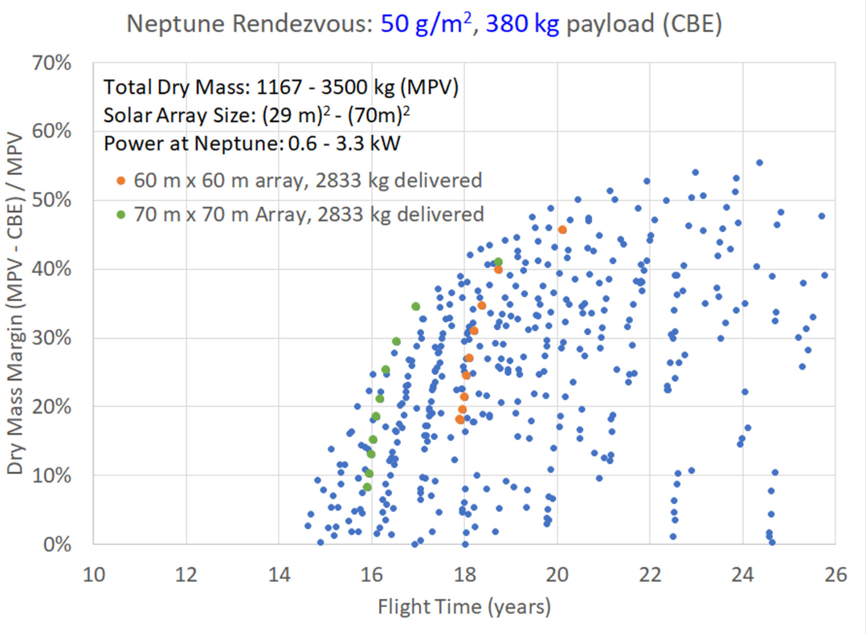

Figure 3.9: Dry mass margin versus flight time for a Neptune orbiter mission with a solar array areal density of 50 g/m^2 and a payload CBE mass of 377 kg. Flight times to enter Neptune orbit are 16.5 years or more for mass margins greater than 30%.

the net CBE mass available, we took the delivered mass from the trajectory analysis and assumed this corresponded to the MEV mass. We divided by 1.43 to get the CBE mass and then subtracted the mass of the solar array, the xenon tank mass, and the xenon mass margin. What's left over we refer to as the net spacecraft mass which represents the available CBE mass for the spacecraft plus the instruments. The results of the process are shown in Figures 3.9 and 3.10 for Uranus and Neptune, respectively.

The orange curve in Figure 3.9 indicates that a solar array with characteristic length of 29 m and an areal density of 100 g/m^2 can deliver a net spacecraft mass of over 300 kg to Uranus orbit in a flight time of 10 years. The larger 60-m solar array could deliver this same net spacecraft mass in about 9 years. As before, significant increases in net spacecraft mass can be obtained with slightly longer flight times, a feature that could potentially provide substantial risk reduction during flight implementation.

Similar results for Neptune are shown in Figure 3.10. In this case, a 300-kg net spacecraft mass could be delivered to Neptune orbit in about 15 years with a 60-m solar array with an areal density of 50 g/m^2. At Neptune, the 29-m and 60-m array would provide 0.6 kW and 2.4 kW, respectively.

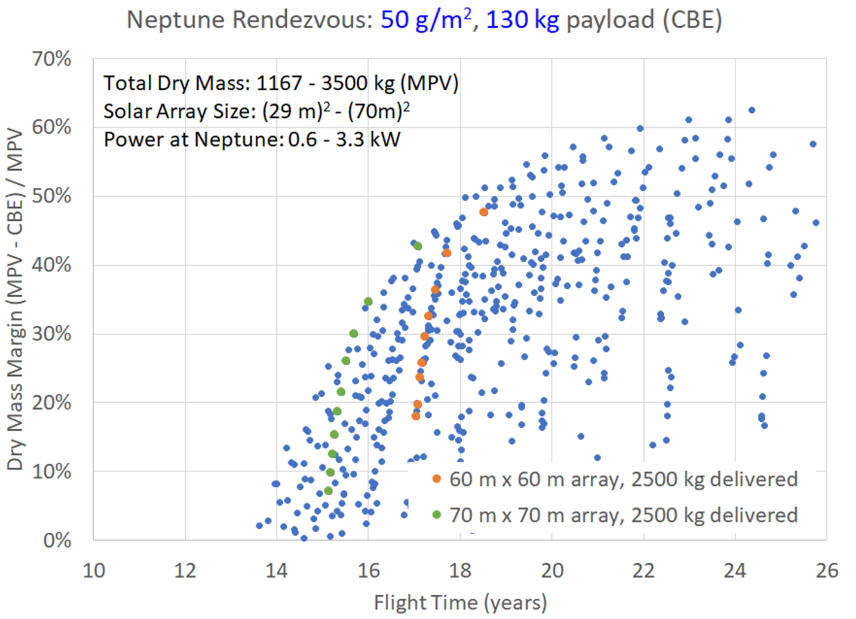

Figure 3.10: Reducing the payload mass from 377 kg to 130 kg, with a solar array areal density of 50 g/m^2 reduces the minimum flight time to 15.7 year for a mass margin of >30%.

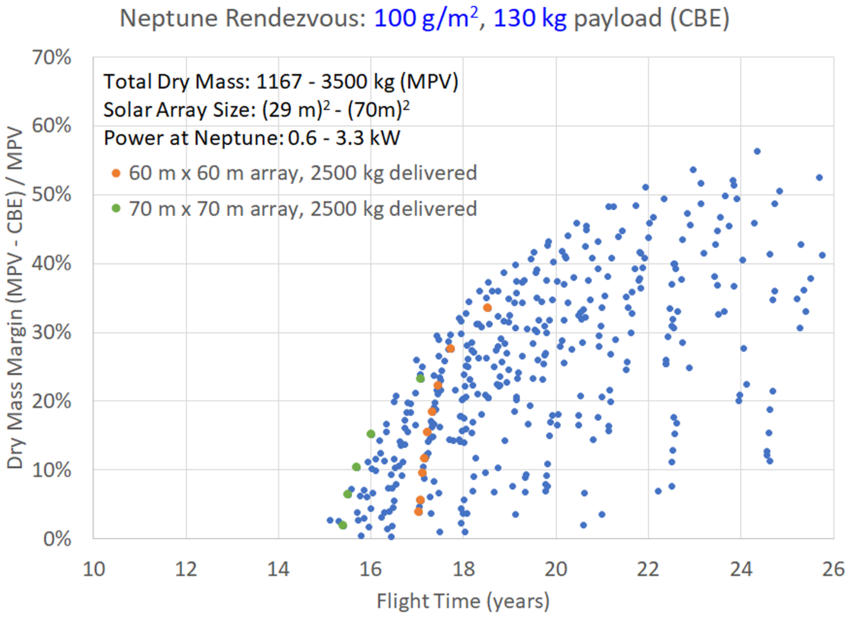

Figure 3.11: Using a less aggressive solar array areal density of 100 g/m^2, with all else being equal, increases the flight times by more than a year relative to the results in Figure 3.4.

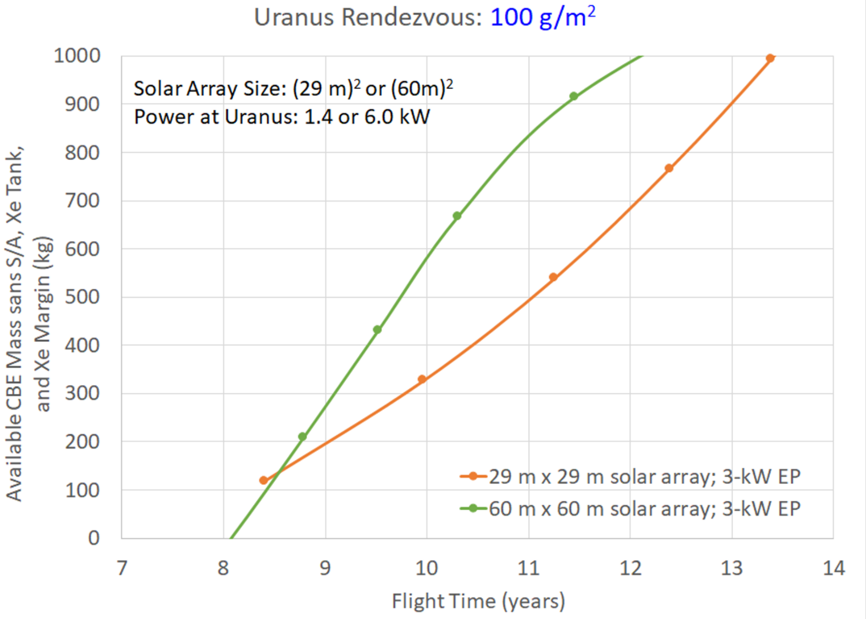

Figure 3.12: Coupling large, lightweight solar arrays with low-power EP systems can deliver net spacecraft masses to Uranus orbit of several hundred kilograms in flight times of less than 10 years. The net spacecraft mass, as defined here, is the delivered mass minus the solar array, xenon tank, and xenon mass margin.

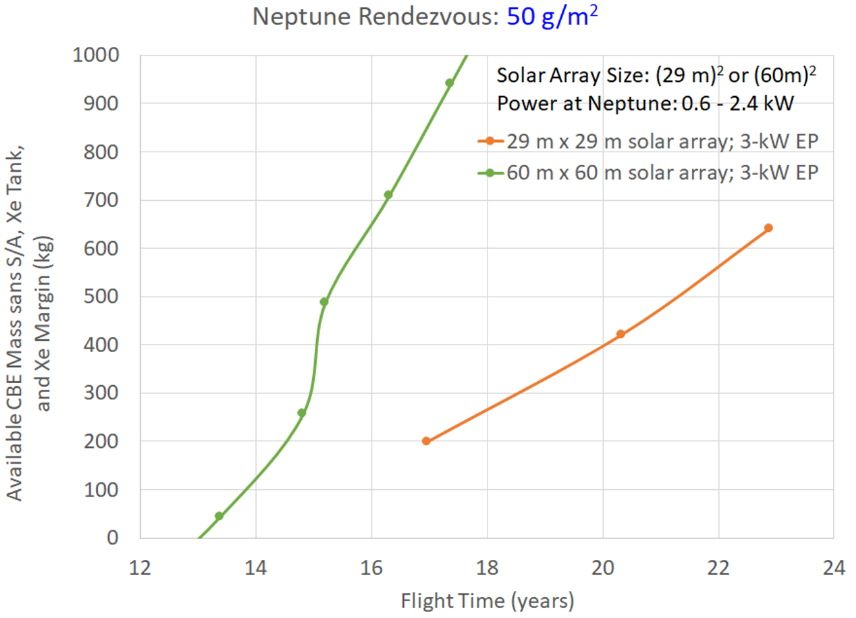

Figure 3.13: Net spacecraft masses of 300 to 500 kg can be delivered to Neptune orbit with flight times of around 15 years with a 60-m solar array that has an areal density of 50 g/m^2. Such an array would provide roughly 2.4 kW at Neptune.

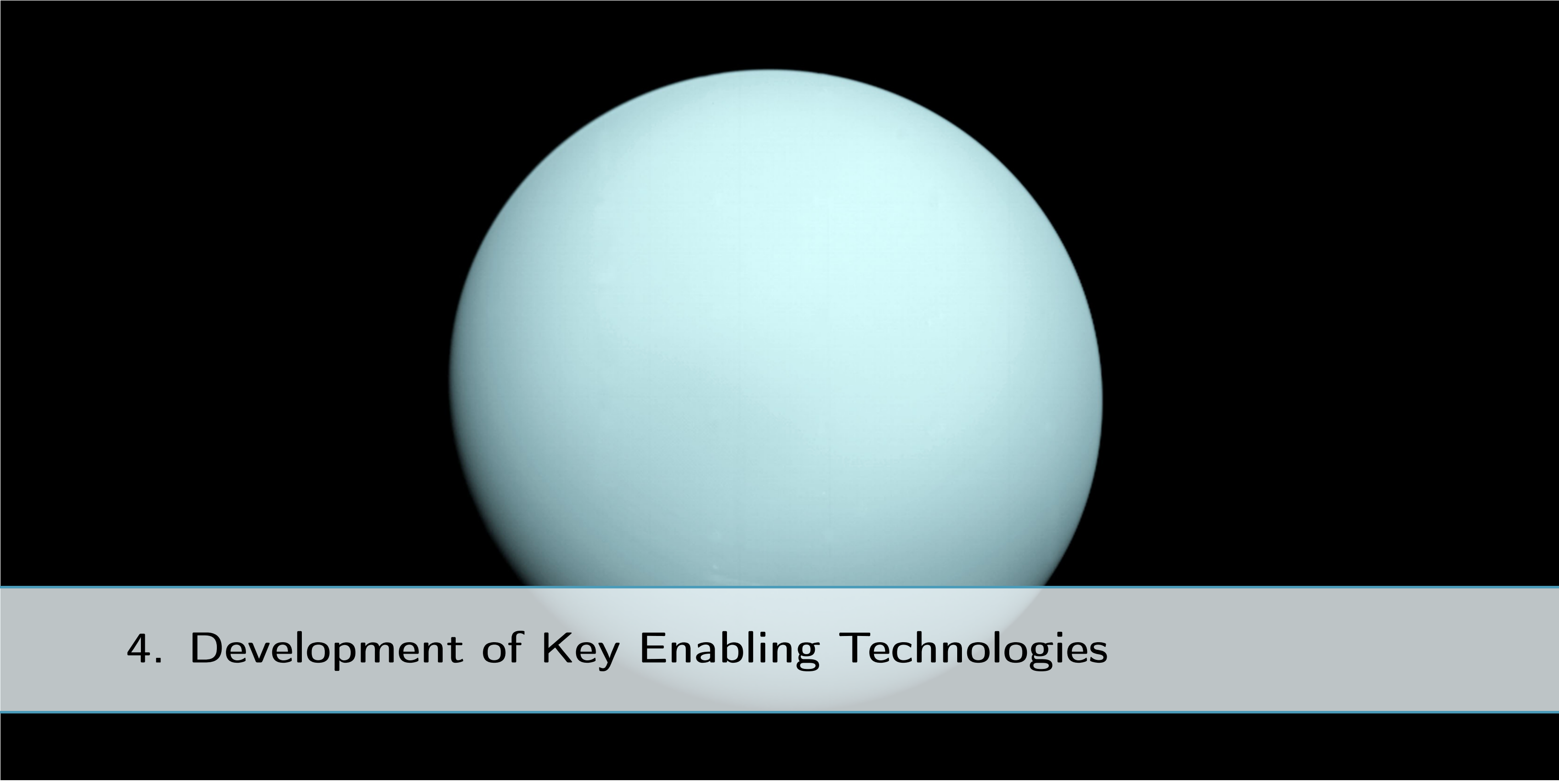

4. Development of Key Enabling Technologies

The status and possible future development paths for the key enabling technologies: very large, lightweight solar arrays; electric propulsion; and power beaming are presented in the following subsections.

4.1 Large, Lightweight Solar Arrays

Deployable solar arrays currently come in two architectures: accordion-folded rigid panels connected by hinges and flexible blankets tensioned by one or more deployable booms. The first architecture does not scale well to very large arrays and will not be discussed further. The second architecture is relevant to the present objective and the state of art for flexible blanket arrays is discussed next. An example of a flexible blanket layout is shown in Figure 4.1.

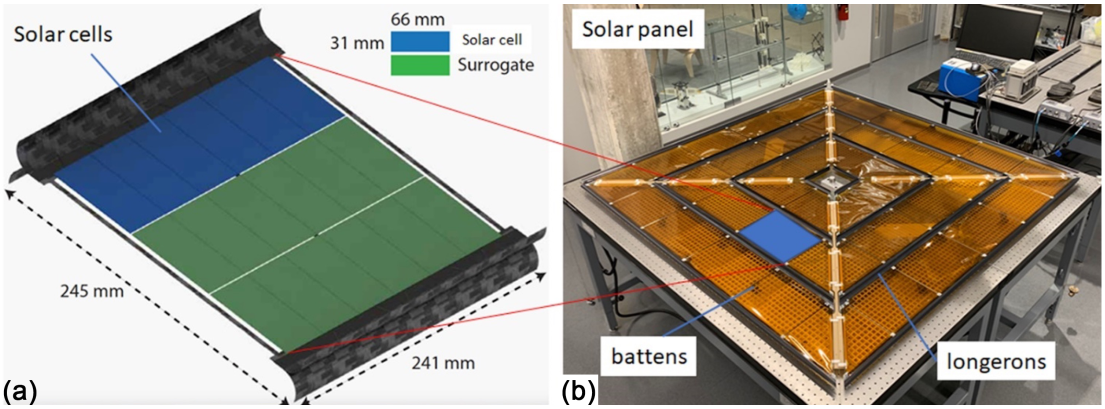

Figure 4.1: Schematic layout of solar array flexible blanket.

Data on four flexible-blanket arrays with PV area ranging from 44 m^2 to 301 m^2 is shown in Table 4.1. MegaROSA is a derivative of the ROSA arrays installed on the ISS in 2021 to enable scaling to much larger sizes.

Parameter	Terra	Milstar	ISS	MegaROSA	MegaFle
Rectangular (R)/circular (C)	R	R	R	R	C
Deployed PV area A, m^2	45.3	44.0	301	74.3	
Acceleration load a, 9.81 m/s^2	0.015	0.050	—	0.060	0.100
Fundamental frequency f, Hz	0.16	0.16	—	0.21	0.10
Length L, m	8.95	14.8	32.9	14.9	5.70
Width W, m	5.06	2.97	9.15	4.99	—
Number of booms	1	1	1	2	10
Cantilever mass density γ, kg m	2.06	1.52	1.78	1.29	1.16
Primary booms (γ_{pb}), kg/m^2	0.077	0.102	0.463	0.135	0.191
Blanket (γ_b), kg/m^2	1.66	1.22	1.20	1.07	0.967
Blanket (γ_b), kg/m^2	0.323	0.203	0.121	0.083	0
Root mass density γ_r, kg/m^2	1.09	0.857	0.574	0.172	0.593

Table 4.1: Data on three heritage arrays and two prototypes, based on Banik and Maji (2016).

A typical architecture of a small flexible blanket array is shown in Figure 4.2. It consists of a single boom, under compression, that applies a tension to the blanket. Given the blanket areal density and total length, the tension in the blanket is set at 20% of the boom buckling load and the fundamental natural frequency of vibration of the combined boom-blanket system, *f*, is given by the following expression (Banik and Maji, 2016):

$$f = 0.425\sqrt{\frac{EI}{wL^4}}$$

where *EI* is the flexural stiffness of the boom, *L* is the length of the boom, and *w* is the combined linear density of the boom and blanket.

An extensive study (Banik and Maji, 2016) has reached the conclusion that this architecture incurs significant mass penalty as the number of booms and the length of the booms are increased. In other words, shorter and wider arrays with fewer booms are preferable.

The alternative architecture developed by the Caltech Space Solar Power Project (SSPP) is considered more efficient for future, ultralight arrays based on next generation thin PV films. The SSPP architecture is a square structure composed of long and narrow, parallel strips that

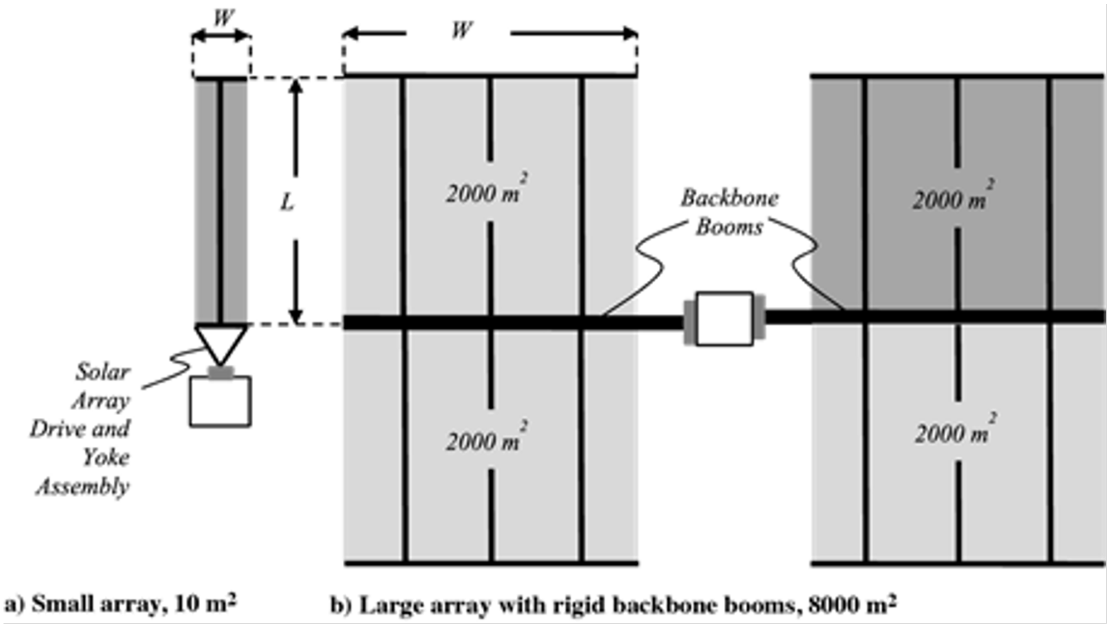

Figure 4.2: Architecture of solar array consisting of flexible blanket(s) and deployable boom(s). (a) Small array with a single boom. (b) Large array with multiple booms mounted on backbone booms. (Edited from Banik and Maji, 2016).

support photovoltaic (PV) and power radiation tiles. The strips are bending-stiff structures that are supported by four diagonal booms, also loaded in bending, through four diagonal cables. Each cable is connected to the central hub and to the tip of a boom. Bending of the booms and strips is the main load-carrying mode for this structure when it is loaded by a transverse pressure (Figures4 4.3 and 4.4) and the structure can be efficiently packaged through a combination of origami-inspired folding and coiling (Figure 4.5; Arya et al., 2016). The main advantages of the SSPP architecture include:

- Modular and scalable design.
- The thin PV films are supported and stabilized along the edges, which facilitates handling, testing and integration (Fig 4-6).
- The load path in the structure is statically determinate, and hence insensitive to manufacturing errors and thermal gradients.
- Main electrical conducting network can be integrated within the longerons.
- More efficient use of structural material, through avoidance of buckling of booms.

The fundamental frequencies of the structures in Table 4.1 all greater than 0.1 Hz. This is a typical requirement for large deployable appendages. A discussion of the control of very large, lightweight structures with much lower natural frequencies is given in Section 4.1.3.

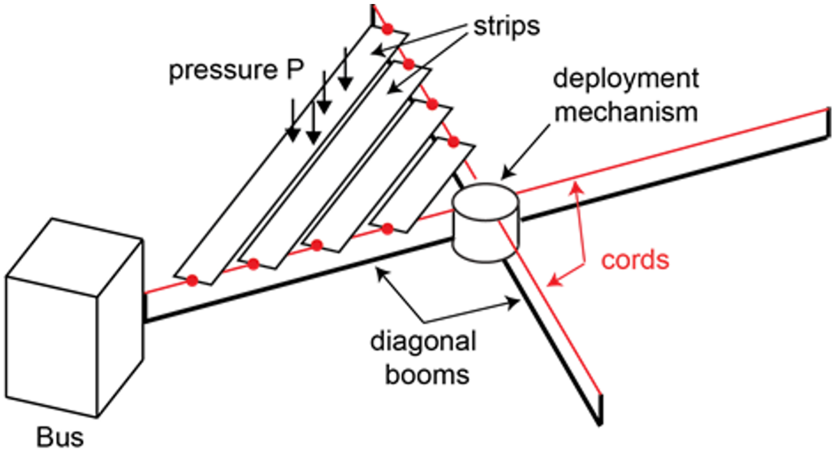

Figure 4.3: Schematic description of SSPP structural architecture.

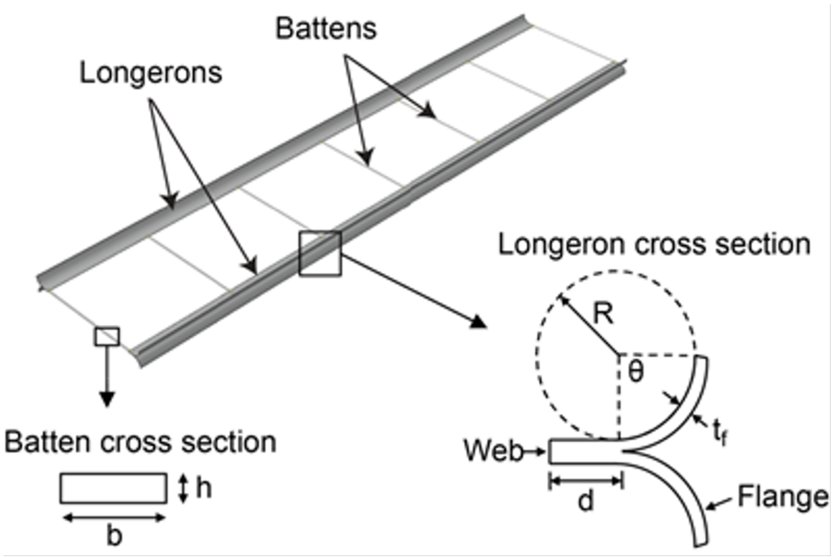

Figure 4.4: Schematic of strip of structure.

As an example, an optimal design for a structure with size $L = 40$ m that is required to carry a pressure $P = 10^{-3}$ Pa with a deflection limit of $0.1L = 4$ m, was developed by Lee and Pellegrino (2021). The values of the boom length, radius, and thickness, as well as the strip longeron angle and total areal density are listed in Table 4.2. The areal density is 28.4 g/m^2.

The strips are limited by excessive deflection. The bending architecture booms are also limited by excessive deflection. The deflected shape under the pressure 10^{-3} Pa is shown in Figure 4.8.

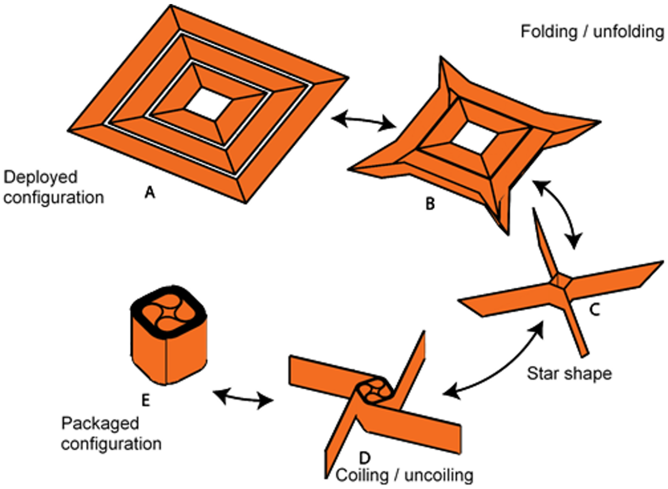

Figure 4.5: Packaging and deployment scheme.

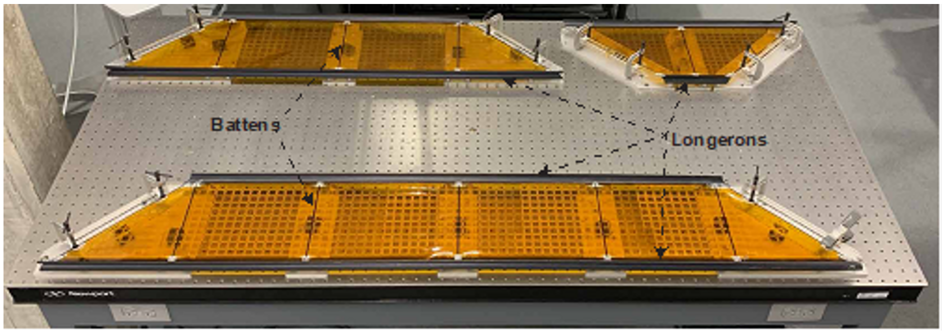

Figure 4.6: Examples of strips of three different lengths.

There are 20 strips in each quadrant and the total maximum deflection of 4 m occurs at the center of the outermost strips.

r (mm)	t (mm)	θ(deg)	ρ_{total} (g/m^2)
20	0.6	130	28.4

Table 4.2: Geometry, areal density, and design limiting conditions for optimal design with $L = 40$ m, $P = 10^{-3}$ Pa, and $w = 0.1L$.

4.1.1 Deployment / Structure

Deployable structures with areal density of order 50 g/m^2 are an enabling technology for the large ultralight solar arrays required for non-nuclear exploration of the outer planets. The lightest deployable structures that can be scaled to large arrays and have been demonstrated to-date are prototypes of the Caltech SSPP deployable structure (Gdoutos et al., 2020).

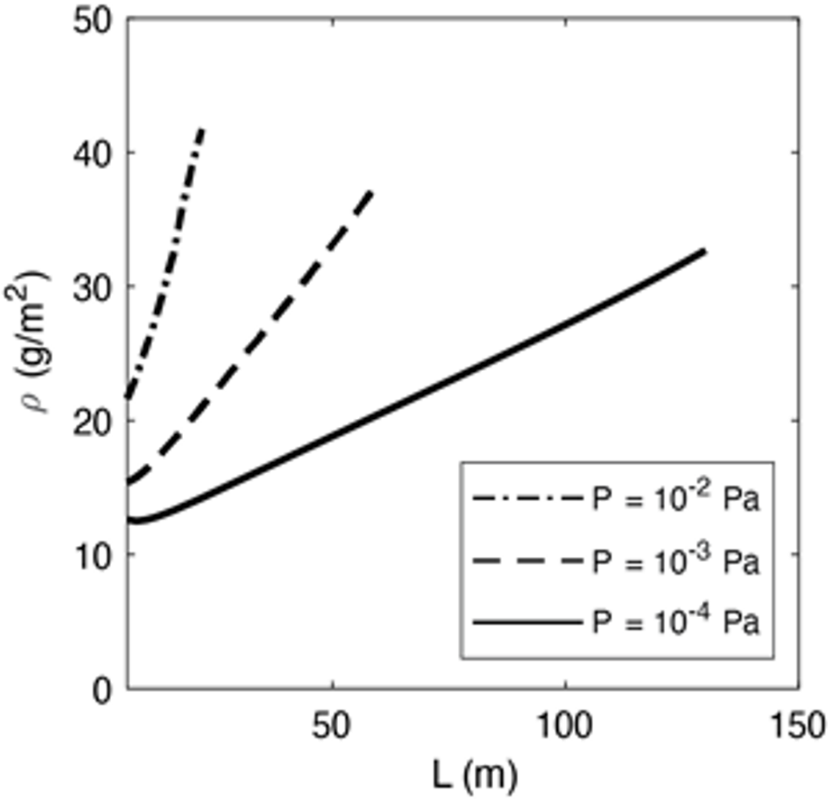

Figure 4.7: Areal densities vs. span L for three pressure values. The maximum boom deflection, cable sag, and strip deflection are $0.05L$, and the total maximum deflection is $0.1L$.

The Caltech SSPP deployable structures differ from existing architectures in that they are assembled of modular structural elements (strips) which can be ground-tested independently and do not rely on boom tension for stiffness.

The state-of-the art Caltech SSPP deployable prototype measures 1.7 m × 1.7 m, weighs ~100 g/m^2, and can be packaged in a cylinder with 185 mm diameter and 255 mm height inside a deployment mechanism (Figure 4.11a). The structure's repeated deployment and stable response to thermally accelerated aging while stowed have been demonstrated for the qualification campaign of the Deployable on-Orbit ultraLight Composite Experiment (DOLCE) technology demonstration payload, part of Caltech's Space Solar Power Demonstration-1 (SSPD-1) mission (Gdoutos et al., 2022).

The Caltech SSPP deployable is a promising technology with the potential to enable large ultralight solar arrays. A number of prototypes have been built and demonstrated at the ~2-m × 2 m scale and the areal density for sizes greater than 7 m × 7 m is calculated to be less than 30 g/m^2 (Gdoutos et al., 2022). In order to mature the Caltech SSPP deployable

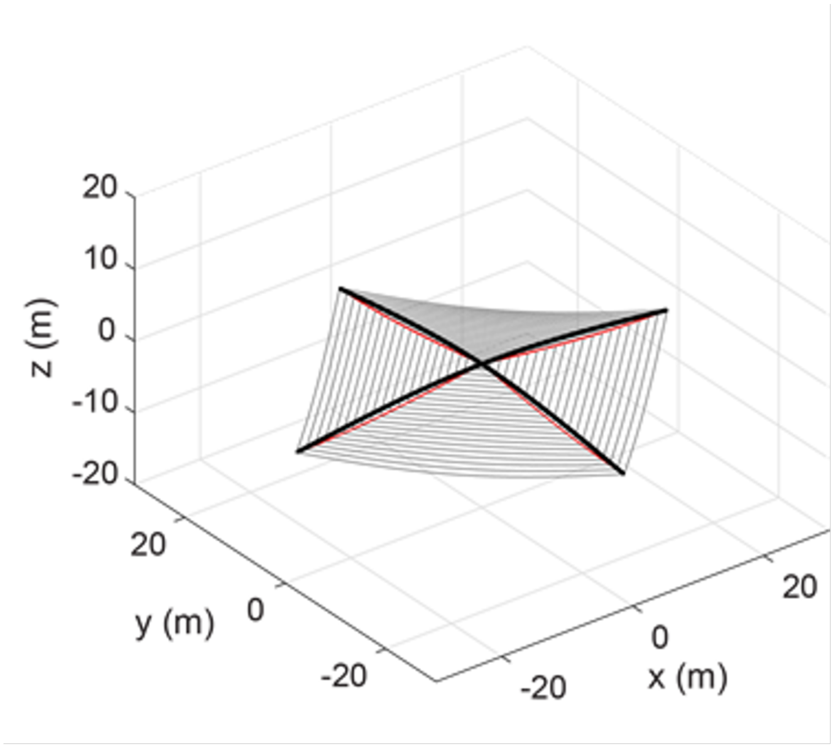

Figure 4.8: Example 40-m solar array.

structure technology for consideration for an outer planet mission, the following five key milestones have been identified:

1. On-Orbit deployment demonstration of prototype-scale (~2-m × 2-m) Caltech SSPP structure. The goals of the ~2-m × ~2-m on-orbit milestone are to demonstrate the Caltech SSPP deployment in zero gravity, the structure's thermal stability under orbital cycles, and to mature the deployment mechanism to a flight design. Achieving these goals will establish the flight feasibility of this novel deployable concept, with solar array functionality and scale-up to be demonstrated in milestones 2–5.

2. Functional and environmental qualification of medium-scale (~7-m × ~7-m) Caltech SSPP solar array strip (~2-m × 1-m). The goals of this milestone are to integrate photovoltaics with the deployable structure and demonstrate the integrated solar array's ultra low areal density (~100 g/m^2), coilability around a tight mandrel (40 mm diameter), and performance under temperature and vacuum. For this milestone, it is sufficient to demonstrate that a representative strip (shown in blue Figure 4.12a) of the overall structure meets the performance targets. This reduces the complexity of the gravity off-loading setup that may be required, utilizing the architecture's modularity to reduce complexity. Achieving this milestone will demonstrate the space applicability of the lightest deployable solar array to-date as well the anticipated reduction in areal

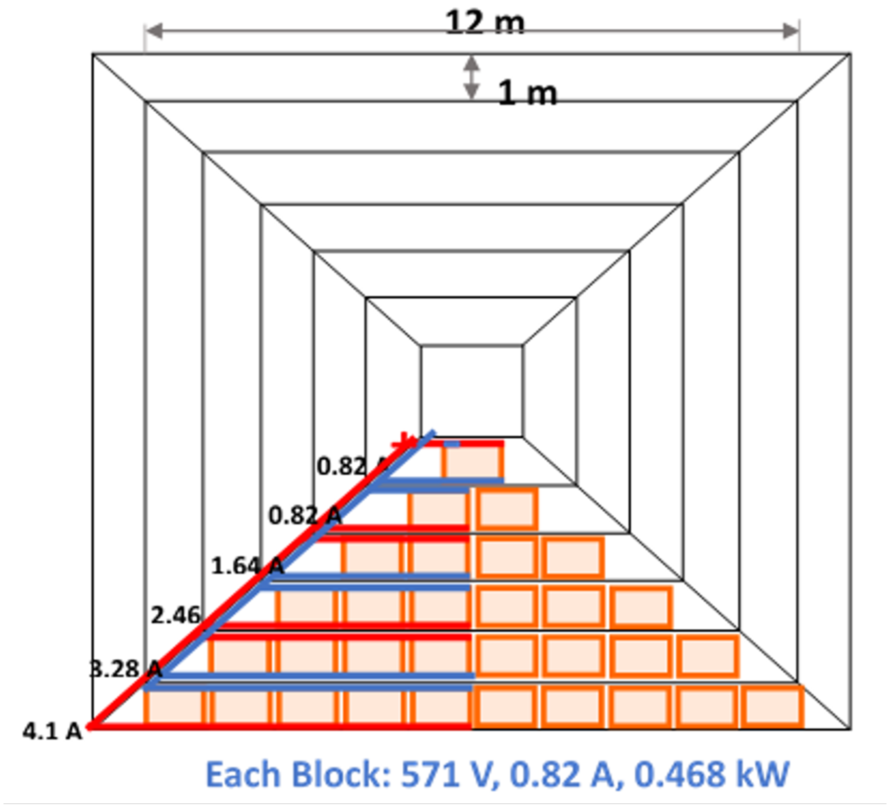

Figure 4.9: Example electrical layout of 12 m × 12 m array, 60 kW under AM0 conditions. Courtesy of Dr. Wen Luo, personal communication.

density that is achieved when scaling up the structure size. The deployable structure demonstrated in this milestone is a modular component of the ~7-m × ~7-m deployable but can also be implemented on its own for missions requiring ~2-m × ~1-m deployables.

3. Functional and environmental qualification of medium-scale (~7-m × ~7-m) Caltech SSPP solar array quadrant. The goal of this milestone is to demonstrate the deployment and thermal performance of a quadrant of the ~7-m × ~7-m Caltech SSPP deployable structure (shown in orange in Figure 4.12a). At the same, this milestone will highlight the modularity of this design, building up a quadrant out of an assembly of previously demonstrated strips and packaging and deploying the quadrant with the same scheme as for the full structure. For this milestone it is sufficient that only a fraction of the quadrant be populated with functional photovoltaic, with the remainder populated with a mass and stiffness surrogate or other functional element such as flexible electronics. The quadrant demonstrated in this milestone is one fourth of the ~7-m × ~7-m deployable but can also be implemented on its own for missions requiring ~12-m^2 deployables.

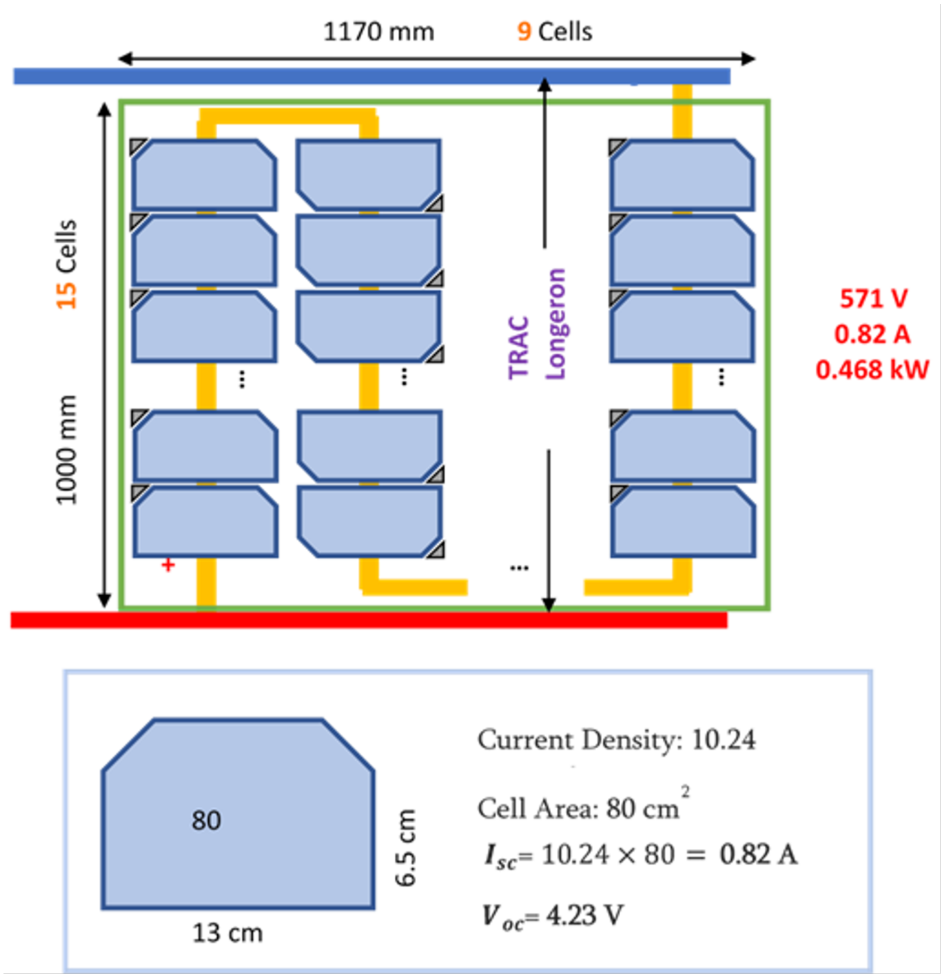

Figure 4.10: Wiring scheme for one block of cells.

4. Medium-scale (~7-m × ~7-m) low-cost (class C/D) mission utilizing the Caltech SSPP solar array. The goal of this milestone is to establish the flight heritage of the Caltech SSPP solar array. With the deployable technology demonstrated on-orbit at small scale (milestone 1) and integration into a solar array and scale-up to ~7-m × ~7-m demonstrated in-lab (milestones 2 and 3) at the quadrant-level, a low-cost/high-risk (class C/D) mission would leverage the ultra-low areal density (<100 g/m^2) of the Caltech SSPP deployable and qualify the architecture for future missions.

5. Functional and environmental qualification of large-scale (~25-m × ~25-m) Caltech SSPP solar array quadrant. The final milestone to mature this deployable technology for candidacy toward a mission to the outer planets builds on the already-demonstrated modularity of the architecture and establishes the manufacturability, assembly, and deployment at larger scales. Demonstrating these parameters for the structure's quadrant (shown in green in Figure 4.12b) is sufficient as the scale-up from quadrant

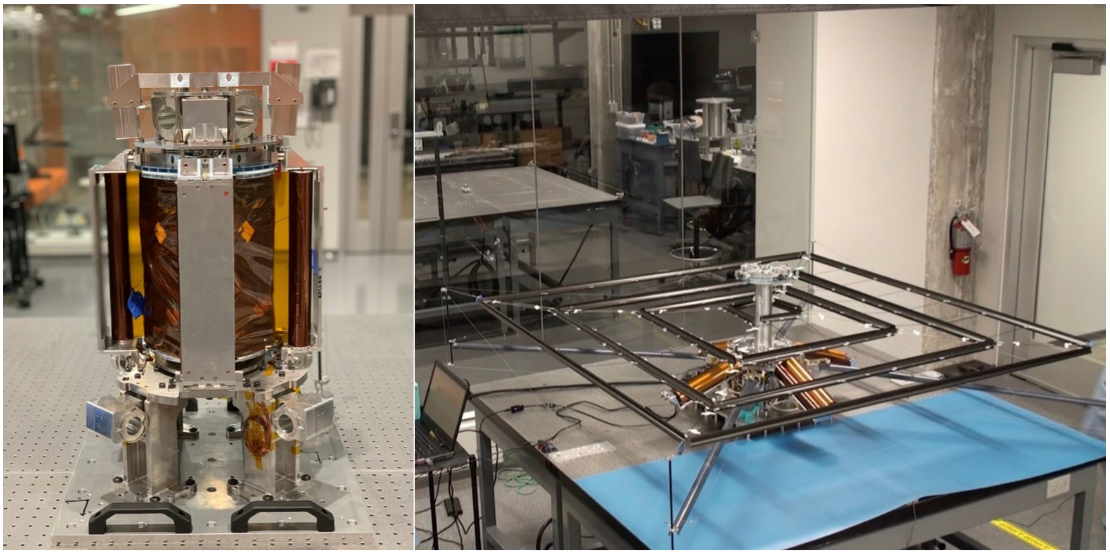

Figure 4.11: Caltech SSPP deployable structure prototype (a) packaged inside deployment mechanism; (b) fully deployed. The fully deployed structure measures 1.7 m × 1.7 m and weighs 100 g/m^2.

to full structure would have been previously demonstrated. It is further sufficient to populate only a fraction of the surface with functional photovoltaic. These simplifications result in significant complexity and cost reduction, in particular with gravity off-loading, manufacturing, and photovoltaic procurement. Achieving this milestone will demonstrate a large (~25-m × ~25 m) ultra-light (<100 g/m^2 structure and PV, <50 g/m^2 structure only) deployable structure with the potential to enable the non-nuclear exploration of the outer planets when used at full scale and a host of other missions requiring a ~150 m^2 deployable.

4.1.2 PV Blanket / Cell technology

High-efficiency thin-film photovoltaic blankets emerged from this study as one of the key technologies required for non-nuclear exploration of the outer planets. In order to provide direction and focus to technology development efforts in this area, it might be worth summarizing what performance requirements are needed/assumed for this concept, and listing some of the key challenges that have to be overcome before the technology can be infused into a flight mission.

The primary performance requirements for the PV-blanket are:

- Areal density: ~50 g/m^2. The mass tally should at a minimum include solar cells, interconnects, wiring harness or traces, any encapsulation or shielding for maintaining

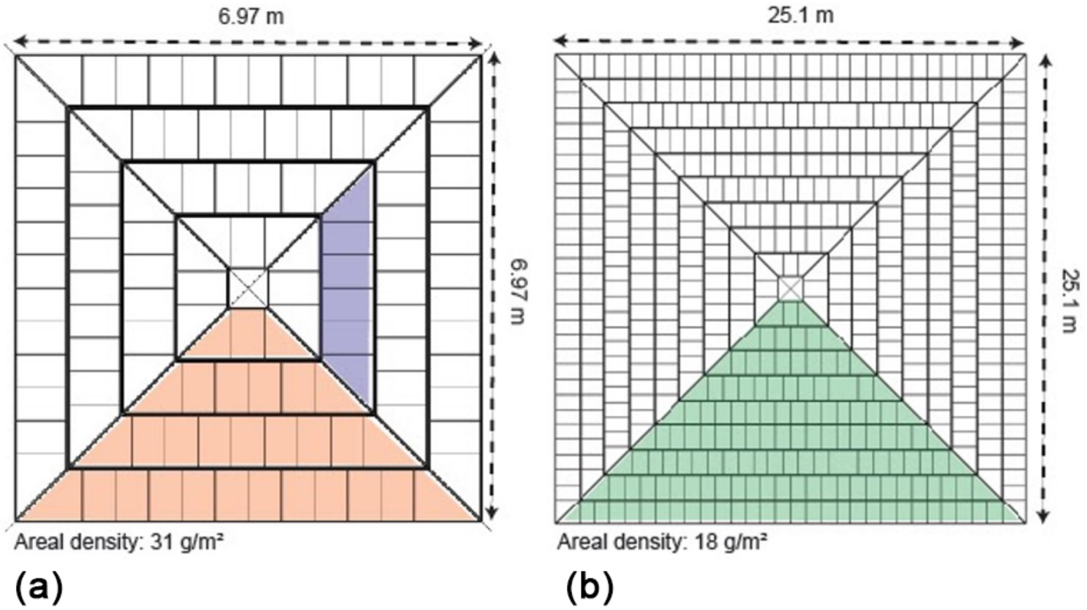

Figure 4.12: Designs for (a) ~7-m × 7-m and (b) ~25-m × ~25-m Caltech SSPP deployable structures. A modular component called "strip" is shown in blue; assemblies of strips into quadrants are shown in orange and green.

solar cell performance stability and/or for preventing destructive electrostatic discharges, provisions for attachment to the structure, etc. The rationale here is that the 100 g/m^2 mass allocation at the array level would be divided evenly between mechanical components such as the structure and deployment mechanisms, and electrical components such as the PV blanket with all of its constituent components;

- Array-level efficiency: ~25% under Neptune operating conditions of 1.5 W/m^2 AM0 irradiance and -220°C temperature (or 3.7 W/m^2 and -200°C for Uranus, the "easy" case, relatively speaking). This array-level efficiency should take into account cell-level efficiency at the operating conditions, together with losses such as packing factor (active area as a fraction of total solar array area), series resistance drops in the wire harness or traces, optical transmission of the encapsulation, any charged-particle or UV radiation losses to the PV device and/or the encapsulation, current or voltage mismatch, bypass diode drops if any, operating-voltage ratio to max-power voltage, etc.

It goes without saying that the above two requirements must be met simultaneously. Another way to state this is that at the PV-blanket level the end-of-life specific power goal is 7.6 W/kg at 30AU and -220°C.

Multiple challenges must be overcome before this technology can be proposed for a flight mission. Solutions need to be found to each of the following problems (not an exhaustive list!), and these solutions must all be combined into a single technology, implemented in scalable prototype hardware, and brought to a TRL-6 level through test and analysis:

- Efficiency at Uranus/Neptune conditions, for statistically significant sample quantities
- Performance stability to pre- and post-launch conditions, i.e., in air, sunlight, vacuum etc.
- Mechanical durability to integration processes as well as to launch and flight conditions
- Lightweight blanket feasibility including harness or printed-trace scalability
- Large-scale, repeatable (quality-controlled) cell and blanket manufacturing capability
- Compatibility of PV blanket with the stowed/deployed mechanical structure
- ESD mitigations as needed, especially for the high voltage (~1kV) applications
- Tolerance to space radiation, primarily full spectrum of solar protons and ultraviolet

4.1.3 Control

Juno, Lucy, and Europa Clipper feature the largest solar arrays of any NASA deep-space spacecraft. Hence, they epitomize the current state-of-practice for attitude dynamics and control of spacecraft with large solar arrays. Juno is a spin-stabilized Jupiter-orbiter with a reaction control system (RCS) for attitude control and three solar array wings, each approximately 9 m long and 2.6 m wide (Bolton et al., 2017). Lucy and Europa Clipper are both three-axis stabilized spacecraft with reaction wheels for fine attitude control and RCSs for reaction wheel desaturation. Lucy launched to the Trojan asteroids in 2021; Europa Clipper is under development for a 2024 launch to Jupiter. Both spacecraft have two solar arrays with total deployed areas of approximately 80 m^2 (Lucy) and 100 m^2 (Europa Clipper). Europa Clipper's solar arrays each include a single-axis gimbal to reorient the arrays independently of the spacecraft bus, e.g., to increase power generation or decrease solar heating (Bayer et al., 2019). Each spacecraft's solar arrays are *dynamically passive*, which means that each spacecraft's attitude control system (ACS) perceives solar array flexibility as a disturbance. Dynamically passive solar arrays are standard on NASA deep-space spacecraft.

Deep-space spacecraft with large solar array wings are traditionally designed and operated to move sufficiently "slowly" to prevent the excitation of flexible modes. For example, the standard practice for ACS design is to set its closed-loop bandwidth an order of magnitude lower or more than the frequency of the dominant flexible mode (Spanos, 1989). This guarantees sufficient gain and phase margins relative to the flexible mode, and by doing so, effectively reduces the ACS design problem to that of a rigid-body spacecraft. The control system bandwidth determines how quickly an ACS is capable of rejecting disturbances. Stiffer solar arrays allow for higher bandwidth, and therefore, more agile and precise pointing. However, stiffness is heavy, so larger solar arrays tend to result in lower bandwidth controllers with slow slew and acquisition times. Slew times are typically an order of magnitude longer than the dominant mode period, again to minimize the excitation of flexible modes. In practice, however, other constraints often result in slower slew times than those due to the structure alone. The ACS design philosophy based on moving "slowly" is referred to herein as the *passive architecture*.

Building solar-powered spacecraft for outer planet exploration requires solar arrays an order of magnitude or more larger and lighter in weight than the current state of the art. Achieving an order of magnitude or more reduction in areal density entails the use of aggressive new structural architectures that are ultralight, packageable, and self-deployable, like the Space Solar Power Project (SSPP) structural architecture (Arya et al., 2016) described previously in Section 4.1, to package the solar arrays into the confines of existing launch vehicles. The strain energy stored in the elastic folds in the packaged structure facilitates self-deployment in space. Generally speaking, increasing packaging efficiency and array size both decrease structural stiffness, whereas increasing array size increases inertia. The combination of very low stiffness and high inertia are the main challenges for ACS design.

The critical question is whether operating a spacecraft with solar arrays at the scale required for a Uranus or Neptune mission is feasible using a passive ACS architecture. To that end, this section aims to demonstrate the feasibility of slewing such a spacecraft using a benchmark numerical model. Altogether, the results highlight how the solar array structure is not likely the limiting factor, at least insofar as slewing is concerned (although it does limit control system bandwidth). Instead, other constraints, like those due to the ACS hardware (torque or momentum limits), are likely to drive slew time requirements.

4.1.3.1 Benchmark Spacecraft Model

The benchmark spacecraft model is adapted from Marshall (2022) and consists of two square solar arrays, each based on a simplified version of the SSPP architecture, attached to a central bus modeled as a spherical point inertia. The solar array model eliminates the diagonal cords that support the strips, instead attaching each strip directly to the corresponding diagonal boom using revolute joints. A solar array then consists of four quadrants tiled with bending-stiff strips. Each strip is assembled out of two TRAC longerons with the nominal material and geometric properties (12.7-mm radius, 8-mm web width, and 90-degree flange opening angle) from Leclerc and Pellegrino (2020) connected by 1 m-long battens. Strips have a uniform areal mass density of 100 g/m^2 to account for both the photovoltaics and the underlying structure. To reduce the size of the numerical model, rectangular strips modeled as elastic beams replace the thin-shell trapezoidal strips described in Section 4.1.

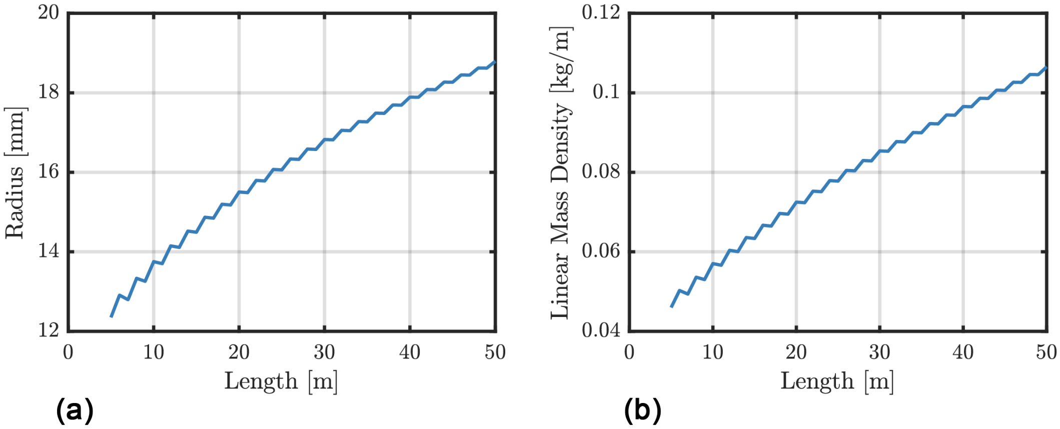

Figure 4.13: (a) Boom radii as a function of solar array dimension. (b) Boom linear mass density as a function of solar array dimension.

Each strip attaches to two diagonal booms. The booms are modeled as isotropic thin-walled cylindrical tubes with the material properties from Lee and Pellegrino (2021) (density 1600 kg/m^3, elastic modulus 70 GPa, and Poisson's ratio 0.3), and a wall thickness-to-radius ratio of 0.03. Figure 4.13a plots the boom radii as a function of the solar array dimension. For each radius, Figure 4.13b then depicts the corresponding boom's linear mass density. The boom radii are from the design study in Marshall (2022) for a spacecraft with a single Caltech SSPP solar array mounted to a central bus. Each quadrant has an innermost strip of length 2 m, an outermost strip of length l attached to the ends of the booms, and uniform spacing between strips. The deployment mechanism at the center of each array is modeled as a 40.4-kg point mass. This estimate is based on scaling the engineering model of the deployment mechanism for the DOLCE technology demonstration mission (Gdoutos et al., 2022) to accommodate 1-m-wide strips. The solar array wings are then cantilevered to the 5000-kg-m^2 spherical point inertia used to model the spacecraft bus (including propellant). This assumes that each solar array is significantly more flexible than the interface attaching it to the bus. 5000 kg-m^2 is an order-of-magnitude estimate based on the inertia properties of the fueled bus for Europa Clipper.

The benchmark spacecraft is modeled as a nonlinear flexible multibody system using geometrically nonlinear Timoshenko beam finite elements to discretize the booms and strips. The specific elements are an updated version of the geometrically exact beam finite elements from Cardona and Geradin (1988). Strips are slender, thin-shell structures. Modeling strips as elastic beams requires evaluating their equivalent beam stiffness properties. This is done using a displacement-based homogenization procedure applied to a high-fidelity strip finite element model sans photovoltaic material implemented in SIMULIA Abaqus 2020. The homogenized stiffness properties extracted from the Abaqus model are inputs to the flexible multibody dynamics model. The flexible multibody dynamics model is then linearized in its undeformed configuration to facilitate a fixed-base modal analysis, i.e., a modal analysis where the spacecraft bus node has its three translational and three rotational degrees of freedom fully restrained. Due to symmetry, the modal analyses for each solar array wing are decoupled. Thus, it is sufficient to only analyze the modes of a single solar array, as is done here.

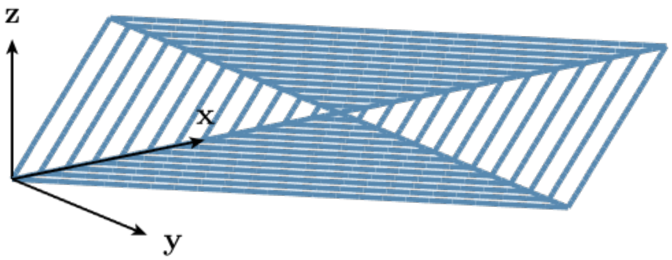

Figure 4.14: Solar array wing reference frame. The spacecraft bus is the origin of the reference frame.

Standard (canonical) methods for flexible spacecraft ACS analysis and design use single-axis modal models (Spanos, 1989; Wie, 2008). Preliminary analysis and design in particular often rely on so-called single-axis, single-mode models, i.e., a single-axis modal model with one rigid body mode and one flexible mode, although retaining additional flexible modes is often required for detailed analysis and design. With this in mind, we use a single-axis, single-mode model for estimating slew times. Such a model requires the spacecraft's rigid body inertia, the natural frequency of the most significant mode, and the corresponding effective modal inertia as inputs, all of which are derivable from the flexible multibody dynamics model. The solar arrays are softest in the out-of-plane direction, meaning a y-axis slew is likely the worst case for exciting structural vibrations. Hence, we exclusively focus on a y-axis slew in what follows.

The moments of inertia of an undeformed solar array wing about the cantilever point (the origin in Figure 4.14) are an output from the flexible multibody dynamics model. Figure 4.15 depicts the principal moments of inertia about the axes from Figure 4.14 as a function of the outer dimension of the solar arrays. With a 5000-kg-m^2 spherical point inertia for the bus and two solar array wings, the solar array wings dominate the rigid body inertia for all but the smallest solar arrays. The total inertia about a principal axis is the inertia of the bus plus twice the inertia from Figure 4.15.

The ratio between the slew time and the spacecraft's dominant natural frequency determines the magnitude of the flexible dynamics. Figure 4.16a compares the first mode and dominant mode natural frequencies as a function of solar array size. Figure 4.16b then shows the

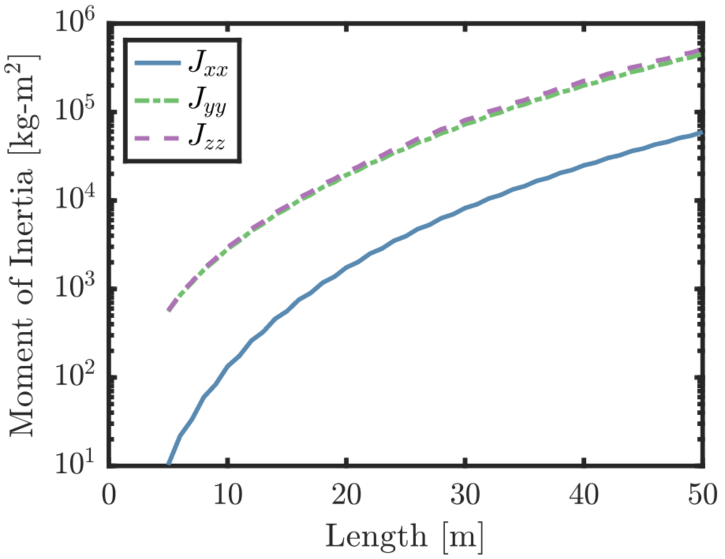

Figure 4.15: Moments of inertia about the origin of the solar array wing reference frame from Figure 4.14 as a function of solar array size for a 100 g/m^2 areal density square solar array.

corresponding natural periods. The dominant mode corresponds to the mode with the highest effective interface mass (Kammer and Triller, 1994), i.e., the mode with the highest average dynamic reaction forces and moments on the spacecraft bus. The dominant mode falls somewhere between modes 2 and 7 and contains between 41% and 48% of the effective interface mass, both depending on the size of the solar array. Likewise, modes between 2

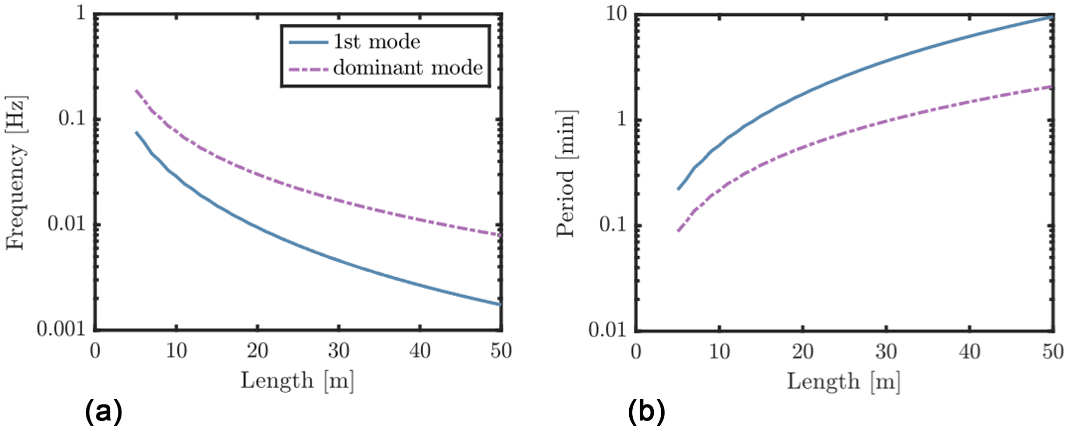

Figure 4.16: (a) Comparison of first mode and dominant mode frequencies as a function of solar array dimension. (b) Comparison of first mode and dominant mode periods as a function of solar array dimension.

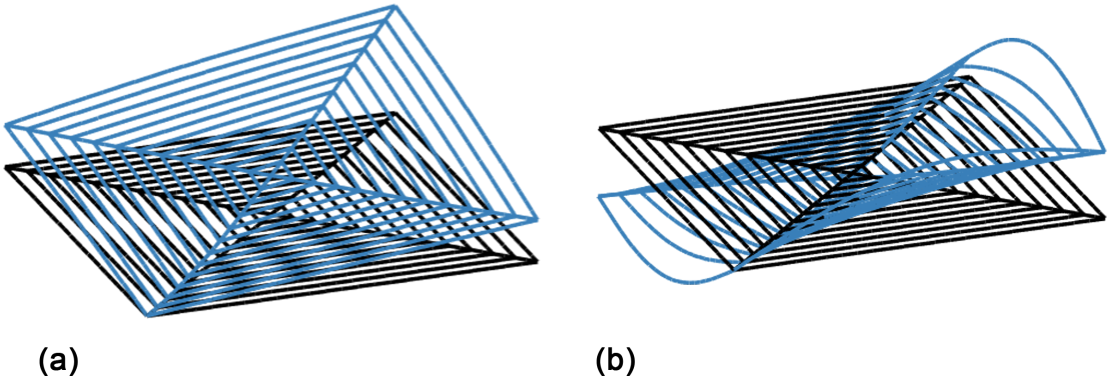

Figure 4.17: (a) First mode for a 24 m × 24 m solar array. (b) Mode with highest effective interface mass for a 24 m × 24 m solar array.

and 7 contain upwards of 95% of the total effective interface mass, again depending on the size of the solar array. This emphasizes that the dominant mode is not necessarily the lowest frequency mode. With periods on the order of 1–10 minutes, we intuitively expect slew times on similar or longer time scales.

Figure 4.17 depicts two representative vibration modes, both from the modal analysis of a 24 × 24 m solar array. The first mode (Figure 4.17a) is a cantilever mode that predominantly consists of boom bending with little to no excitation of the strips. The dominant mode (Figure 4.17b), however, is more complicated; it involves significant interactions between the booms and strips. In both cases, the solar array attachment to the spacecraft bus is located at the tip of the lower-left boom.

For calculating slew times, the correct mode to include in a single-axis, single-mode model is the one with the highest effective modal inertia about the corresponding axis because it leads to the largest disturbance on the spacecraft bus. For a y-axis slew, this is the first mode, independent of the size of the solar array, although this is not necessarily true for other axes. In this case, the effective modal inertia about the solar array is only marginally smaller than its total inertia.

4.1.3.2 Minimum Slew Time Estimates

Space structures are typically very lightly damped (0.5% is typical; Balas, 1982), resulting in extremely long settling times in the absence of additional (either active or passive) dampers (Marshall, 2022). Rather than relying on damping out flexible excitations, it is preferable to simply slew the spacecraft in a way that keeps any flexible excitations to a tolerable level (e.g., Banerjee et al., 2001). Moreover, an ACS can more easily tolerate errors in angular position than angular velocity. This is particularly important for obtaining high-quality scientific measurements where even small angular velocity errors can lead to undesirable effects, e.g., smearing. Hence, our preferred criterion for estimating slew times is based on the amplitude of the residual elastic angular velocity. For a nominally rest-to-rest slew maneuver, this is simply the amplitude of the bus angular velocity after the slew, which in this case is entirely due to flexibility.

We specifically estimate the minimum slew time as the maximum time for which the amplitude of the post-slew residual angular velocity is less than a specified requirement. To better explore the design space, we consider two residual angular velocity requirements: 0.01 deg/s and 0.001 deg/s. Relatively speaking, these correspond to coarse and fine pointing, although additional settling or an independent fine pointing stage may still be required to meet science requirements. We calculate slew times for an undamped system with the expectation that system performance is only going to improve with damping.

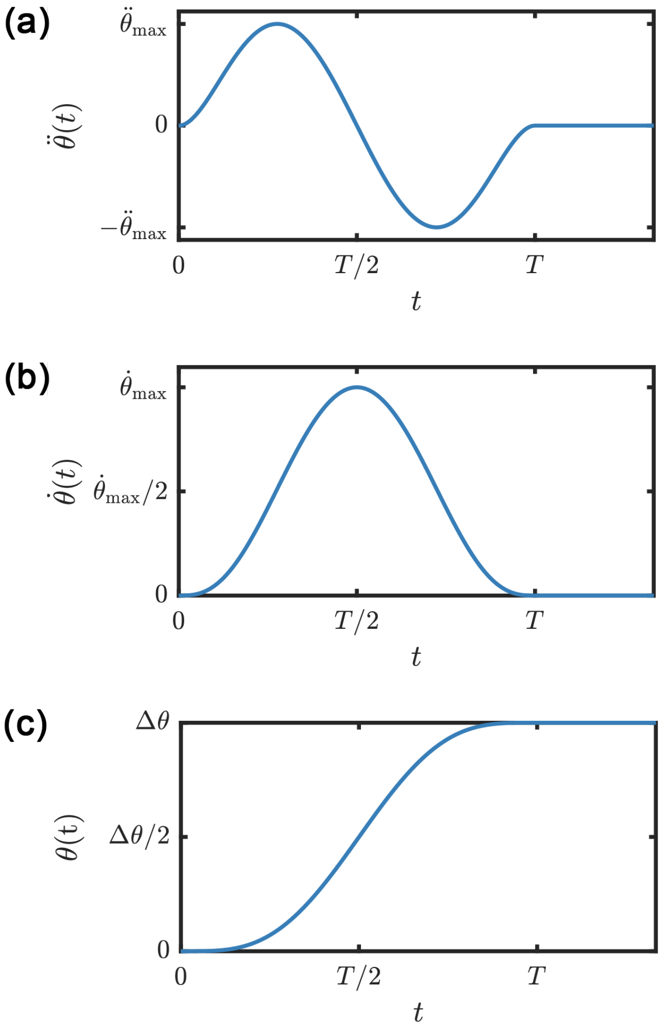

Figure 4.18: Smooth attitude slew maneuver profile for a slew through an angle $\Delta\theta$ in time T. (a) Angular acceleration $\ddot{\theta}(t)$. (b) Angular velocity $\dot{\theta}(t)$. (c) Slew angle $\theta(t)$.

Slew time calculations require a slew maneuver profile, in this case, the 7th-order polynomial depicted in Figure 4.18. The slew maneuver nominally rotates the spacecraft through an angle $\Delta\theta$ in time T. A 7th-order polynomial is chosen because it can simultaneously satisfy zero velocity, zero acceleration, and zero jerk boundary conditions. The polynomial smoothly accelerates and decelerates the spacecraft, resulting in lower excitation of the flexible mode compared to more standard slew profiles, e.g., bang-bang or bang-off-bang.

We consider a reaction-wheel stabilized spacecraft executing a 90-deg y-axis slew maneuver. Two reaction wheels are considered: a baseline wheel with momentum storage and torque representative of a large commercially available wheel, and a wheel with five times more momentum storage and torque; see Table 4.3. Typically, momentum and torque are allocated for different ACS functions. Hence, only a fraction of the total momentum storage and torque are ever available for slewing. We set these thresholds at 60%. Increasing the amount of available momentum storage typically imposes higher propellant requirements to increase the depth of desaturation before a slew. In any case, the available momentum storage and torque impose additional angular velocity and acceleration constraints on slew maneuvers.

	Baseline	**5× Baseline**
Momentum storage [N·m·s]	100	500
Maximum torque [N·m]	0.2	1

Table 4.3: Momentum storage and torque for baseline and 5× baseline reaction wheels.

Figure 4.19 depicts the minimum slew time as a function of the solar array size. For a given reaction wheel and residual angular velocity requirement, the top-most curve dictates the minimum slew time. Depending on the solar array size, the residual angular velocity requirement, the available momentum storage, and the available torque, all impose limits on the minimum slew time. In particular, for the large solar arrays required for Uranus (23 m × 23 m) and Neptune (37 m × 37 m), the reaction wheel capabilities largely drive the minimum slew times, not the structural vibrations. The predicted minimum slew times with the 5× baseline wheel are comparable to other deep-space missions. As a result, provided a sufficiently capable ACS is available, we conclude that it is likely feasible to use the passive architecture for a deep-space spacecraft with very flexible solar arrays at the scales required for outer planet exploration.

The passive architecture, however, often leads to overly conservative ACS designs. Improved performance translates into improved science return and is achievable using modern control design and analysis techniques and/or non-classical ACS architectures. For example, modern optimal control methods can design slew maneuver profiles that simultaneously are robust to any structural uncertainties in the solar arrays, minimize the magnitude of the flexible excitations, and satisfy constraints on the system, e.g., on the available angular momentum

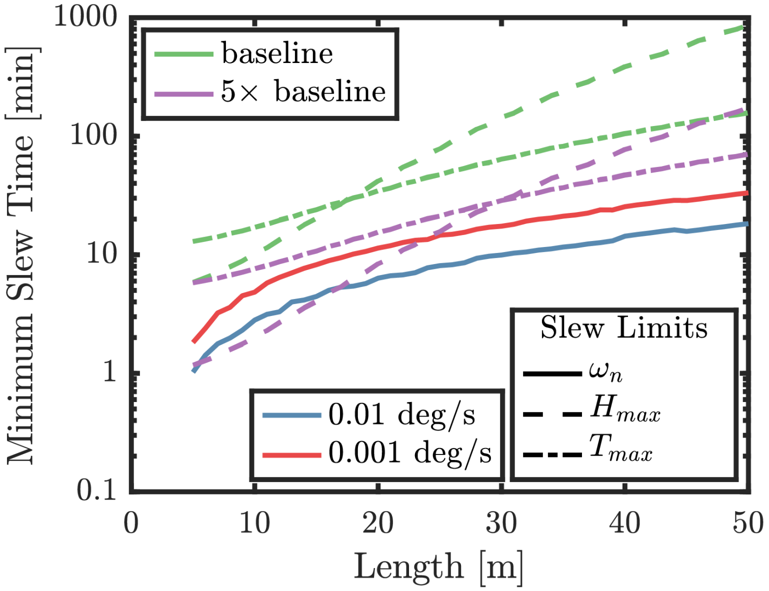

Figure 4.19: Minimum slew times based on (i) natural frequency (ω_n) and a residual angular velocity requirement, (ii) MCS momentum limits ($H_{\max}$), and (iii) MCS torque limits ($T_{\max}$). The minimum slew times based on (i) are calculated without momentum and torque constraints.

or torque. Likewise, modern multivariable control techniques like model predictive control (MPC) can simultaneously control the rigid body motion of the bus and the dominant solar array modes. Further performance improvements are likely derivable from non-classical ACS architectures. Such non-classical architectures can potentially make use of active mass translators (Orphee et al., 2018), embedded sensors and actuators, and/or distributed electric propulsion thrusters or reaction wheels, among others. Active mass translators are propellant-less actuators that use sliding masses to vary the offset between a spacecraft's center of mass and center of (solar) pressure. As a result, they are capable of generating torques about two axes for attitude control and/or momentum control system desaturation. Embedded sensors and actuators can enable dynamic stiffening and active damping. Embedded piezoelectrics can even convert an entire solar array wing into an ACS actuator (Chilan et al., 2017). Alternatively, distributed electric propulsion thrusters or reaction wheels can facilitate simultaneous control of both the spacecraft's rigid body and flexible dynamics. All told, there are multiple possible paths for the development and eventual flight implementation of higher performing ACS technologies for flexible spacecraft.

Lastly, large deployable solar arrays introduce additional risk factors that must be considered during ACS design. An important example is the loss-of-control risk posed by the dynamic deployment of a large solar array. Dynamic deployments are characterized by the conversion of stored strain energy into kinetic energy and large configuration (inertia) changes, which together introduce a potential for spacecraft loss-of-control either during or immediately after deployment. Even if active attitude control is disabled during deployment, uncertainties in a deployment's terminal conditions, e.g., due to a partial deployment, can conceivably introduce an attitude control instability. For these reasons, plus the difficulties associated with testing large solar array structures on Earth, computational tools are likely to play an outsized role in demonstrating that the spacecraft is stable and controllable throughout the expected flight envelope. Hence, the availability of efficient and robust computational tools is imperative for verification and validation of critical ACS mission events. Importantly, many of the requisite computational tools do not currently exist at a sufficient level of maturity for use in the development of a full-scale flight system.

Altogether, there are challenges on the path toward developing and implementing an ACS for a full-scale flight system. However, these are primarily engineering challenges in that the fundamental technologies currently exist, just not at a suitable level of maturity for flight implementation. Thus, the main challenges for the ACS are associated with design maturation and risk reduction.

4.2 Electric Propulsion Technology

Electric propulsion technologies are divided into primary propulsion to provide all the ΔV requirements for solar-powered missions to the ice giants, and secondary propulsion that could potentially be used to provide or enhance attitude control of spacecraft with very large, ultralightweight solar arrays.

4.2.1 Primary Propulsion

With available power for electric propulsion possibly varying by more than a factor of 100 for a mission to the outer planets multiple thruster technologies were considered since no single electric thruster technology has this range capability. The trajectory analyses to date for the Uranus and Neptune missions limited the input power range to the electric propulsion system, but larger throttle ranges may provide increased performance. Figure 4-20 shows the thrust and power range of multiple thruster candidates considered. Hall and ion thruster thrust and power data are presented as continuous curves representing the capability of a single thruster. Multiple thrusters can be flown and operated simultaneously to achieve higher thrust levels and larger dynamic ranges. The electrospray thruster thrust and power data are presented as markers representing a number of integrated propulsion modules from 1 to 100 in a distributed thruster propulsion architecture that could provide both primary and secondary propulsion functions. These systems can be throttled in thrust and power between the markers as will be discussed later.

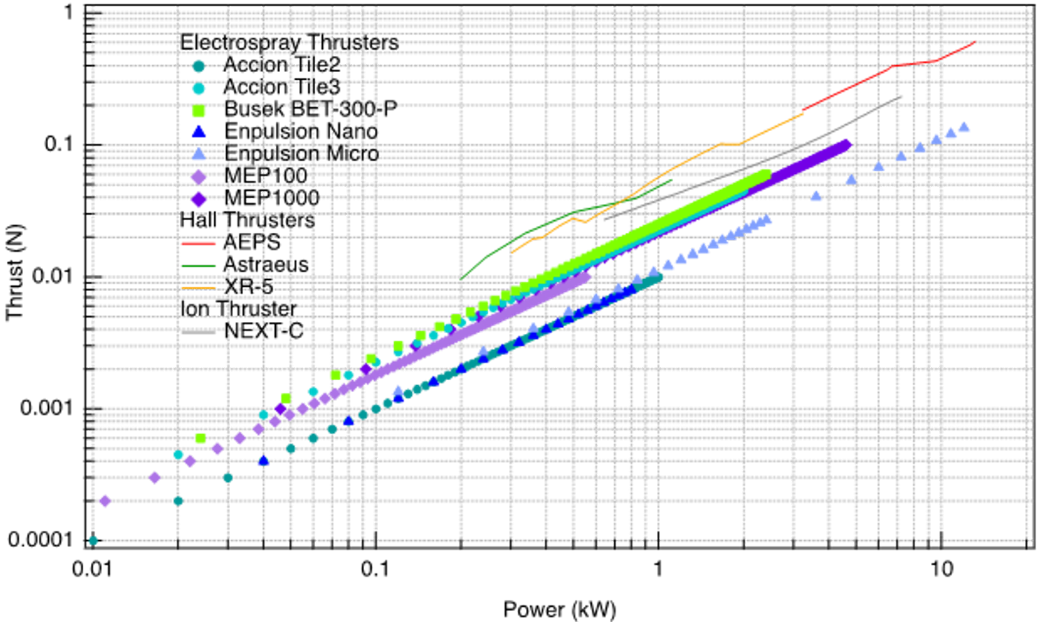

Figure 4.20: Electric propulsion technology candidates considered in this study for primary and secondary propulsion.

Ion thrusters currently have the most flight heritage on interplanetary spacecraft with the NSTAR ion thrusters used on Deep Space 1 and Dawn, the IES/mu thrusters on Hayabusa 1 & 2, the T6 thruster on Bepicolombo, and NEXT-C on DART. Hall thrusters, traditionally not been favored in this context due to their lower Isp (leq ~2000 s), but will soon be demonstrated in deep space on the Psyche mission. Electrospray thrusters have been demonstrated as far out as Sun-Earth L1 for disturbance rejection on the LISA Pathfinder mission. The Isp of electrospray thrusters spans the range of Hall thrusters and ion engines, but the technology development has been driven by potential applications requiring fine control or by spacecraft with very low available power. Consequently, the technology readiness level (TRL) at kilowatt-scale powers is low. Unlike Hall thrusters and ion engines which suffer from efficiency losses at lower powers, electrospray arrays can be throttled via parallel operation with great flexibility and constant performance per unit.

The NASA's Evolutionary Xenon Thruster - Commercial (NEXT-C) ion thruster is the leading candidate for primary propulsion because of the large power range capability and high specific impulse. It operates over a broad power range of 0.64–7.4 kW at 25–235 mN and high specific impulse range at 1400–4200 s. A picture of the thruster and an electrical block diagram showing the elements of the propulsion system are shown in Figure 4.21 (Shastry et al., 2013). This thruster has a reported xenon propellant throughput capability of >900 kg (Shastry et al., 2014), but was derated to 700 kg for this study due to uncertainty regarding potential facility effects on the results of the NEXT life test. The xenon propellant mass requirement ranged from 515–4400 kg for the Uranus and Neptune trajectory analyses assuming an ion thruster with a specific impulse of 4000 s. Processing 40 kW of power and 4400 kg of xenon propellant for the mission would require up to 6 NEXT ion thrusters and PPUs. A seventh thruster and PPU would be added for redundancy to meet a single fault tolerant requirement. The NEXT propulsion system includes thrusters, PPUs, a high-pressure feed system, a xenon flow control assembly and xenon propellant tank. The NEXT thruster mass is 13.3 kg. The single high-pressure feed system for multiple thrusters is 5 kg. The xenon control assembly for each thruster has a mass of 2.5 kg. The standard PPU mass is 34 kg.

Having solar arrays that could operate at high output voltages in the range 1000–2000 V would enable direct drive power systems with significantly lower masses than traditional PPUs. A direct drive PPU is simplified greatly by replacing the beam power supply in a standard PPU with a switch and a capacitor. Direct drive has been successfully demonstrated with multiple Hall thrusters (Snyder et al., 2014). While it is expected that the NEXT-C PPU mass can be reduced from 30 kg to 10 kg with the direct drive, it must be developed and demonstrated. The mission analyses performed in this study assumed a conventional PPU architecture.

The thruster technology baseline for primary propulsion is the NEXT-C ion engine. NASA's Evolutionary Xenon Thruster–Commercial (NEXT-C) was developed at NASA GRC and Aerojet Rocketdyne (AR) for deep space robotic missions and high total impulse defense and commercial missions and is now built by AR.

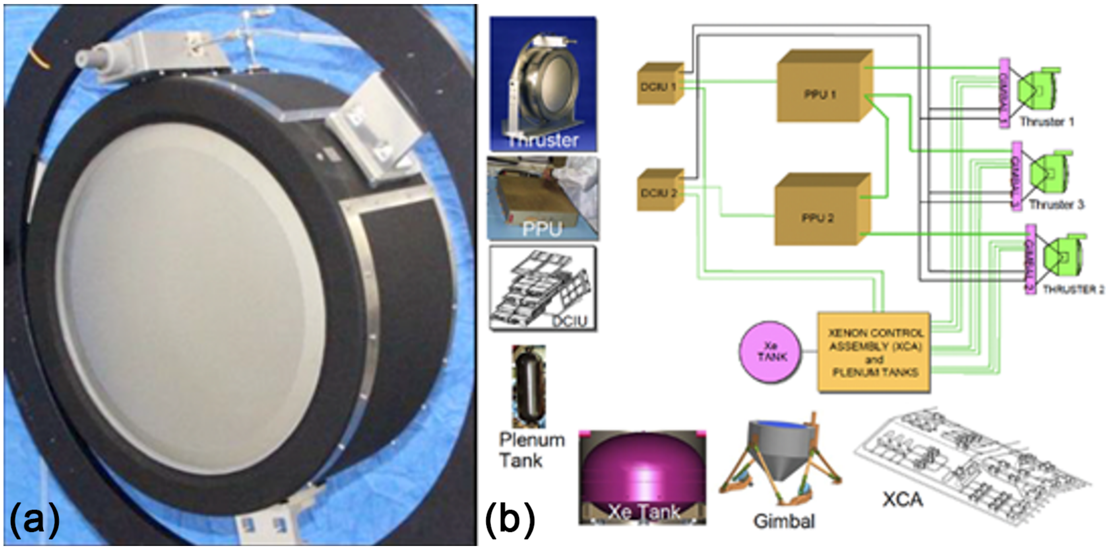

Figure 4.21: (a)The NEXT-C Ion thruster, and (b) ion propulsion system elements (Thomas et al., 2019).

A technology roadmap for the NEXT-C for possible application to solar-powered missions to the ice giants is shown in Figure 4.22, starting with the SOA system that is currently flying on the DART mission. The next step is flight qualification for the full thruster throttle range from 0.6 to 7.8 kW. Then a direct-drive PPU could be developed as a mission performance enhancement. A small-scale mission technology demonstration of a direct-drive NEXT-C system could be done with all of the other required technologies before the much larger Neptune/Uranus mission to reduce risk.

4.2.2 Reaction Control

Electrospray thrusters are considered to support spacecraft attitude control and/or momentum management because they are small, highly integrated and compact. This combination of characteristics provides the possibility to design and integrate with the solar arrays a distributed propulsion system. With the very large solar arrays required for solar-powered missions to the ice giants, electrospray propulsion may offer a lower mass and quieter approach to attitude control to supplement or potentially replace than reaction wheels in the spacecraft body (Sec 4.1.3).

Electrospray thrusters have already flight demonstrated low-noise spacecraft control on the LISA Pathfinder mission (*LISA Pathfinder* n.d.). Electrospray thrusters have been developed for cubesats as highly integrated system modules that include the thrusters, propellant and PPUs operating at tens to hundreds of micronewtons of thrust. Integrating them into the solar array panels could provide adequate slewing and pointing with rotational rates of several degrees/min without introducing structural jitter and vibrations. The system could be designed to enable each thruster assemble to draw power locally from a solar array panel and be commanded wirelessly from the spacecraft bus. For example, sixty 100-μN thrusters located up to 60 m from the spacecraft bus on the solar arrays would provide slew rates greater than 0.08 deg/s—comparable to typical spacecraft slew rates with reaction wheels or chemical thrusters.

A conceptual illustration is provided in Figure 4.23 with thruster modules integrated into the solar array panels. The panels are sized to provide the required thruster power at the destination with margin. Each panel would have opposing thrusters pointing 180° from each other, with one operating at a time. A mission would require 4-m × 4-m panels for 14.8 W/panel at Uranus to power a single electrospray thruster for about 100–200 μN of

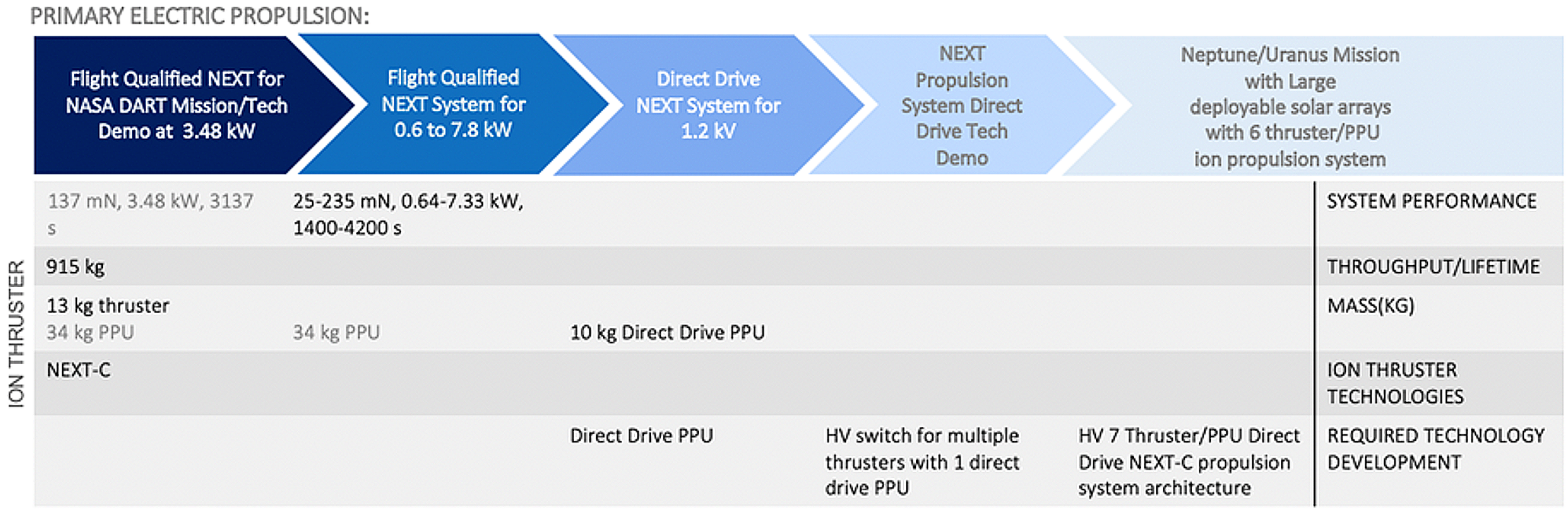

PRIMARY ELECTRIC PROPULSION:

ION THRUSTER

Flight Qualified NEXT for NASA DART Mission/Tech Demo at 3.48 kW	Flight Qualified NEXT System for 0.6 to 7.8 kW	Direct Drive NEXT System for 1.2 kV	NEXT Propulsion System Direct Drive Tech Demo	Neptune/Uranus Mission with Large deployable solar arrays with 6 thruster/PPU ion propulsion system	
137 mN, 3.48 kW, 3137 s	25-235 mN, 0.64-7.33 kW, 1400-4200 s				SYSTEM PERFORMANCE
915 kg					THROUGHPUT/LIFETIME
13 kg thruster 34 kg PPU	34 kg PPU	10 kg Direct Drive PPU			MASS(KG)
NEXT-C					ION THRUSTER TECHNOLOGIES
		Direct Drive PPU	HV switch for multiple thrusters with 1 direct drive PPU	HV 7 Thruster/PPU Direct Drive NEXT-C propulsion system architecture	REQUIRED TECHNOLOGY DEVELOPMENT

Figure 4.22: NEXT-C technology roadmap for SEP missions to Uranus and Neptune.

thrust. If this thruster is operated at Uranus at the low end of its power and thrust range capability, then it could operate at much higher power and thrust on the way to Uranus. A thruster that could operate at 0.1 mN at less than 14.8 W at Uranus and up to 1.0 mN at higher power along the way, could be used for both primary and secondary propulsion if there are a few hundred of them, providing the same thrust as 1 or 2 NEXT-C thrusters at 235–470 mN.

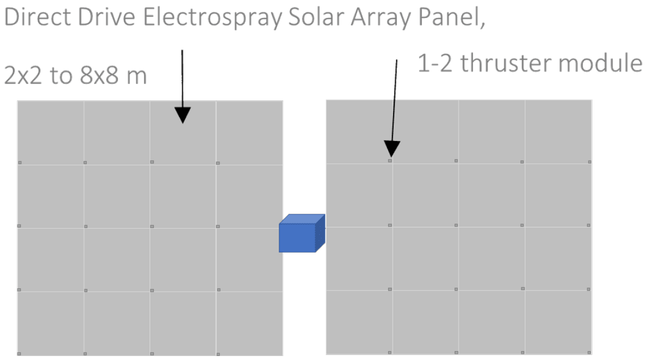

Figure 4.23: An illustration showing how electrospray modules could be integrated into large HV PV arrays of a spacecraft. It shows each wing with an 4 × 4 configuration of solar array panels, where each panel is 4 m × 4 m in order to provide enough power at Uranus for an electrospray thruster. At Neptune, the panels would need to be 5 m × 5 m. These could be used to control the central rigid body indirectly, or it could be controlled separately using small reaction wheels.

Advanced microfabricated or highly integrated, compact electrospray thrusters are considered for this mission application because their lightweight and small size enable highly scalable configurations. Existing electrospray thrusters are shown in Fig 4-24 including the Busek BET-300P, the ACCION TILE2 and 3, Enpulsion Nano R3, the MEP100 and the JPL MEP100. These systems are highly modular with the propellant and feed systems integrated with the thruster head and 10 cm × 10 cm cubesat-sized PPUs. The BET-300-P thruster operates in two configurations as indicated in Table 4-4. In configuration B, it has a nominal thrust level of 55 μN and operates up to 100 μN at 2300 s with a total impulse of 250 Ns. The BET-Max-300-P is a 4-thruster system with a single PPU that can operate 4 thrusters simultaneously at a nominal power of 14 W and max power of 24 W with a wet mass of 0.8 kg and volume of 1250 cm^3 (*BET-MAX: Multi-axis precision electrospray thruster system* n.d.). The ACCION TILE2 thrusters operate at 40–100 μN of thrust and 4–10 W of power with a system wet mass of 0.48 kg (*Tile Propulsion: Propulsion, Reinvented for New Space* n.d.). The ACCION TILE3 operates at 100–225 μN of thrust with a system wet mass of 1.25 kg and power of 10–20 W (*Tile Propulsion: Propulsion, Reinvented for New Space* n.d.). The Enpulsion Nano R3 operates at 10 400 μN of thrust with a system wet mass of 1.4 kg and power of 10–45 W. The MEP100 thruster operates at an estimated 10–100 μN of thrust, system mass of 0.314 kg and power of 2–5.5 W (Marrese-Reading, 2016; Marrese-Reading and Anderson, 2016).

While it is still under development, the MEP has the potential to be the lowest wet mass option because it is microfabricated with a highly integrated capillary force driven feed system, has the highest specific impulse capability to minimize propellant mass for the mission and operates on a very high-density indium metal propellant to minimize the tank volume and mass. The disadvantage over some of the other electrospray technologies is higher power because the thruster has to be heated to melt the indium and it runs at higher current levels than the thrusters using ionic liquids like EMI Im and EMI BF4. The mass of all of these systems could be significantly reduced for this type of application. Also, much higher total impulses may be possible from some of the technologies with additional propellant loading. The MEP100 was loaded with only 2.8 grams of propellant for the first demonstration of the technology with an integrated thruster, capillary force driven feed system and a small propellant reservoir after a feed system demonstration in a test fixture (Marrese-Reading, 2021). The lifetime and propellant throughput of this thruster has not yet been characterized.

All of the electrospray thrusters in Table 4.4 require additional development including flight qualification. The flight qualification of the BET-300-P and Enpulsion Nano R3 thrusters is currently underway. Both the ACCION TILE2 and Enpulsion Nano R3 have been flight demonstrated on cubesats. However, significant investment is still required to develop performance and lifetime models and conduct long duration testing to characterize their lifetime and propellant throughput capability.

Most of these electrospray thrusters operate at 1000-2000 V also, which would enable significant PPU simplification and mass savings with high voltage PV arrays (1000–2000 V) powering direct drive PPUs. The direct drive PPU is expected to reduce the mass of the PPU by more than 50%. This technology has extraordinary potential for a broad range of spacecraft propulsion and control applications for small and large spacecraft.

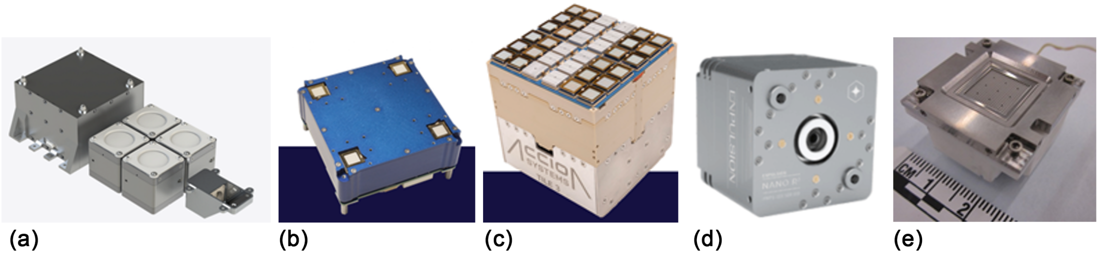

Figure 4.24: Electrospray thrusters, including (from left to right) the Busek BET-MAX-300P, ACCION TILE2 and TILE3, Enpulsion Nano R3, JPL MEP100.

	Busek BET-300-P		**ACCION TILE2**	**ACCION TILE3**	**Enpulsion Nano R3**	**JPL MEP100**	**JPL MEP1000**
	Config A	**Config B**					
Propellant	EMI IM		EMI-BF4	EMI-BF4	Indium	Indium	Indium
Thrust (μN)	55–150	55–100	40–100	225–450	10–350	10–100	100–1000
	55–600 (4 thrusters)						
Isp (s)	850	2300	1650	1650	2000–6000	3100	5724
Power (W)	0.85–2.25	1.38–2.5	4–10	10–20	10–45	5.5	8.4–46
	12–24 (4 thrusters)						
Wet Mass (g)	166 (1 thruster)		480	1250	1400	314	1135
	800 (4 thrusters)						
Propellant Mass (g)	230	230	1.3	46.7	230	3	550
Total Impulse (N · s)	92	250	21	755	5000	94	30852
Specific Mass (kg/kW)	195–74	120–66.4	120–48	120–60	117–26	57	70–13

Table 4.4: Electrospray thruster technologies currently under development that were evaluated as candidates for application to solar-powered missions to the ice giants.

The last row of Table 4.4 gives the specific mass (kg/kW) of various state-of-the-art electrospray systems which can be used for mass scaling estimations. The specific mass of the propulsion system does not need to be driven as low as the solar array because it will not be the leading contributor to the mass of the overall vehicle. The specific mass of electrospray systems is useful for evaluating the configuration of thrusters for attitude control purposes. The state-of-the-art electrospray systems weigh anywhere from 10^1 to 10^2 kg/kW (note that state-of-the-art systems process only tens of watts of power and weigh hundreds of grams). Lighter electrospray systems may be more easily integrated and deployed on a large flexible array structure. The specific mass of the electrospray thruster can be decreased by:

- Increasing the emitter density (more power per unit area with minimal mass penalty)
- Through development of direct-drive PPUs which will eliminate the need for HV transformer electric hardware.

Table 4.5 below shows projected specific mass values for each component of an electrospray thruster system with further technology development in each of these areas. The driving component of the specific mass value (both current and future) is the PPU. All current electrospray PPUs are required to transform a low voltage spacecraft bus to the 1+ kV required to generate the ion plume. Projected improvements in specific mass scale with the operating power of the PPU. The green curve in Figure 4.25 shows the projected electrospray system specific mass, α, as a function of operating mass. It is projected that electrospray systems and their PPUs can achieve an overall lower specific power than Hall thrusters or ion engines due to the compact propellant storage and relatively simple power electronics requirements.

Component	**Specific Mass (kg/kW)**	
	SOA (10 W)	**Future**
Thruster	1	0.05 (high thrust density, all powers)
PPU	18	0.5 (high power)
Propellant Tank	2	«1
Flow System	(embedded in thruster and tank mass)	(will decrease with shared tankage)

Table 4.5: Specific mass for state-of-the-art and future electrospray systems.

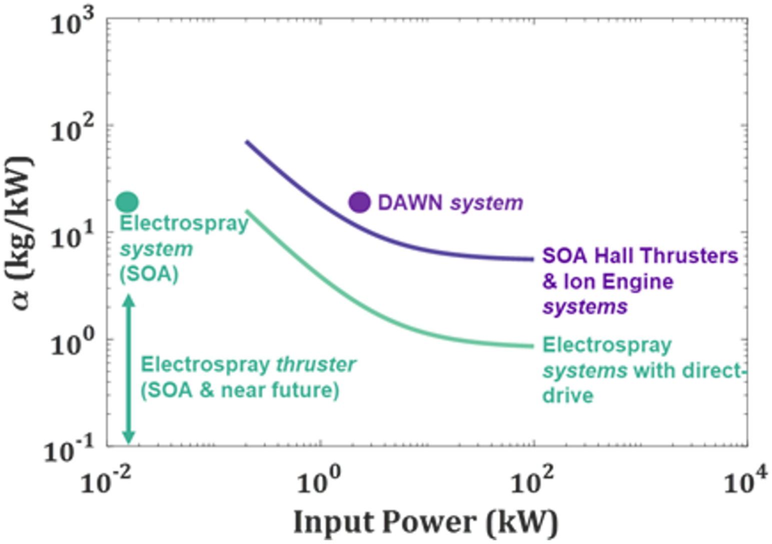

Figure 4.25: Projected electrospray system specific mass, α, as a function of operating mass.

A road map for electrospray propulsion for ACS for this mission concept is included in Figure 4.26. Significant electrospray thruster development is required for this mission concept application beyond the current SOA. The systems need to be very low mass to be deployable with the PV arrays, therefore, only the microfabricated thruster approach may be feasible. Such systems are under development and some have been flight demonstrated.

A lab-scale demonstration of direct drive control of electrospray thrusters via high-voltage photovoltaic wiring would be readily achievable and would pave the way to flight demonstrations. Such a demonstration would require modification of the electrospray PPU to remove the high voltage transformer board and replace bus power conditioning with conditioning from array power.

A pathfinder mission for risk reduction could include two twin SimpleX class ~50 kg spacecraft versions of the much larger spacecraft to Uranus and Neptune. This mission concept could demonstrate the following key elements:

1. Direct-drive high-voltage (HV) electrospray thruster propulsion systems.
2. High-voltage PV array panels.
3. Packaging and deployment of the high-voltage PV arrays with integrated electrospray propulsion systems.
4. Spacecraft attitude control with electrospray propulsion systems on large deployable high-voltage PV array structures.

This demonstration would only require 1 m^2 high-voltage PV panels to power a single 1 mN electrospray thruster propulsion system with significant margin.

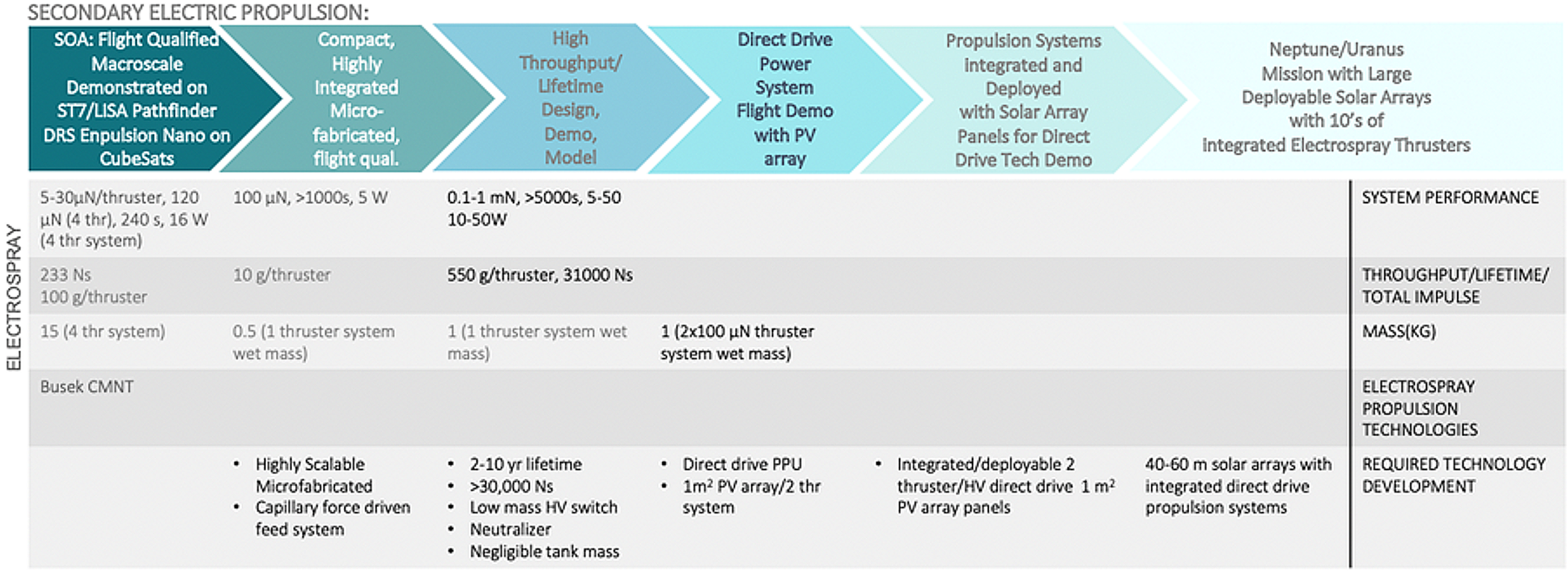

SECONDARY ELECTRIC PROPULSION:

ELECTROSPRAY

SOA: Flight Qualified Macroscale Demonstrated on ST7/LISA Pathfinder DRS Enpulsion Nano on CubeSats	Compact, Highly Integrated Micro-fabricated, flight qual.	High Throughput/ Lifetime Design, Demo, Model	Direct Drive Power System Flight Demo with PV array	Propulsion Systems Integrated and Deployed with Solar Array Panels for Direct Drive Tech Demo	Neptune/Uranus Mission with Large Deployable Solar Arrays with 10's of Integrated Electrospray Thrusters	
5-30µN/thruster, 120 µN (4 thr), 240 s, 16 W (4 thr system)	100 µN, >1000s, 5 W	0.1-1 mN, >5000s, 5-50 10-50W				SYSTEM PERFORMANCE
233 Ns 100 g/thruster	10 g/thruster	550 g/thruster, 31000 Ns				THROUGHPUT/LIFETIME/ TOTAL IMPULSE
15 (4 thr system)	0.5 (1 thruster system wet mass)	1 (1 thruster system wet mass)	1 (2x100 µN thruster system wet mass)			MASS(KG)
Busek CMNT						ELECTROSPRAY PROPULSION TECHNOLOGIES
	• Highly Scalable Microfabricated • Capillary force driven feed system	• 2-10 yr lifetime • >30,000 Ns • Low mass HV switch • Neutralizer • Negligible tank mass	• Direct drive PPU • 1m² PV array/2 thr system	• Integrated/deployable 2 thruster/HV direct drive 1 m² PV array panels	40-60 m solar arrays with integrated direct drive propulsion systems	REQUIRED TECHNOLOGY DEVELOPMENT

Figure 4.26: Electrospray technology roadmap for SEP missions to Uranus and Neptune.

4.3 Modular Architectures

A flight system consisting of a large deployable structure can be seen as a single monolithic structure or as an assembly of smaller, modular structures. If all the modular structures are assembled together on ground prior to launch, then such a structure is limited by the mass and volume of the launch vehicle lift capacity and most likely by the volume and diameter of the launch vehicle shroud. An alternative which allows for higher system scalability beyond the capacity of the launch vehicle, is to launch multiple (N) modular structures into orbit, for example to LEO, and using multiple launch vehicles, and then these modules either self-assemble in space or get assembled using specific robotic manipulators, into the final flight assembly. In the latter case, the flight system is potentially unbounded other than constraints driven by system complexity and flight system control complexity. However, modular structures also have the potential advantage of being able to possibly self-assemble, reassemble due to failures in flight, and provide for long-term survivability in space.

A modular architecture flight system that is to self-assemble in space to form a large, modular, flight system, needs to be specifically designed for such a purpose from the onset. Each module would likely be identical and there would have to be a way for each module to communicate with other modules either neighbor-to-neighbor or using omnidirectional antennas to broadcast to other modules its existence and position in the overall structure. Each module would need to store information about itself and also keep information about the system as a whole. Consider a large system of N modules where each module is composed of a 60 m × 60 m deployable structure launched separately into LEO. Each module first deploys in space and then these modules self assemble into a very large (uber) structure. The central portion of each module consists of an identical spacecraft module that has electric propulsion, communication, navigation, computing, data storage, and science sensing capabilities and power from the deployable solar array structure. Each module has attach and detach capabilities and the system is reconfigurable in the presence of permanent failures. Furthermore, each module in the N-module system can also carry a small payload (modular lander) module for the target destination, which can also self-assemble prior to encountering the target destination.

From an architectural and technological point of view, it is worth mentioning that the above described scenario is in-line with where the space technological roadmap is advancing in the future. That is, there is already a national initiative in the area of (In) Orbit Servicing Assembly and Manufacturing (OSAM). This consortium of national agencies, national laboratories and industry is coordinating the national efforts in this field of development as it is seen as a strategic area for the USA to have a leadership role. That is, this field is critical for both civil and defense applications in the future. For civil purposes, there is a need for large deployable structures such as telescopes, servicing platforms, refueling stations and more. For strategic purposes there is a need for situational awareness, space asset protection and much more.

4.4 Power Beaming Technology

The transmit side of state-of-the-art directed-energy (DE) systems are solid state, efficient (~50%), low mass (~1 kg/kW$_{\text{opt}}$), long lifetime (~10^5 hrs), and improving rapidly driven by the photonic revolution along with consumer and industrial demand. Much like Moore's Law for electronics, there is exponential growth in photonics with a doubling time of about 20 months (Lubin, 2016). There are many possible system designs depending on the requirements in terms of delivered power and distance from the "server" or DE system and the "client" or laser power converter (LPC) as indicated in Table 4.6. The general term of beamed power refers to the entire system. The LPC can be very efficient (with conversion efficiencies of ~50%) due to the nearly monochromatic nature of the laser light. Laser tuned LPCs can also be relatively low mass (< 1kg/kW$_{\text{e}}$) with new thin film PV promising to be >10× lower mass still (<0.1 kg/kW$_{\text{e}}$). LPCs are similar in many ways to solar PV, but LPCs typically only use a single junction for efficient conversion due to the narrow wavelength of the incoming laser light.

Technique	Pro	Con	Extensibility
Beamed Power: Laser (Infrared or visible)	Scalable/multiple client capability	Modest end-to-end efficiency (~20% currently—goal 30% in future—largely independent of client distance)	Long range capability with little efficiency an mass change
Beamed Power: Radio Frequency (RF)	Scalable/multiple client capability	Similar eff to IR. Much larger optics needed Ex: 10,000× optics size for 30 GHz	Not easily extended to long range due to extremely large optics
Wires—direct to asset and possible charging stations/battery swapping	Simple and high eff for short ranges. Possible high temp superconductor option for PSR/lunar night	Not easily extended to longer ranges and mobile clients. For central charging stations rovers have to return each time.	Difficult to extend. High wire and tower masses needed for long range

Table 4.6: Pros and cons of power transfer technologies.

DE Power Levels. Current SOA for CW DE power is close to 1 kg/kW$_{\text{opt}}$ (Figure 4.27) with a volumetric power density that is generally limited by the thermal management and not the semiconductor volume. Packaged devices can easily exceed 1 W$_{\text{opt}}$/cm^3. DE devices can be either free space or fiber coupled and the thermal management can be accomplished with either direct thermal conduction or liquid /gas cooling. For space applications the direct thermal conduction is

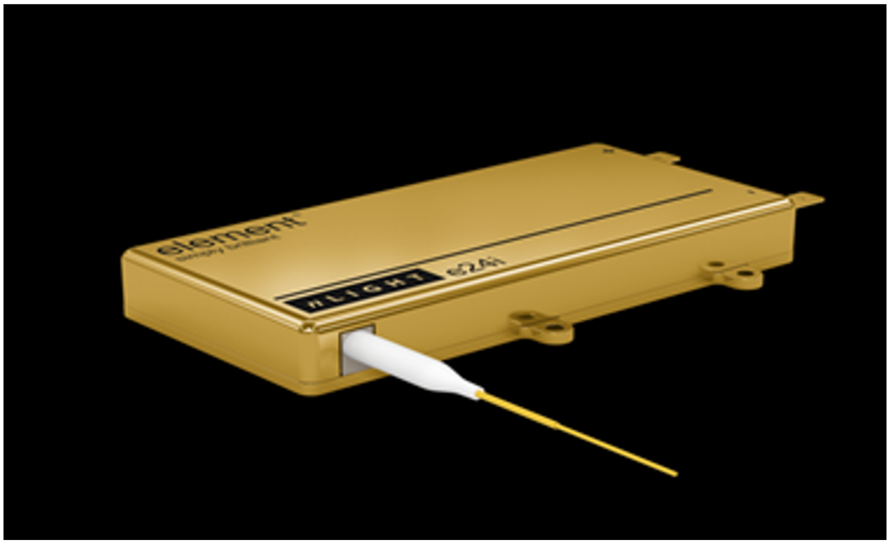

Figure 4.27: Example of a fiber coupled semiconductor laser diode: 400 W_{opt} 976-nm device (~10 × 10 × 1cm) has a mass of 500 g, efficiency of 50% and conductively cooled. These units can be space qualified.

generally simplest and most reliable. Hand held DE to approximately 1 kW_{opt} is feasible currently.

DE Optics. For long range operation (>1 km) the DE system will normally be operated in a single spatial mode simply known as "single mode" (Figure 4.28) while for shorter range operation "multi-mode" (Figure 4.29) is often preferred as multi-mode is generally more efficient and lower mass as well as being "more forgiving" in system design and optics. For a single mode system, the optics should operate in a diffraction limited configuration with wavefront errors of better than 1/10 wave to yield high Strehl or optical efficiency. Optics can be reflective, refractive or diffractive. Given the narrow laser bandwidth extremely lower areal mass diffractive optics (<1 kg/m^2) is viable. The low mass optics allow a large range of mission options.

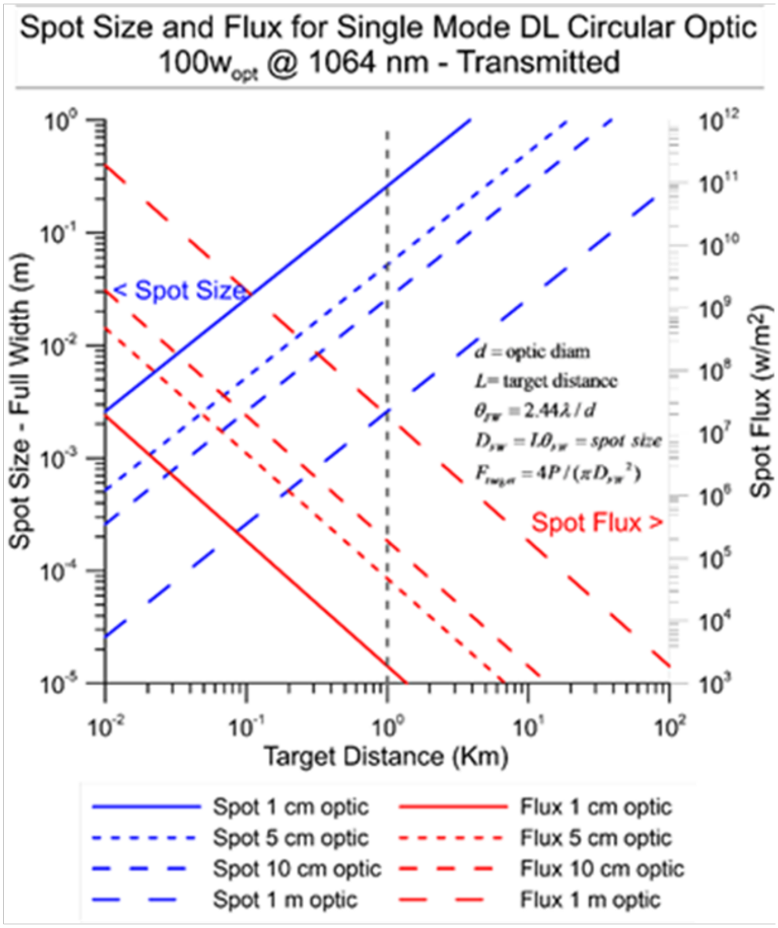

Figure 4.28: Single mode diffraction limited beam diameter (Airy disk) and target flux for circular aperture vs. distance to target from 10-m to 100-km distance with optical diameters of 1, 5 ,10, 100 cm at a wavelength of 1.06 microns with 100 watts.

LPC. Laser power converters can be operated in either an unconcentrated (no optics) or concentrated (with optics) mode (Figure 4.30). For the case of concentrated optics, the LPC is almost always run in a multiple mode free space coupled configuration. The trade space between using optics (concentrated LPC) or not with depends on several issues including:

- If high quality thermal power is needed then concentrated LPCs are generally desired.
- If the radiation environment is high then concentrated LPCs facilitates shielding.

- If the flux is very low then concentrated LPV may be desired.

Concentrated LPCs required a pointing system on the LPC optics which adds complexity, mass, and is less reliable. In most applications, including in this study, we assume no concentration.

Combined Power and Data—Beamed power allows a natural combined data and power link which can be bi-directional if there is a laser or modulatable retro-reflector on the client side.

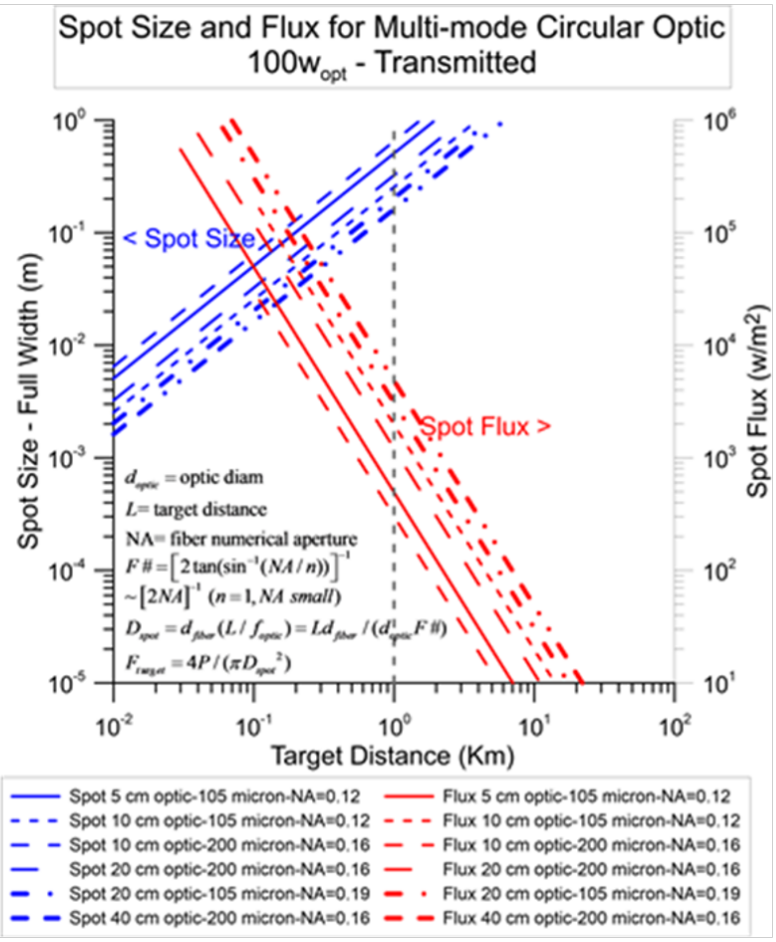

Figure 4.29: Multi-mode beam diameter and target flux for circular aperture with various fiber geometries vs distance to target from 10-m to 100-km distance with optical diameters of 5,10, 20, 40 cm with 100 W$_{opt}$ transmitted. The flux scales as the power transmitted.

4.4.0.1 Radiation Effects

1. The typical way to achieve single mode operation is to multi-mode optically pump a single mode doped fiber which then yields a single mode. The multi-mode optical

pump is generally a laser diode that is often multi-mode fiber coupled to the doped single mode fiber. The fiber that couples the multi-mode pump fiber is not doped and is simply high-quality glass that is generally very radiation resistant though it can also be shielded if necessary.

2. SOA DE devices are semiconductor InGaAs/AlGaAs/GaAs which are generally inside of a metal body for thermal and alignment reasons and hence can be very well shielded against moderate energy radiation. If the DE is fiber coupled then we have to be concerned with radiation effects on the fibers, and shielding may be required.
3. The LPC is similar to solar PV and the radiation effects have similar effect on both. Solar PV radiation effects have been extensively studied on a wide variety of materials. Cover glass is often used for low energy radiation protection.

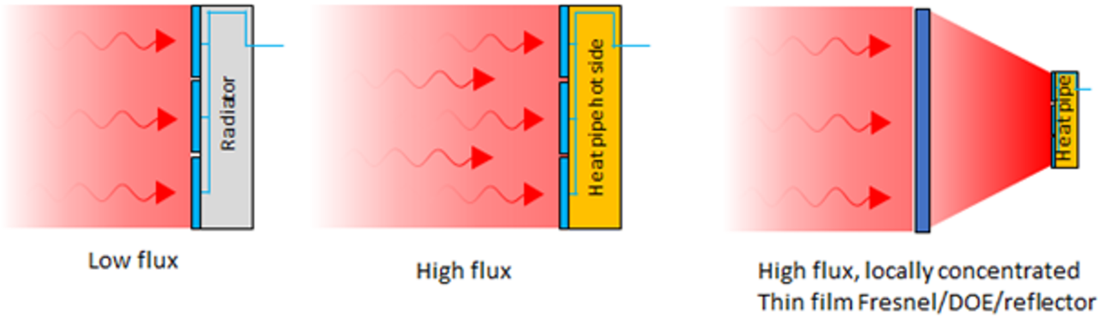

Figure 4.30: PV and heat sink for low flux (~1 kW/m^2) or high flux or locally concentrated PV with heat pipe for thermal control and thermal storage battery charging.

Photovoltaic conversion. Currently the highest efficiency PV cell at near IR wavelengths are made from GaAs or InGaAs or variants of III-V compounds. This is an area of significant research and improvements in efficiency and mass reduction and radiation hardening are expected. As the laser wavelength is narrow the junctions used are single- vs. multi-junction for solar PV, which is broad spectral bandwidth. Currently, InGaAs has achieved in excess of 50% efficiency at about 900 nm and slightly below that at 1064 nm (Figure 4.32). Solar PV of similar construction has flight heritage. In tests of sample (not optimized) InGaAs LPV (Laser tuned PhotoVoltaics) from Spectrolab we measured relative efficiency at various relevant wavelengths from low to high flux (>20 kW$_{opt}$/m^2).

Optimization of PV cell layout is important for power beaming systems. Unlit cells in series with lighted ones reduce the conversion efficiency, while transmitted power that doesn't land on any PV cell is obviously lost. Figure 4.31 is an example of a Spectrolab produced array of small, high flux capable cells, similar to the sort of array we will build for our demonstrator. The cells are arranged in strings and controlled with MMPT electronics.

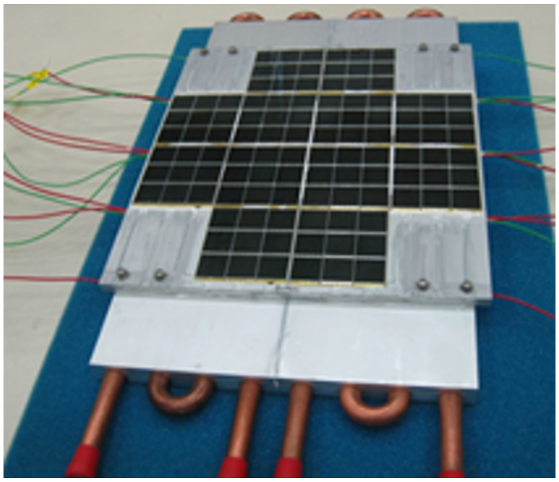

Figure 4.31: Boeing/Spectrolab concentrated optimized laser InGaAs LPV with twelve 3x3 cell subsets. Each cell is 2.25 cm^2. These cells are ~60% efficient at 808 nm. Goal with new cells is 50% efficient at 976 nm.

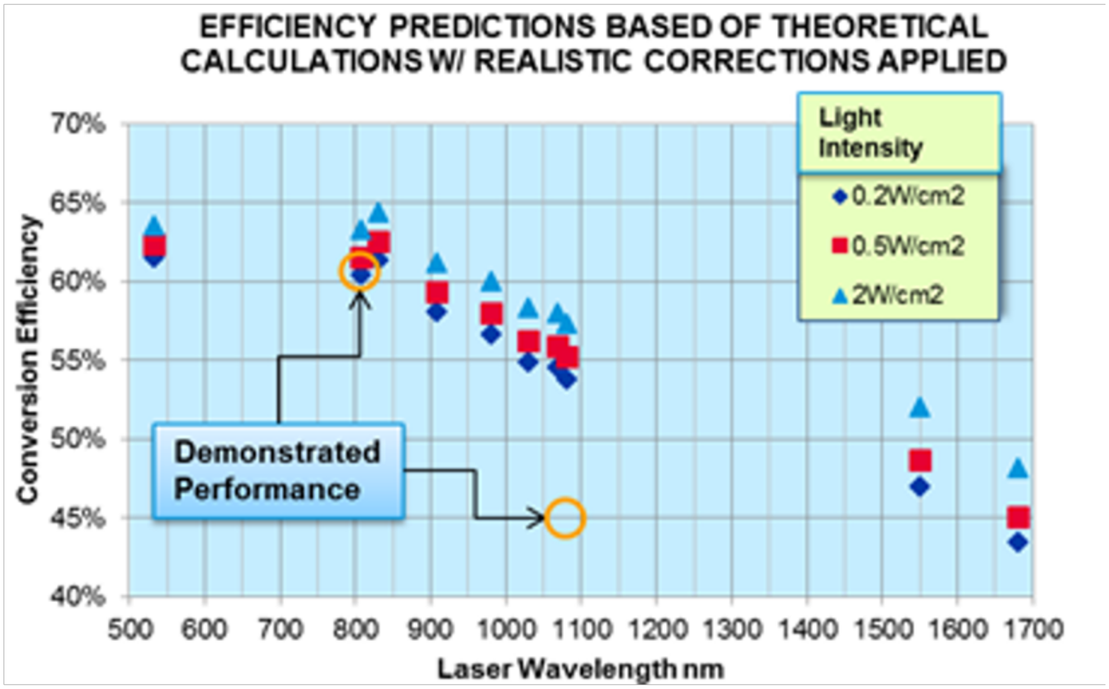

Figure 4.32: Modeled and achieved efficiencies of various laser power converters for common laser wavelengths vs. flux. Note that high flux is more efficient.

Target locking and moving targets. It is possible to beam power to both stationary and moving targets as well as to multiple targets. For example, unique optical beacons on each client and server (if more than one). RF/optical comms allow continuous communication to assess and optimize client needed PV power.

Multi-Mode to Single-Mode Options. There is a straightforward way to go from multi-mode to single mode. By multi-mode cladding pumping a single mode Yb doped fiber (YDF) at 976 nm we get single-mode out at 1064 nm with approximately 85% conversion efficiency. By using multiple 976 nm pumps, $>1\text{kW}_{\text{opt}}$ single-mode 1064-nm output is feasible at a wall plug efficiency of >42%. While not trivial, it does give many options (Figure 4.33).

Further details on power beaming technology are given in the Appendix A.

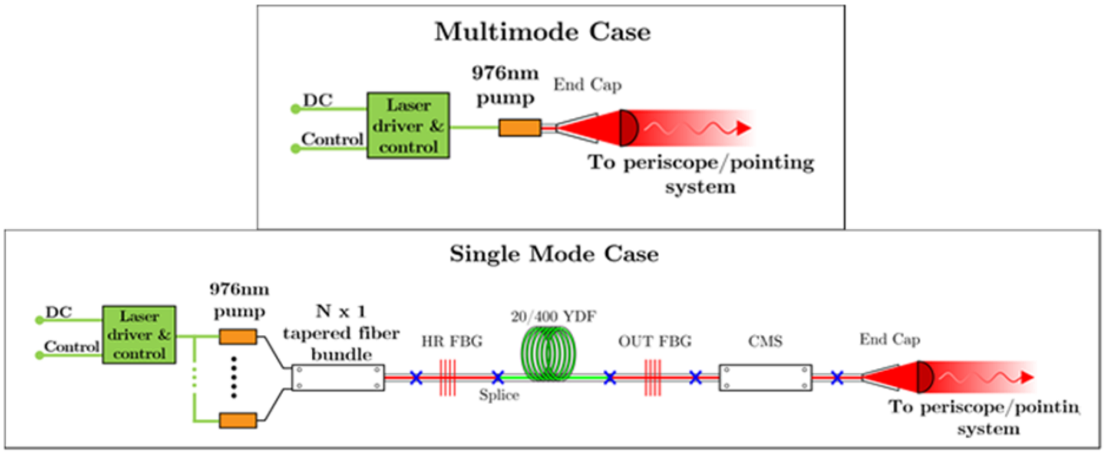

Figure 4.33: Schematic comparison of multi-mode (top) and single mode (bottom) high power lasers.

4.5 System Level Way Forward

The technologies explored in this report are groundbreaking and represent significant steps forward, even revolutionary. To achieve the mega-watt-scale solar arrays envisioned here, we need to both decrease the areal mass density of the solar arrays by more than an order of magnitude beyond current state-of-the-art while increases the array area by up to an order of magnitude. Each of these advances brings its own challenges as discussed in Section 4.1.

A deliberate path to space technology risk reduction is well described in NASA Technology Readiness Assessment Best Practices Guide, SP-20205003605. An appropriate summary graphic from that document is reproduced in Figure 4.34. This indicates the development path of fidelity to flight via modeling, analyses, breadboards, brassboards, and prototypes, and, in

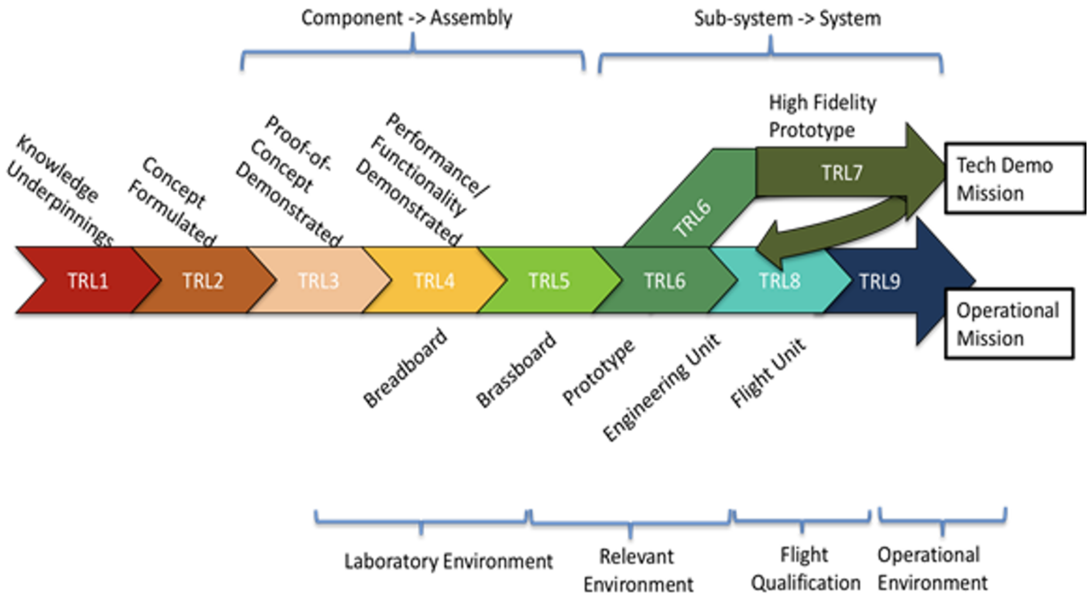

Figure 4.34: Two paths to flight. The most common path progresses from TRL 1 to TRL 6, skips TRL 7, and then progresses through TRL 8 to 9. For new technologies where demonstration in space is critical to risk reduction, TRL 7 is also included. (Copied from NASA SP-20205003605 Technology Readiness Assessment Best Practices Guide).

concert with that maturation, higher levels of assembly, and testing to relevant environments (e.g., zero-g and 30 au). The TRL 7 step is especially germane in that for some technologies key testing can be performed on Earth, but for the large, gossamer solar arrays considered herein it is likely that flight demonstration testing will be required to provide zero-g, if not 30 au solar range.

To achieve TRL 7 or 8, the interaction of all relevant subsystem interfaces must be considered as diagrammed in Figure 4.35. In the present case, this includes most of the spacecraft; power, thermal, attitude control and structure/mechanisms, and is the issue that drives the need for a flight demonstration. A potential shortcut to a solar array flight test at 30 au may be to place a demo mission in a super-Geosynchronous or L2 halo orbit specifically designed to explore the Earth's penumbra, which would allow throttling incident solar flux between 0 and 1 (albeit with spectral distortions due to the Earth's atmosphere). Such a test would be crucial to demonstrating key performance such as (1) array deployment and stability in space (2) momentum management in the presence of solar radiation pressure (SRP) and heat re-radiation (3) attitude control in the presence of the large flexible body and (4) management/distribution of the very large power coming from the solar panels.

Similarly, integration of these solar array advances with other potential uses for this high power level, e.g., SEP (Section 4.2) and Power Beaming (Section 4.3) requires consideration of the maturity of the interfacing. For example, given decades of experience with such hardware, the combination of new SEP thrusters with the large power available may reliably be demonstrated via ground test to achieve TRL7, but the usage of power beaming is revolutionary so would require its own flight test, while demonstrating control of the large flexible solar array simultaneous with the beam pointing stability.

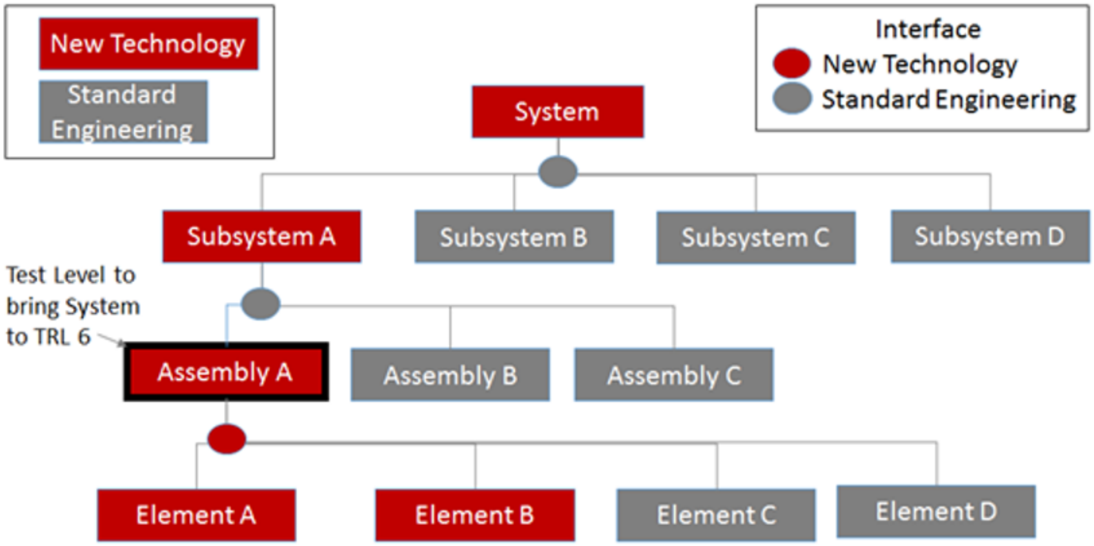

Figure 4.35: Hierarchical breakdown of the system structure (Copied from NASA SP-20205003605 Technology Readiness Assessment Best Practices Guide).

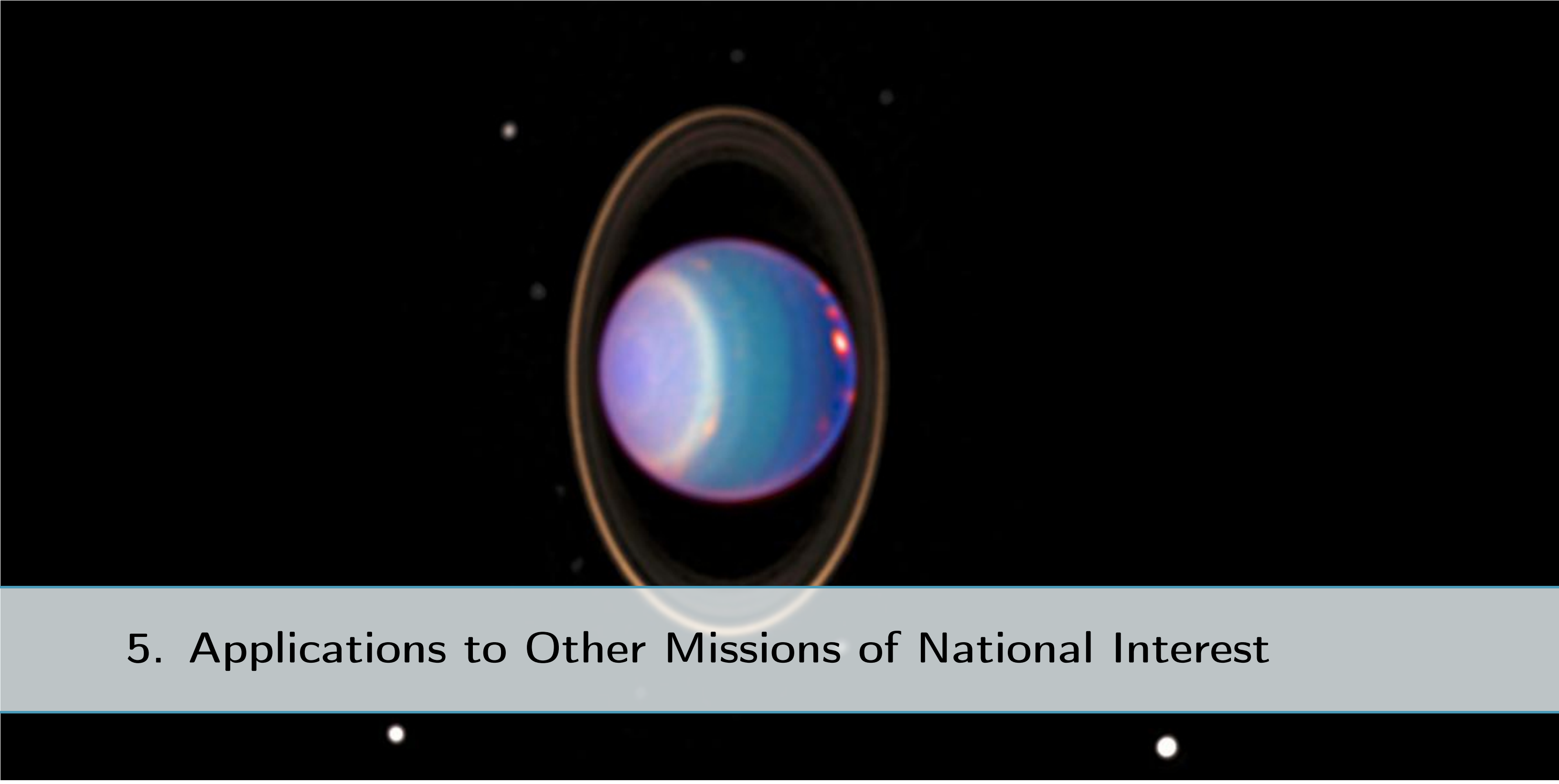

5. Applications to Other Missions of National Interest

The technologies discussed here have the potential to enable a tantalizing arrays of mission applications, which we divide into the following seven categories:

1. Single-system orbiter: A Pluto orbiter is of great interest to the planetary science community, as evidenced by the Planetary Mission Concept Study: "Persephone: A Pluto-System Orbiter & Kuiper Belt Explorer" (Howett et al., 2020). The large, ultra-light solar arrays combined with a state-of-the-art electric propulsion system would make the orbital exploration of Pluto, and a tour of its large moon Charon and smaller moons, possible within a reasonable mass margin. Conventional propulsion systems would require an unreasonably large mass to successfully enter orbit around Pluto, and many RTGs would be required for power.

2. Multi-body flyby: Large, ultra-light solar arrays and a state-of-the-art electric propulsion system would enable a spacecraft to chase down and encounter long-period comets and potentially even interstellar objects. Rapid reaction times could be facilitated by stationing the spacecraft at a Lagrange point or in Mars orbit. The ability to leave this ‘parking orbit,’ flyby a long-period object or interstellar object and then return to the parking orbit to await another flyby is possible using SEP but not conventional propulsion.

3. Multi-body orbiter: SEP enables a spacecraft to orbit multiple bodies using a reasonable propellant mass, e.g., the Dawn mission to Vesta and Ceres. The large, ultra-light solar arrays discussed in this study would enable a Dawn-like mission architecture deeper in the solar system, for example: a Kuiper belt tour, centaur tour or a ‘Grand Tour’ of

the gas and ice giants without the need for the most optimal planetary alignment as with the Voyager missions.

4. Sample return: Sample return is the next frontier in planetary exploration. But returning a spacecraft with the sample is more difficult than leaving the Earth because there is no extra push from a launch vehicle. SEP and the other technological developments discussed here would facilitate sample return from a wide range of bodies including (in order of perceived difficulty): Ceres or Mars, Enceladus or Titan, Triton or Mercury.

5. Power beaming: Beaming power from a large, ultra-light solar array in orbit to a landed asset would allow for surface exploration in a variety of forms: power could be delivered to the poles and permanently shadowed regions of the Moon and Mercury; a spacecraft in a Mars synchronous orbit could provide power to a variety of surface assets; power could be beamed from a decoupled solar array to a space telescope, reducing imaging disturbances; and beamed power could even potentially power melt probes on the icy satellites and drones and/or boats on Titan. The logistics of beaming power through the atmospheres of Mars and Titan needs to be further investigated.

6. Human exploration: A SEP/chemical hybrid spacecraft would avoid transporting humans to Mars with nuclear-electric or nuclear thermal propulsion. Lighter arrays could also reduce flight times, decreasing the exposure of the astronauts to potentially harmful radiation. Power could also be beamed to the surface for habitats.

7. Planetary defense: The Arecibo observatory, which was uniquely qualified to detect and characterize potentially hazardous NEOs, required a large amount of power. Large, ultra-light solar arrays could power an Arecibo-like telescope in space, providing an early-warning system for the Earth. Ion-beam deflection and laser ablation of hazardous asteroids would also be greatly enhanced by these technologies.

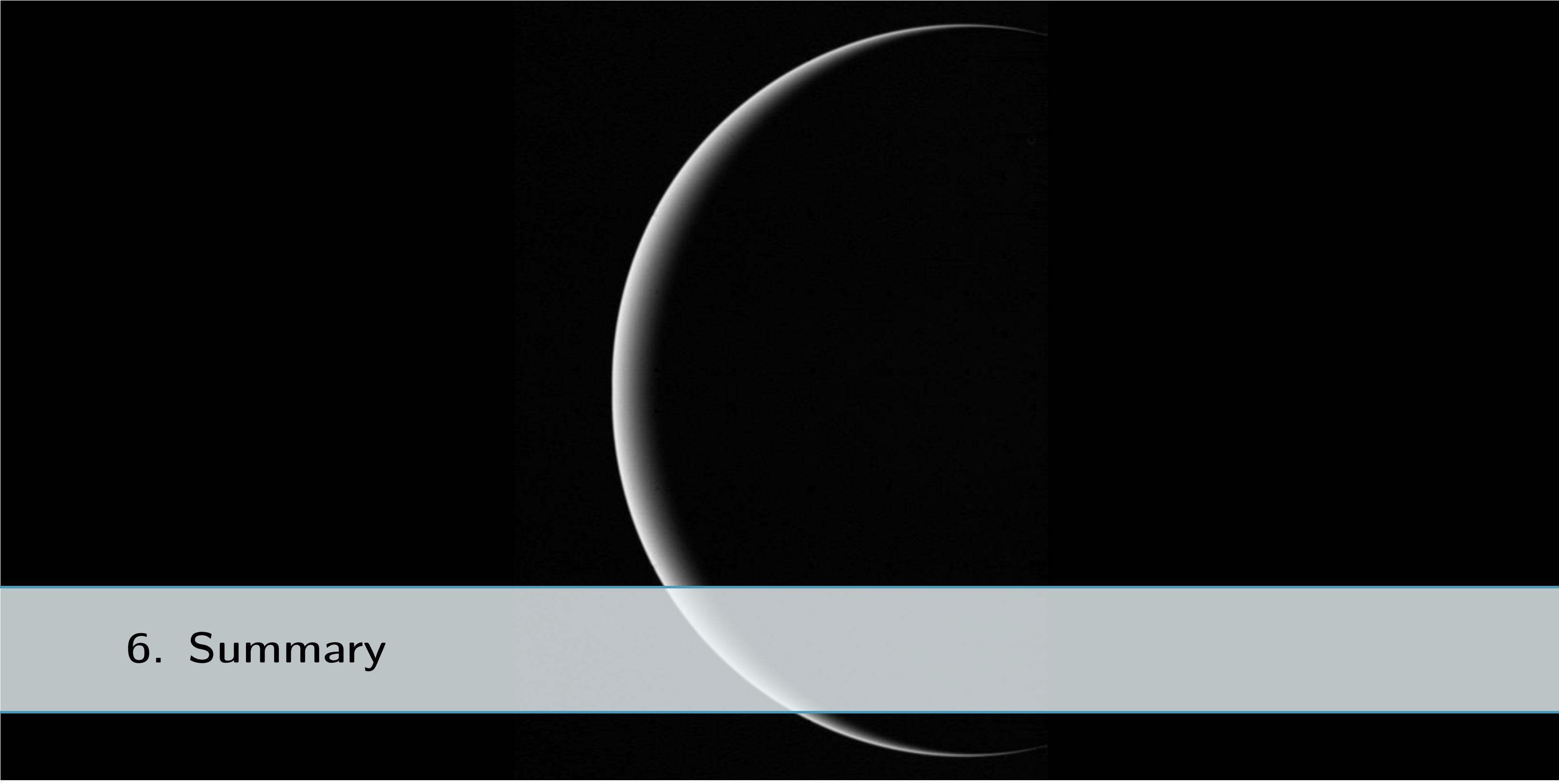

6. Summary

Over the history of space exploration, solar arrays have been getting larger (higher power), lighter (lower specific mass), less expensive ($/kW), and have been used at increasing distances from the Sun. Continued solar array technology development will enable solar powered missions to the ice giants. Solar cells specially designed by Boca, have demonstrated good efficiency and fill factors under conditions roughly equivalent to the same solar range as the orbit of Neptune. The technology goals identified in this report for solar powered missions to Uranus and Neptune are: 1) Cell efficiency of 25% at Uranus or Neptune; 2) Areal density of 100 g/m^2 for Uranus and 50 g/m^2 for Neptune; and a deployable solar array wing with an active area of order 3600 m^2. While solar array wings of this size and areal densities are ambitious goals, reasonable paths to achieving them are identified in this report.

Amazingly, no new electric propulsion technology is needed to perform the all solar-powered missions to Uranus and Neptune. The performance capability represented NASA's NEXT ion propulsion system is sufficient to perform these missions with a reasonable number of thrusters (up to 6 thrusters) and reasonable propellant masses ($<$3000 kg). The NEXT system has some engineering details to complete and the system would have to be flight qualified for the demands of these missions, but no technology development is required. More advanced mission architectures could make use of electrospray thruster technology, but this would fall in the category of mission enhancements rather than being mission enabling. In addition, significant technology development of electrospray thrusters would be required to support missions to the ice giants.

Power beaming is required to provide power to landed assets on the moons of Uranus or Neptune in an all solar-powered architecture. Power would be beamed down from a solar-powered orbiting platform to the landed asset. Power could be provided either continuously to a single asset or intermittently to multiple assets for battery recharging. The requirements for these applications include: 1) Beaming power across hundreds to thousands of kilometers; efficiency of electrical power to laser power conversion of ~50%; efficiency of laser power to electrical power conversion of ~50%; and the ability to use receiver arrays on the landed assets that are acceptably small (i.e., a few meters in diameter). These requirements are beyond the current state-of-the-art, but they appear to be readily achievable with continued technology development.

While the ultimate goal of this study was to evaluate the technology required for a fully non-nuclear exploration of the ice giants, the development of the required technology would likely include a number of demonstration missions that would be potentially beneficial in their own right. Such missions could include: 1) Power beaming from Earth–Moon L1 to the lunar surface; 2) Power beaming to the surface of Mars; 3) Sample return missions using large, lightweight solar arrays and electric propulsion; and 4) Demonstration of ion beam deflection as a viable and effective planetary defense technique that is enhanced by the availability of large, lightweight solar arrays.

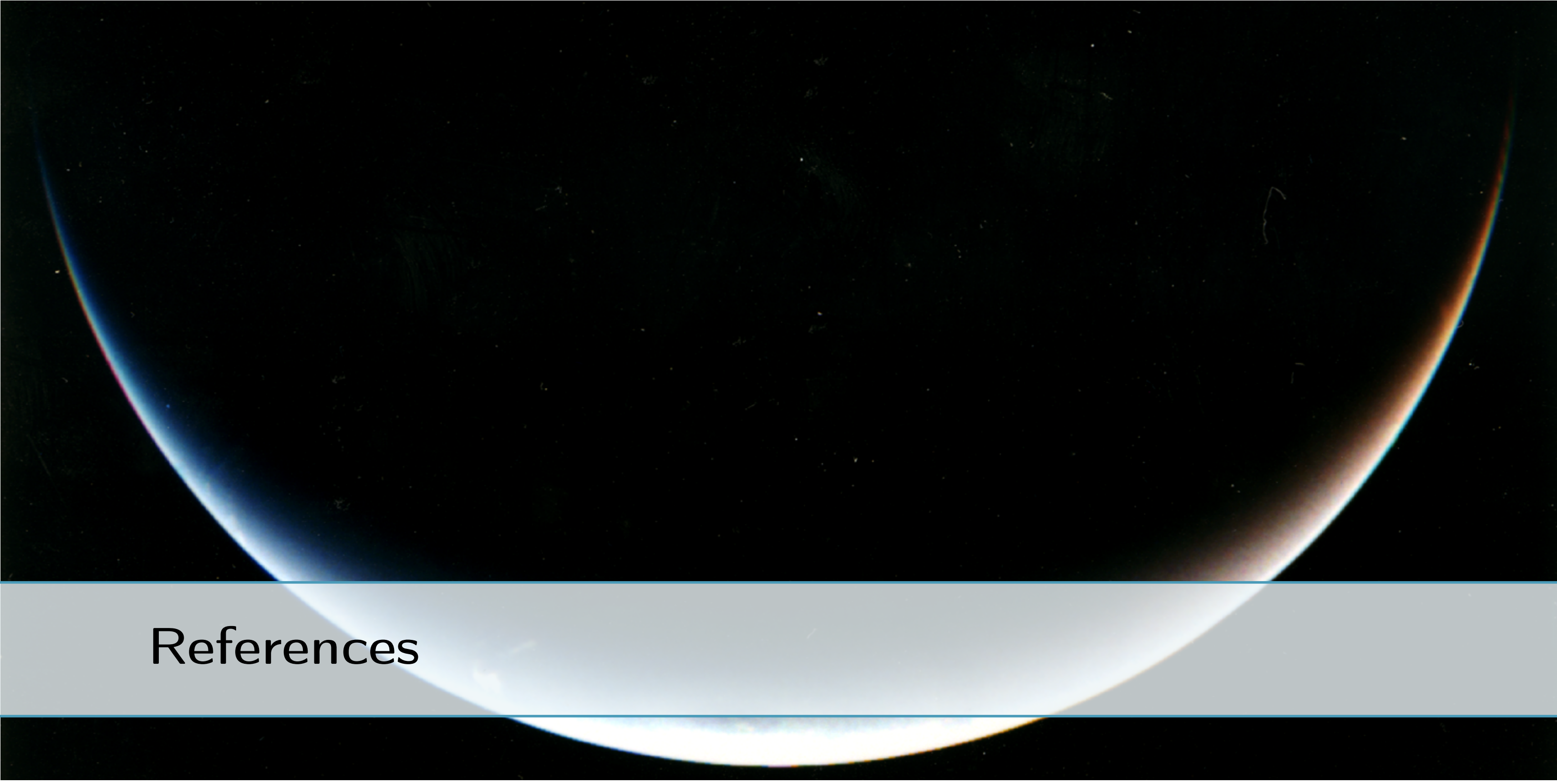

References

Advanced Stirling radioisotope generator (n.d.). Accessed 04/02/2022. URL: `https://en.wikipedia.org/wiki/Advanced_Stirling_radioisotope_generator`.

Arya, Manan, Nicolas Lee, and Sergio Pellegrino (2016). "Ultralight structures for space solar power satellites". In: *3rd AIAA Spacecraft Structures Conference*, p. 1950.

Balas, Mark (1982). "Trends in large space structure control theory: fondest hopes, wildest dreams". In: *IEEE Transactions on Automatic control* 27.3. doi:10.1109/TAC.1982.1102953, pp. 522–535.

Banerjee, Arun K, Nelson Pedreiro, and William E Singhose (2001). "Vibration reduction for flexible spacecraft following momentum dumping with/without slewing". In: *Journal of Guidance, Control, and Dynamics* 24.3. doi: 10.2514/2.4737, pp. 417–427.

Banik, Jeremy A and Arup K Maji (2016). "Structural scaling parameters for rectangular flexible blanket solar arrays". In: *Journal of Spacecraft and Rockets* 53.5. doi.org/10.2514/1.A32895, pp. 936–951.

Bayer, Todd et al. (2019). "Europa clipper mission: Preliminary design report". In: *2019 IEEE Aerospace Conference*. doi:10.1109/AERO.2019.8741777. IEEE, pp. 1–24.

Beddingfield, Chloe et al. (2020). "Exploration of the Ice Giant Systems: A White Paper for NASA's Planetary Science and Astrobiology Decadal Survey 2023-2032". In: *arXiv preprint arXiv:2007.11063*.

BET-MAX: Multi-axis precision electrospray thruster system (n.d.). Accessed 04/02/2022. URL: `https://www.busek.com/bet-300p`.

Bolton, SJ et al. (2017). "The juno mission". In: *Space Science Reviews* 213.1. doi: 10.1007/s11214-017-0429-6, pp. 5–37.

Bozek, John M (Feb. 1995). *Ground-based and space-based laser beam power applications*. Tech. rep. NASA Technical Memorandum 106774.

Brophy, John (2011). "The Dawn Ion Propulsion System". In: *Space Science Reviews* 163. doi.org/10.1007/s11214-011-9848-y, pp. 251–261.

Brophy, John R. et al. (Oct. 2019). *Non-Nuclear Exploration of the Solar System*. Tech. rep.

Cardona, A and M Geradin (1988). "A beam finite element non-linear theory with finite rotations". In: *International journal for numerical methods in engineering* 26.11. doi:10.1002/nme.1620261105, pp. 2403–2438.

Chilan, Christian M et al. (2017). "Co-design of strain-actuated solar arrays for spacecraft precision pointing and jitter reduction". In: *AIAA journal* 55.9. doi:10.2514/1.J055748, pp. 3180–3195.

DART (n.d.). Accessed 04/02/2022. URL: `https://www.nasa.gov/planetarydefense/dart/dart-news`.

Enhanced Multi-Mission Radioisotope Thermoelectric Generator (eMMRTG) Concept (n.d.). Accessed 04/02/2022. URL: `https://rps.nasa.gov/resources/56/archival-content-enhanced-multi-mission-radioisotope-thermoelectric-generator-emmrtg-concept/`.

Fan, T. Y. (2017). "Coherent beam combining of fiber lasers". In: *2017 Conference on Lasers and Electro-Optics Europe European Quantum Electronics Conference (CLEO/Europe-EQEC)*, pp. 1–1. DOI: `10.1109/CLEOE-EQEC.2017.8087019`.

Fan, Tso Yee (2005). "Laser beam combining for high-power, high-radiance sources". In: *IEEE Journal of selected topics in Quantum Electronics* 11.3, pp. 567–577.

Gapontsev, V. et al. (June 2016). "Multi-Kilowatt CW Fiber Laser Systems with Record Wall-Plug Efficiency Exceeding 50%". In:

Gdoutos, Eleftherios et al. (2020). "Ultralight deployable space structure prototype". In: *AIAA Scitech 2020 Forum*, p. 0692.

Gdoutos, Eleftherios et al. (2022). "Development of the Deployable on-Orbit ultraLight Composite Experiment (DOLCE) for the Space Solar Power Project Demonstration Mission". In: *AIAA SCITECH 2022 Forum*, p. 1266.

Gozzard, David R et al. (2020). "Fast beam steering with an optical phased array". In: *Optics Letters* 45.13, pp. 3793–3796.

Hecht, Jeff (Apr. 2016). "Photonic frontiers: High-efficiency optical pumping:'Going green' cranks up the laser power". In: *Laser Focus World*.

Hofstadter, Mark et al. (June 2017). *Ice Giants: Pre-Decadal Survey Mission Study Report*. Tech. rep. JPL D-100520. NASA.

Howett, Carly, Stuart Robbins, Karl Fielhauer, et al. (2020). "Persephone: A Pluto-System Orbiter & Kuiper Belt Explorer". In: *NASA Planetary Mission Concept Study*.

Hughes, Gary B et al. (2014). "Optical modeling for a laser phased-array directed energy system". In: *Nanophotonics and Macrophotonics for Space Environments VIII*. Vol. 9226. SPIE, pp. 20–26.

Jaffe, Paul (2021). *15 Critical Measurements for Power Beaming Links*. URL: `https://hdiac.org/wp-content/uploads/2021/04/2020-07-30-hdiac-webinar-power-beaming-space-solar-innovation-slides.pdf`.

Kammer, DC and MJ Triller (1994). "Ranking the dynamic importance of fixed interface modes using a generalization of effective mass". In: *Modal Analysis: The International Journal of Analytical and Experimental Modal Analysis* 9.2, pp. 77–98.

Kilopower (n.d.). Accessed 04/02/2022. URL: `https://www.nasa.gov/directorates/spacetech/kilopower`.

Klein, Bernard J and John J Degnan (1974). "Optical antenna gain. 1: Transmitting antennas". In: *Applied optics* 13.9, pp. 2134–2141.

Leclerc, Christophe and Sergio Pellegrino (2020). "Nonlinear elastic buckling of ultra-thin coilable booms". In: *International Journal of Solids and Structures* 203. doi: 10.1016/j.ijsolstr.2020.06.042, pp. 46–56.

Lee, A.J. and S. Pellegrino (2021). "Architectures for Lightweight Deployable Plate-Like Space Structures". In: *International Journal of Solids and Structures*. Submitted.

LISA Pathfinder (n.d.). Accessed 04/02/2022. URL: `https://en.wikipedia.org/wiki/LISA_Pathfinder`.

Lubin, P (2016). "A Roadmap to Interstellar Flight". In: *Journal of the British Interplanetary Society* 69, pp. 40–72.

Marrese-Reading, Colleen (2016). "Microfluidic Electrospray Propulsion (MEP) Thruster Performance with Microfabricated Emitter Arrays for Indium Propellant". In: *52nd AIAA/SAE/ASEE Joint Propulsion Conference*, p. 4738.

– (June 2021). "Microfluidic Electrospray Propulsion (MEP) Thruster Demonstration with a Capillary Force Driven Feed System and Propellant Reservoir". In: *68th JANNAF Propulsion*

Conference. Joint Army-Navy-Air Force Chemical Propulsion Information Analysis Center, Columbia, MD.

Marrese-Reading, Colleen and John R Anderson (2016). "Silicon emitter needle and array design for indium electrospray arrays for spacecraft propulsion". In: *52nd AIAA/SAE/ASEE Joint Propulsion Conference*, p. 4547.

Marshall, M. A. (2022). "Dynamics of Ultralight, Flexible Spacecraft during Slew Maneuvers". PhD thesis. California Institute of Technology.

Multi-mission radioisotope thermoelectric generator (n.d.). Accessed 04/02/2022. URL: `https://en.wikipedia.org/wiki/Multi-mission_radioisotope_thermoelectric_generator`.

Orphee, Juan et al. (2018). "Solar torque management for the near earth asteroid scout cubeSat using center of mass position control". In: *2018 AIAA Guidance, Navigation, and Control Conference*. doi:10.2514/6.2018-1326, p. 1326.

Photonics, IPG (n.d.). *YLS-20000 ECO: Highest-Efficiency High-Power Fiber Laser*. URL: `https://www.ipgphotonics.com/en/100/FileAttachment/YLS-10000-ECO+Datasheet.pdf`.

Rymer, Abigail et al. (2020). "Neptune Odyssey: Mission to the Neptune-Triton System". In: *NASA Planetary Mission Concept Study*.

Shastry, Rohit et al. (2013). "Status of NASA's Evolutionary Xenon Thruster (NEXT) long-duration test as of 50,000 h and 900 kg throughput". In: *International Electric Propulsion Conference (IEPC2013)*. IEPC-2013-121.

– (2014). "End-of-test Performance and Wear Characterization of NASA's Evolutionary Xenon Thruster (NEXT) Long-Duration Test". In: *50th AIAA/ASME/SAE/ASEE Joint Propulsion Conference*. AIAA-2014-3617, p. 3617.

Siewert, Andreas (Nov. 2014). "High Power Industrial Grade Fiber Lasers". In: Hamburg. AIME on High Energy Lasers, DESY.

SNAP-10A (n.d.). Accessed 04/02/2022. URL: `https://en.wikipedia.org/wiki/SNAP-10A`.

Snyder, John Steven et al. (2014). "Experimental investigation of a direct-drive Hall thruster and solar array system". In: *Journal of Spacecraft and Rockets* 51.1, pp. 360–373.

Spanos, John T (1989). "Control-structure interaction in precision pointing servo loops". In: *Journal of Guidance, Control, and Dynamics* 12.2. doi:10.2514/3.20399, pp. 256–263.

Sprangle, Phillip et al. (2015). "High-power lasers for directed-energy applications". In: *Applied Optics* 54.31, F201–F209.

Thomas, Robert E et al. (2019). "NEXT Single String Integration Tests in Support of the Double Asteroid Redirection Test Mission". In: *International Electric Propulsion Conference*. IEPC-2019-853. University of Vienna, Vienna, Austria, September 15–20.

Tile Propulsion: Propulsion, Reinvented for New Space (n.d.). Accessed 04/02/2022. URL: `https://accion-systems.com/tile-propulsion/`.

Wie, Bong (2008). *Space Vehicle Dynamics and Control, 2nd Ed.* Reston, Virginia. American Institute of Aeronautics and Astronautics.

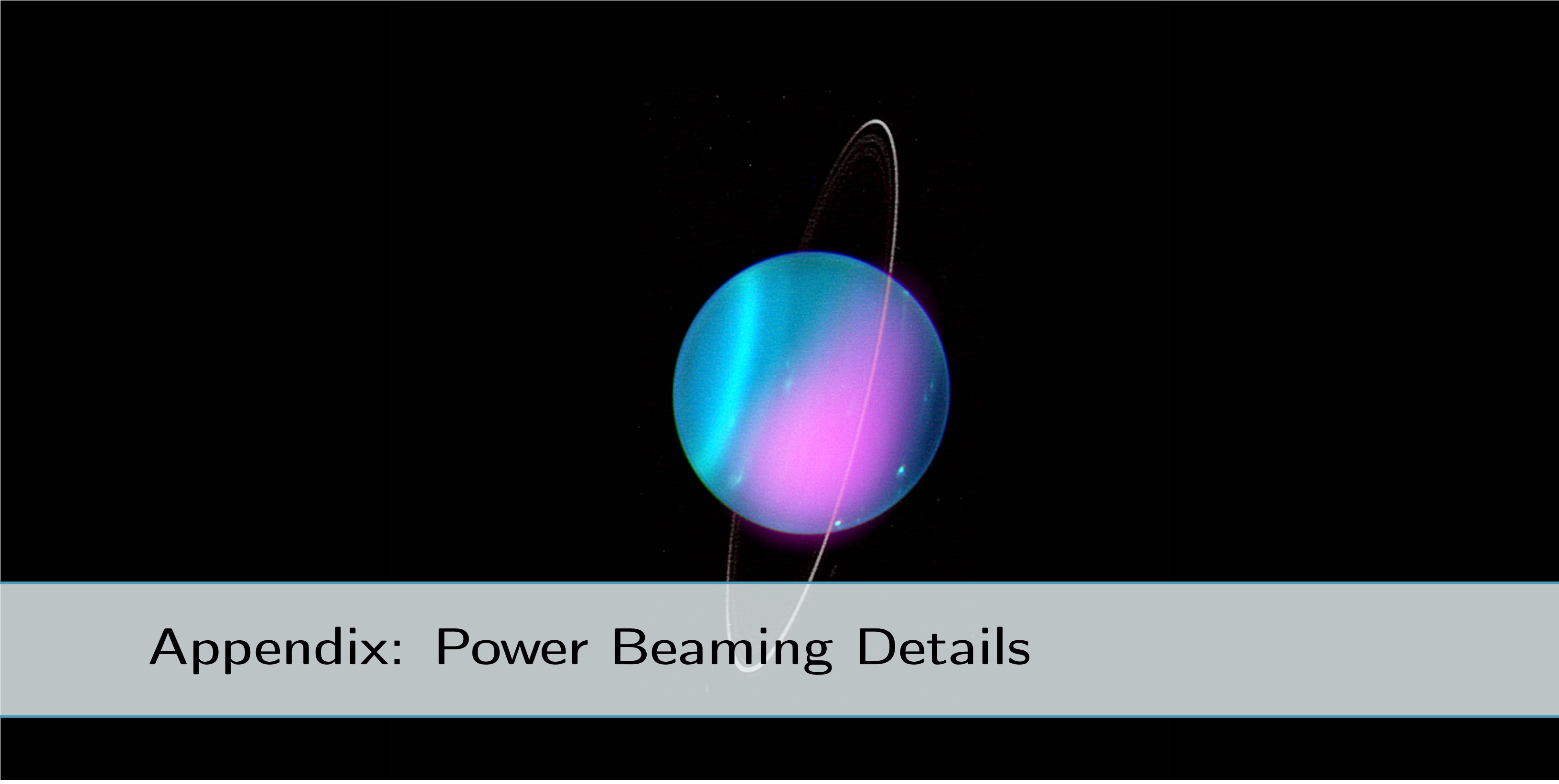

Appendix: Power Beaming Details

(by Abhijit Biswas)

A.1 Introduction

Power beaming has been studied for a number of diverse applications (Bozek, 1995; Jaffe, 2021) over the years. In this appendix power beaming relevant to non-nuclear exploration of the solar system is briefly discussed. Figure A.1 shows a schematic view of the essential elements of a power beaming system.

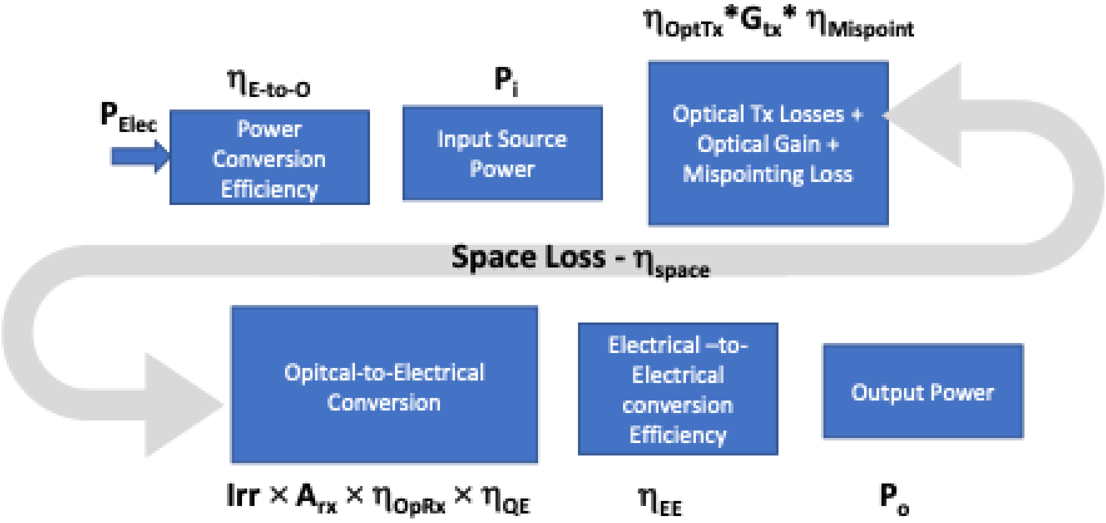

Figure A.1: A schematic representation of system conversion losses for power beaming.

Equation 1 for Irradiance (W/m^2) at target, where λrepresents the laser wavelength, and Equation 2, written separately, for output power and Equation 3 for transmit side electrical to optical power conversion, describes the power beaming system:

$$Irr = P_i \eta_{OpTX} G_{tx} \eta_{Mispoint} \eta_{space} \left[\frac{4\pi}{\lambda^2} \right] \tag{1}$$

$$P_0 = Irr A_{rx} \eta_{OpRx} \eta_{QE} \eta_{EE} \tag{2}$$

$$P_i = P_{Elec} \eta_{E-to-O} \tag{3}$$

The design objective will be to optimize P_o/P_{Elec} while keeping in mind outer space mission durations and environments. Table A.1 lists the parameters in the power conversion equation.

Equation 1 does not explicitly call out thermal dependencies of the conversion efficiencies and pointing control losses. System implementation can be significantly impacted by these dependencies and should be accounted for in the design. For design analysis, the allocation of these dependencies can be distributed amongst the defined parameters. System mass optimization is always a driver for space missions and will need to be addressed.

Lifetime for both the laser and the detector to be deployed will also be a driver. For example, degradation of laser electrical to optical conversion efficiency, detector QE and increase in dark noise with time, associated with total ionization dose (TID) is expected and should be accounted for. Lasers subjected to extended periods in cold dark space have not been designed or deployed and studies to understand the vulnerabilities and mitigations are needed. Likewise, detector lifetime and performance degradation with aging may require special studies for the class of missions under consideration.

In a recent study (Brophy et al., 2019) a design reference mission for a Miranda lander formulated higher level requirements for a power beaming system. These are listed in Table A.2 below as a guide for the discussions to follow.

The mission concept involves power being beamed over a distance of 600 km to a landed asset on the surface of Miranda. This is motivated by the enhanced power density achievable with a laser beam compared to solar power at Uranus distances. A phase array laser was conceptualized as the transmitter, with non-mechanical beam steering to control the laser beam pointing.

P_{Elec}	Electrical power input to the Power Beaming System (Watts)
P_0	Output useable electrical power (Watts)
P_{i}	Optical power output from power beaming laser (Watts)
η_{EO}	Electrical to optical conversion efficiency, largely dictated by laser wall-plug efficiency
η_{OpTx}	Output optical coupling efficiency associated with coupling the laser beam to optics that optimize the beam energy transferred to the target. Optical transmission and scattering losses, wave-front error losses, far-field coupling and/or truncation losses are included in this term
G_{tx}	Antenna gain, to first order dependent on the ratio λ/D, or beam divergence, with D representing the transmitting aperture diameter
η_{Mispoint}	Mis-pointing losses in optimally covering the receiver area, includes dynamic losses due to base platform vibrational disturbance, and static and quasi-static components from pointing offset or bias errors
η_{Space}	Inverse square of distance loss due to beam spreading
Irr	Irradiance incident at target (W/m^2) presumed to be approximated by a spatia gaussian distribution
A_{Rx}	Collection antenna aperture area (m^2)
η_{OpRx}	Optical coupling efficiency between collection area and light incident on detectc includes optical transmission and scattering, possible overfilling or blocking losse of the detector
η_{QE}	Optical-to-electrical conversion following electro-optic conversion, will include quantum efficiency of detector and other secondary losses of converted photoelectrons
η_{EE}	Electrical-to-electrical conversion losses i.e. DC–DC converters or other signal conditioning losses

Table A.1: Power Conversion Parameters

Within the framework described above the remainder of this writeup is organized as follows. Section A.2 will discuss the laser transmitter side of a power beaming system including the laser itself.

A.2 Transmitter

A.2.1 Lasers Transmitter (LT) Requirement Drivers

From Eq. 3 laser transmitter average power, P_i, is determined by the wall-plug efficiency (WPE) of the laser or the electrical-to optical conversion efficiency. The power beaming Laser Transmitter (LT) key requirements based on Table A.2 are:

- Wavelength of approximately 1064 nm
- Output power 2 kilowatt
- WPE of 50%.

Paramet	Quantity	Units	
1	Wavelength (textlambda)	1064	nm
2	Power Output	2	kW
3	EO Conversion Efficiency	50	%
4	Transmitter Aperture Diameter	50	cm
5	Range	600	km
6	Receiver Collection Diameter	2.13	m
7	Receive Side Conversion Efficiency	50	%
8	Power at Lander	243	W

Table A.2: Requirements for power beaming to a lander on Miranda.

Additional critical requirements for the LT that are:

- M^2 of approximately 1.2.
- Efficient waste heat removal

The low M^2 value is needed in order to efficiently couple the laser power to the target. Thermal management of the 2 kW of waste heat around the "hot spots" associated the diodes used for pumping the gain medium is required to avoid damage or severe reduction in lifetime. While thermally stable laser operation is desired, tight spectral control may not be required for power beaming.

Practical packaging and aggressive mass saving will be required for the class of missions under consideration. Another critical requirement will be the reliability and lifetime of the LT. Technology development may be required to ensure that the laser lifetime exceeds the cruise and mission duration, with margin, with cruise duration expected to far exceed the mission duration. Gain medium like fibers or crystals surviving in cold dark space for prolonged periods will need to be addressed, possibly with mitigation to periodically power up lasers to anneal out darkening of the gain medium.

Two broad classes of laser transmitters that operate in the wavelength, power output and WPE regime targeted are: (i) phase combining of lower power unit lasers to achieve higher power, with closed loop spatial pointing control for optimal energy transfer to the receiver; (ii) a single or a few high-power lasers, with built-in redundancy, coupled to suitably sized optics with a separate pointing control sub-system.

Figure A.2: 1070 nm laser module with approximately 1 kW output (M^2~1.1; Siewert, 2014)

A.2.2 LT State of Art

A.2.2.1 Incoherent Combining

High power laser development has advanced significantly with the required power levels and WPE being commercially advertised. Ytterbium doped lasers (Gapontsev et al., 2016; Hecht, 2016) with wavelengths in the vicinity of 1060 nm and kW class power with WPE of 30–50%, are available for industrial materials processing applications. The IPG product line (Siewert, 2014) advertises a 1070 nm 1 kW laser module with single mode output (M^2 ~1.1), WPE of approximately 30%, packaged with a mass of 11 kg and a 2-m length of delivery fiber (see Figure A1.1). Larger core (100–200 µm) lasers (Photonics, n.d.) also around 1070 nm with 10 kW output and 50% WPE are also advertised but the reported mass of 400 kg for these systems give the impression of them being too massive for space applications.

Recently the DSOC Project at JPL developed a Coherent Inc. SPADE amplifier, shown in Figure A.2, for use as a ground-to-space transmit with CW output power of 2 kW and approximately 30% WPE, M^2 of 1.2 and < 0.25 nm spectral linewidth. The as-built mass of these lasers is about 20 kg, with no effort expended to optimize the mass.

The lasers described above approach the power output and WPE targeted for the non-nuclear deep space missions. Nonetheless, a single string implementation would be too high risk and it would be better to implement beam combination and de-rated operation thereby achieving redundancy and longer lifetime. These lasers for the class of missions under consideration would likely be incoherently combined (Sprangle et al., 2015) because the spectral width (coherence time) and polarization state of these lasers would not lend themselves to efficient coherent combining. Incoherent combining for directed energy applications usually involve propagation through atmospheric propagation the turbulence parameters dictate the spot size on target. For space applications without atmospheric turbulence incoherent combining can use wavelength combining (Fan, 2017; Fan, 2005) methods. Here the component lasers would operate at slightly different wavelengths and the separation in wavelength would be determined by the spectral η_{QE} of the receiving detector and the availability of robust dichroic coatings for implementing wavelength combining schemes on the transmit side.

The proven waste heat management for these lasers would involve use of heat pipes with circulating coolant and possible use of radiators. Innovative ways of utilizing the waste heat should be given some consideration. A research concept being pursued to ease waste heat management is to transmit a train of high peak power pulses so that the average power delivered is the same but the waste heat management is eased through use of pulsed battery power sources.

Figure A.3: SPADE amplifier-based laser developed for DSOC Project ground uplink laser assembly.

A.2.2.2 Coherent Combining

Coherently combined lasers to achieve desired power levels with built-in redundancy and even beam steering capability by phase control offers an appealing and elegant solution. The complexity of these systems is formidable and to date demonstrations have operated at 10s-to-100s of watts power levels. These systems use sophisticated phase loop control algorithms (Fan, 2017; Fan, 2005; Gozzard et al., 2020) that would introduce higher risk for space environment implementation. The scaling of these systems to the kilowatt level has been simulated (Hughes et al., 2014) for a 1064 nm laser transmitted through an effective 1 m diameter aperture to achieve 1.8 µrad pointing with $\lambda/8$ to $\lambda/10$ of phase control. The advantages offered by coherent phaser array lasers are compelling but whether the targeted power levels and efficiencies can be met needs further study and development.

A.2.3 Beam Delivery

Referring back to the system equation (Eq. 1) the product $\eta_{OpTx} \times G_{Tx} \times \eta_{Mispoint}$ is related to the beam delivery.

The use of high-quality optics and coatings minimizes η_{OpTx}, as does minimizing the number of optical surfaces between the beam exiting the LT and exiting the transmitter aperture. For the durations of the class of missions being considered coatings must not only withstand high powers but should also be resistant to aging and cumulative radiation. Heating of optics and thermal gradients caused by the residual optical absorption and the resulting refractive index changes need to be carefully factored into the design. Small space closed-loop beam steering to ensure autonomous alignment is using feedback from optical and/or thermal sensors is critical so that beam walk does not cause burning and permanent damage of structural mounts. Wave-front error (WFE) losses are estimated using a rms number of waves of error but need to be verified through testing to ensure that the allocation is met.

Ideally G_{Tx} is given by $20 \times \log_{10}(\pi D/\lambda)$. The ideal gain is reduced by efficiency terms arising from beam truncation and obscuration (Klein and Degnan, 1974).

Smaller λ/D results in larger G_{Tx} but also results in increased pointing difficulty. Ideally the optical design should optimize the product $G_{Tx} \times \eta_{Pntg}$. For power beaming open loop pointing is risky because the power delivery efficiency will be uncertain. Closed loop pointing requires feedback from the receiving target. For 600-km distances this can be achieved with retroreflectors on the edge of the receiver or a low power beacon transmitted from the landed asset. The latter is more complex and demanding in resources. The retro-reflector approach for 600-km distances may be an optimal choice. Furthermore, use of modulated retroreflectors will also provide a low burden means of returning sensor data and telemetry from the surface. The added optical receiving function should be traded with RF approaches to ensure overall improvement in system efficiency. With or without the modulated retroreflector signal returned for closed loop pointing of the power beam is highly recommended.

A.2.3.1 Example

λ	1064	nm		
P_i	2000	W	33.01	dBW
η_{OTx}	0.39		-4.09	dB
GTx			123.33	dB
η_{space}			-256.96	dB
Peak Power at Target			-104.70	dBW
Peak Irradiance at Target	371.58	W/m^2		

Table A.3: Link parameters and peak irradiance.

η_{Tx} is a combination of an allocated optical transmission, wave-front error and truncation loss. Ideal truncation of a 1064 nm beam with a gaussian footprint on a circular exit aperture with 0.5 m diameter is presumed so that the ratio of the exit aperture radius to the beam waist is 1.12. With these idealized assumptions the peak irradiance at the target is 371.6 W/m^2. Figure A.4 shows a gaussian approximated irradiance distribution plotted as a function of beam diameter from the center of the beam on target.

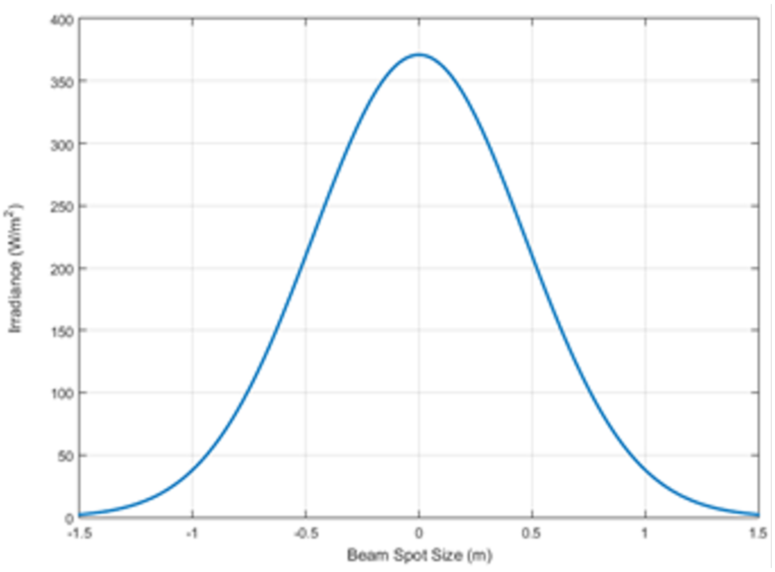

Figure A.4: Irradiance distribution at target with a 2 kW, 1064 nm, laser transmitted through a 0.5-m diameter aperture with ideal truncation to achieve maximum on-axis irradiance.

With a 2-m diameter collection area 96% of the power could be collected, however, if there is a 1 µrad per axis pointing error corresponding to a radial error is 1.4 µrad then only 64.6% of the power would be converted. A radial error of approximately 1.1 µrad is needed to achieve close to 70% power conversion.

A.3 Receiver

A.3.1 Receiver Collection Area

From the discussion in Section 1.1.3.1 2-m class collector areas will be required. The entire array could be made of Laser Power Converters (Brophy et al., 2019). The active detectors could either be placed behind a "lenslet array" architecture designed to maximize fill-factor, or in a "solar-Panel" architecture like photo-voltaic solar cells.

Materials for maximum absorption and quantum efficiency over a narrow spectral band can be selected in order to obtain maximum conversion. Based on maintaining a 70% collection efficiency due to mis-pointing from the transmitter the power would end up being about

950 W. With a 50% QE and a 50% electrical-to-electrical conversion about 210 W of power output could be achieved.